NASA TM-81780

NASA Technical Memorandum 81780

A DESIGN ASSESSMENT OF MULTIWALL, METALLIC STAND-OFF, AND RSI REUSABLE THERMAL PROTECTION SYSTEMS INCLUDING SPACE SHUTTLE APPLICATION

L. ROBERT JACKSON AND SIDNEY C. DIXON

APRIL 1980

National Aeronautics and
Space Administration

Langley Research Center
Hampton, Virginia 23665

A DESIGN ASSESSMENT OF MULTIWALL, METALLIC STAND-OFF, AND RSI REUSABLE THERMAL PROTECTION SYSTEMS INCLUDING SPACE SHUTTLE APPLICATION

L. Robert Jackson and Sidney C. Dixon
Langley Research Center

SUMMARY

Reusable thermal protection systems (TPS) have been studied for hypervelocity vehicles for over 20 years. Three concepts of current interest are Reusable Surface Insulation (RSI) used for the space shuttle, metallic stand-off TPS and multiwall TPS. TPS design goals are given. Each of the thermal protection systems is briefly described, and the ability of each system to satisfy design goals is discussed. Equations for calculating apparent conductivity of multiwall TPS and parameters needed for strength predictions are given. Thermal performance is given for multiwall TPS and mass estimates are compared for all three thermal protection systems as applied to the space shuttle.

Results indicate that multiwall has the potential to satisfy the TPS design goals better than the other systems. The total masses of each of the metallic systems (stand-off TPS and multiwall TPS) are comparable to that of RSI for shuttle application. Moreover, the metallic systems require less primary structure mass than the RSI system; since the nonbuckling skin criteria, required for the RSI system, may be removed. Continued development of multiwall TPS is required to verify its potential and to provide the necessary data base for design.

INTRODUCTION

Reusable thermal protection systems for hypervelocity vehicles have been the subject of research and development for over 20 years. These thermal protection systems include the Reusable Surface Insulation (RSI), currently used on the space shuttle (ref. 1), metallic stand-off TPS (ref. 2), and multiwall TPS (refs. 3-5).

Reusable thermal protection systems are shown in figure 1. The RSI system consists of load-bearing insulating silica tiles bonded to a strain isolation pad, which in turn is bonded to the primary structure. The metallic stand-off TPS consists of a nonload-bearing insulation protected by a metal shield that is segmented to allow unrestrained thermal expansion. The shield is mechanically attached to the structure through flexible stand-off supports. Multiwall TPS consists of a load bearing foil enclosure, strengthened by sandwich faces, that contains either a fibrous or a metallic insulation. The enclosure forms a metallic tile that is mechanically attached through slip joints to the structure.

An effective TPS must control the peak temperature of the primary structure with low mass. The TPS should be reusable and have long life for minimum life cycle cost and acceptable operational turnaround time. The TPS must have sufficient strength and stiffness to support various mechanical, air, and thermal loads and resist flutter. Water and hot gas ingestion are to be avoided and a smooth surface is beneficial. Moreover, an effective TPS must be readily installed and removed for inspection and repair of the TPS and the primary structure.

This paper contains an assessment of how well three thermal protection systems (RSI, metallic stand-off TPS, and multiwall) satisfy the design goals. Thermal and structural properties of multiwall TPS are given to aid in design. In addition, the thermal performance of multiwall and estimated masses for all systems are given for specific application to the space shuttle.

SYMBOLS

A	fractional area of through metal or of expansion gap
F	configuration factor
D	diameter of dimple contact area
f	view factor
H	heat transfer coefficient
j	total number of dimpled and plain foils in thickness, L
k	thermal conductivity
L	total or incremental thickness of multiwall tile
n	number of dimple contacts per unit area of one face
P	conduction path length measured along diagonal pitch of dimples
p	diagonal pitch of dimples
T	temperature
t	thickness of dimpled sheet
z	sum of thickness of j foils in thickness, L
X	slant length of edge seals
β	factor used in calculation of radiation heat transfer coefficient
ϵ	average emittance
σ	Stefan-Boltzman constant

Subscripts:

a	apparent
ave	average
c	cold face
g	gas or expansion gap
h	hot face
i	insulation
m	metal
r	radiation

Additional symbols used in the Appendix are defined as they are used.

TPS DESIGN GOALS

The fundamental design goal of any TPS is to limit the peak temperature of the structure to its specified operating temperature, which is 450 K (350°F) for the aluminum structure of the space shuttle (ref. 1). However, the TPS must satisfy several other goals to be effective. The TPS design goals are listed in Table I and discussed herein. In addition to the fundamental TPS role of limiting the primary structure to its maximum operating temperature, the three most significant design goals, indicated in Table I, are low mass, low life-cycle-cost, and short turnaround time. All of the other goals are required either to meet these goals or to insure that the TPS performs its functions as a structural-insulation system throughout the complete mission of an earth-to-orbit transportation system.

A smooth surface is desirable to minimize local heating and to avoid tripping the laminar boundary layer to minimize both peak heating and the

overall heat load to the vehicle. The TPS must be resistant to hot gas ingress and flow of hot air within the insulation, which could overheat the primary structure.

The mass of the TPS must be low since an increase in TPS mass results in an equal decrease in payload for a space transport. Low mass must be achieved with a TPS that provides the required insulating and load bearing functions. These functions are equally important since insufficient strength or stiffness could cause loss of the TPS, and thus the insulating function it provides. In flight, such a loss can be catastrophic. The TPS must not induce high local loads or thermal stress in the structure. Moreover, the TPS should not require increases in structural mass beyond that required to support structural loads. That is, the TPS should be compatible with structural deformations and skin buckling. The TPS must be resistant to water retention (some insulations are capable of absorbing more than their mass in water). Water retention may also result in such deleterious effects as damage due to expansion upon freezing and possibly corrosion.

For economical operation of a space transport, the TPS should have a short turnaround time between flights and a low life cycle cost. Thus, the TPS should be reusable and have long life. The materials of construction must survive the environment with low oxidation and creep rates, and the strength and stiffness must be adequate to support wind shear, differential pressure, and thermally induced loads without failure or flutter. The TPS must have the durability to survive high acoustic levels, numerous thermal cycles, and damage from foreign objects, ground handling, rain, and possibly hail impingement in flight.

A further design goal for a TPS is that it be economical to fabricate and readily installed on the vehicle. Moreover, it should be readily removed for repair and inspection of both the TPS and the primary structure.

REUSABLE THERMAL PROTECTION SYSTEMS

Various reusable thermal protection systems have been under study to varying degrees for over 20 years. Three of current interest are the Reusable Surface Insulation (RSI), baselined for the space shuttle (ref. 1), metallic stand-off TPS (ref. 2), and multiwall TPS (refs. 3-5), and each is briefly described in the following paragraphs.

RSI Thermal Protection System

The RSI thermal protection system is aptly described in reference 1; however, a brief description is given here along with a discussion of how well RSI satisfies the TPS design goals.

Description.- Figure 2 shows a typical RSI tile arrangement as used on the space shuttle. On the lower surface of the shuttle the tiles are nominally 15 cm (6 in.) square and of various thicknesses dependent on the local heat load. RSI on the lower surface has a high solar absorptance coating and is called HRSI. On the upper surface the tiles are 5.1 cm (2 in.) and 20.3 cm (8 in.) square, and have a low solar absorptance coating and called LRSI. The tiles are made of quartz fiber that is sintered to a bulk density of either 144 kg/m^3 (9 lb/ft^3) or 352 kg/m^3 (22 lb/ft^3), which provides load bearing qualities. A glassy coating is applied in manufacture to control emittance and absorptance and to prevent water ingress. A Nomex felt strain isolation pad is used to prevent tile failure when the primary

structure undergoes mechanical and thermal strains. The coating is omitted along the inner portion of the surface of all four edges of the tile adjacent to the strain isolation pad to permit venting the tile interior. It is currently proposed that after each flight, the gaps between tiles will be sprayed with a water repellant that is permeable to air to allow tile venting. The Nomex felt strain isolation pad is bonded to the tile prior to bonding to the primary structure. Nomex felt filler bars, coated with RTV adhesive, are also bonded to the structure along the four edges of the tile to prevent hot air in the gaps from impinging on the aluminum structure. Numerous tiles have a gap filler to reduce hot air flow in the gaps. Each tile is pre-fabricated including precise machining to suit the local design contour of the vehicle.

Assessment.- RSI is an effective insulation, but it has relatively low strength (ultimate tensile strength is only about 172 kPa (25 lb/in.^{2})). Its thermal reusability has been demonstrated in numerous arc-jet tests simulating entry heating conditions and overtemperature cycles. RSI is a brittle, low-strength material susceptible to damage. Thus, acceptable durability for an operational vehicle remains to be demonstrated by flight experience. Fabrication and handling experience has shown RSI can have a very high breakage rate, particularly the thin LRSI tiles used on the upper surface of the shuttle. However, use of a peel sheet, continuous over the outer surface of several tiles, greatly improves handling qualities. The tiles are stiff and early analyses, based on an assumed linear strain isolation pad (SIP) behavior, showed no flutter for the shuttle trajectory. Recent advances in understanding the SIP nonlinear properties have yet to be incorporated in flutter analysis. A complete assessment of sonic fatigue and other dynamic response phenomena have not been completed.

Water ingestion is avoided by the repellant; however, the repellant will be vaporized during entry when gap heating is severe (refs. 6-8) and the glass coating is easily cracked. Thus water ingestion and retention may occur if the vehicle is exposed to rain after entry during descent or upon landing. The expansion joints permit hot gas ingress between tiles and since the repellant is permeable or vaporized, hot gas may seep through the tiles since all four edges are vented. Gap fillers (ref. 9) are inserted between numerous tiles of the shuttle to prevent catastrophic hot gas ingress.

Approximately 31,000 different tiles are required to cover the space shuttle. The HRSI tiles are limited to a maximum size of 15 cm (6 in.) square on the lower surface because of the limit of the strain isolation pad to prevent structural strains from cracking the tiles. However, the strain isolation pad is not sufficient to isolate the tiles from skin buckling of the structure. Therefore, considerable stiffening has been added to the shuttle primary structure to satisfy a nonbuckling skin criteria. This stiffening is not required to support structural loads, thus it logically represents a RSI TPS mass penalty.

Another consequence of the large number of tiles is the difficulty of installation. Since tile joint gaps or irregularities could induce boundary layer transition resulting in an increased heating rate and total heat load, fairly stringent requirements on allowable gap widths and step heights have been imposed (refs. 1 and 9). However, as with all large vehicles, the local contour of the fabricated shuttle varies to some degree from the design contour. Due to the precision fit required between the tiles and the structure, numerous tiles must be either remachined or completely remanufactured. An additional shortcoming of RSI is that it cannot be easily removed from the vehicle without damaging the tiles.

In summary, RSI has excellent thermal performance at temperatures to 2555 K (2300°F) with overtemperature capability to 2955 K (2700°F) and has low mass. But its fragile quality renders it costly to fabricate and handle and fraught with potential operational problems. Work is continuing on Fiber Reinforced Composite Insulation (FRCI) in an attempt to solve some of the problems with RSI.

Metallic Stand-off TPS

Stand-off concepts were studied rather extensively during the Shuttle Technology Program. Concepts were studied for use in the 1255 K (1000°F) to 1589 K (2400°F) temperature range using nickel and cobalt-base superalloys (refs. 10 and 11) and TDNiCr (refs. 12 and 13) and coated columbium (refs. 14 and 15). Many design concerns were identified (ref. 16), and NASA Langley Research Center is coordinating a broad-based research program to improve the technology. The program has focused on tests of large panels including realistic thermal, acoustic, and aerothermal tests of flat concepts (refs. 10-15). Improvements in creep prediction and creep characteristics (refs. 17 and 18) have occurred and roughness induced local heating and drag tests (refs. 19-21) have been performed. Much of the heating work is summarized in reference 20. The most recent stand-off concept is described in reference 22. A brief description of stand-off TPS is given here with the aid of figure 3 followed by a discussion of how well metallic stand-off TPS currently satisfies the TPS design goals.

Description.- The metallic stand-off TPS (fig. 3) consists of a corrugated metal shield supported at its ends by flexible stand-off supports. The shield is about 0.5 m (20 in.) long and protects a layer of fibrous insulation, which may be packaged in a foil container. A slip joint is provided at the shield

ends, and as the shield is heated, it expands relative to the cooler primary structure to which the stand-offs are mechanically attached. Transverse expansion of the shield is accommodated by flexing of the corrugations that form the shield. Longitudinal expansion is accommodated at one end by flexing of the stand-off supports; the other end is fixed to resist wind shear. Consequently, the thermally induced loads transmitted to the structure are negligible. Conversely, strains of the primary structure are not transmitted to the shields.

Assessment.- Metallic stand-off TPS is also an effective insulation system and has sufficient strength for many flights (refs. 10-15), and the fibrous insulation is a more effective insulator than RSI. But the additional mass of the shield results in overall mass efficiencies that are, at best, about equal to RSI (ref. 2) as projected in 1977. Metallic stand-off TPS may be attached to the structure at ring frames and spars and thus accommodate skin buckling with a considerable reduction in structure mass compared with RSI TPS, which requires additional stiffeners to satisfy a nonbuckling skin criteria required to avoid loss of tiles should the skin buckle.

The cavity between the structure and shields, which is partly or completely filled with insulation, is vented to the base of the vehicle, which is essentially a low pressure sink. The outer surface of the shields is exposed to the static pressure in the boundary layer, which is essentially a high pressure source. The shields have a rearward facing overlap with a small clearance; consequently, the shield assembly acts as a permeable membrane imposing resistance to inflow of hot gas. Thus, the static pressure between the structure and shields could be about equal to the base pressure. In previous design studies of metallic TPS (refs. 22 and 23) it was assumed that a zero absolute pressure exists inside the shields during the period of high

heating rate. Then for the lower surface of the shuttle the pressure difference acting over the heated shields ranges from 1.07 kPa (0.155 psi) to 3.45 kPa (0.50 psi). (Space shuttle data given in this report were taken from a Rockwell International Corporation document and supplied by the Johnson Space Center of NASA.) The amount of hot gas inflow and the pressure history inside the shields is not fully understood, nor has this subject been extensively studied in wind-tunnel tests or design studies. In fact, one of the big unknowns for any reusable TPS is the design pressure difference. Hot gas ingress can increase the apparent thermal conductivity of the fibrous insulation, particularly when the insulation is not packaged, as in the design of reference 22.

The seriousness of the inflow problem has not been fully ascertained. Aero-thermal tests of one concept (ref. 10) experienced hot gas ingress (possibly due to the test setup) and potentially unacceptable performance, whereas tests of a more advanced concept (ref. 11) indicated no inflow problem. Flow seals at the shield ends have been studied, but no practical seal that permits thermal expansion (other than the simple overlapping joint (ref. 11)) has been developed to date. The incentive to develop effective flow seals awaits results of needed wind-tunnel tests of relatively large conical or cone-cylinder models that could determine the seriousness of the inflow/pressure differential problem.

One consequence of the pressure difference over the shields is the permanent creep-induced deflection. In cases where the shields operate at the maximum use temperature of the metals and at significant stress levels, creep deformation may limit stand-off TPS reusability. Significant progress has been made in improving creep properties for cobalt-base alloys (ref. 18).

Work is underway (Contract NAS1-15975) on similar improvements for nickel-base alloys. However, creep is still a design consideration and warrants continued investigation.

A further consequence of vented shields is water ingress. A foil container can be used to inhibit water ingress. However, a study (ref. 24) that included a nickel foil container for the insulation concluded that thermal cycle tests caused the foil package to buckle excessively, and its exposed ends and hot face broke after relatively few cycles, which included two overtemperature cycles to 1422 K (2100°F). These tests indicate that life of a foil container is a design concern requiring additional effort to result in a practical approach. Tests to study water ingress are required to fully assess the problem and to demonstrate container designs (if required) that successfully sustain thermal cycle tests.

Stand-off TPS shields have been shown by analyses and tests (ref. 25) to be flutter resistant. However, analyses indicate a drastic reduction in flutter resistance at flow angles greater than 15° to the axis of the corrugations. Moreover, the analyses (ref. 22) assumed full shear stiffness of the shield, but open end corrugations, used in the shield design, have appreciably less shear stiffness than calculated by the methods used. Therefore, wind tunnel tests at various cross flow angles are needed to verify flutter resistance of actual stand-off TPS designs.

Corrugations impose a relatively rough surface for cross flow which may cause local overheating and laminar-turbulent transition. Reference 19 studied a wavy surface, typical of a stand-off TPS surface, and found the roughness effect to be insignificant for flow angles of 15° or less. For larger flow angles there is an effect that could be significant. References 16 and 17 looked at wavy surfaces, but not necessarily typical of a TPS shield.

and concluded local heating may necessitate a change in material selection (cobalt base for a nickel base, TD-Ni-Cr for a cobalt base, etc.). Since the shuttle enters at an angle of attack in excess of 40°, considerable cross flow will occur. Thus, surface roughness remains a design concern. Inadequate data exist to fully define the problems--particularly laminar-turbulent transition--thus, additional work is needed.

Sonic fatigue tests (ref. 26) of a concept employing a low mass shield indicated a need to carefully design the attachment of the shield to the stand-offs to prevent cracking of the shield. References 12-15 indicate stand-off concepts that were successfully tested for 100 shuttle-type acoustic cycles.

Stand-off TPS is installed on the vehicle as numerous small pieces (insulating spacers under the stand-offs, stand-offs, insulation packages, heat shields, and numerous fasteners); that is stand-off TPS is not prefabricated for installation and removal ease.

Although heat shields have been tested for many of the environments encountered, there are still potential problems with metallic stand-off TPS. What is needed is a complete definition of the loads and requirements, and a stand-off TPS designed to satisfy all TPS goals and tested for all environments in a thorough effort. Although stand-off TPS has not had as thorough testing as RSI, it has had more testing than the newer multiwall TPS concept presented in the next section. With more in-depth effort, metallic stand-off TPS should become a workable system.

Multiwall TPS

A forerunner to multiwall TPS was initially studied for an integral liquid hydrogen tank where the multiwall simultaneously performed the

functions of TPS, primary structure and tank (refs. 3 and 4). The original concept used evacuated multiple layers of dimpled and plain foils welded together and welded to a similar structural sandwich that had relatively thick face sheets; the core of the structural sandwich was helium purged to detect hydrogen leakage. The vacuum was shown analytically to be beneficial in reducing boil-off of the liquid hydrogen. As described in reference 4, a truncated conical model was successfully fabricated, except for retaining a vacuum in the insulating outer layers.

More recently, in 1975 multiwall was proposed as a TPS fabricated as tiles (ref. 5) with the interior of the tiles vented to the local static pressure. This concept has been shown to be attractive in several design studies of hypersonic vehicles (refs. 5, and 27-29). The multiwall thermal protection system is described in this section followed by a discussion of how multiwall satisfies the TPS design goals.

Description.- For the space shuttle the lower surface "acreage" TPS has the most influence on overall TPS mass. Variations of multiwall TPS are needed for the higher temperature areas on the lower surface and for lower temperature areas on the upper surface. Thus, variations of multiwall TPS are described first for acreage areas then for high and low temperatures, respectively.

Basically, multiwall TPS is a load-bearing foil container (fig. 4) filled with an efficient fibrous insulation. Unlike the unstiffened foil bags used for stand-off TPS, the multiwall foil container must carry thermal, mechanical, and aerodynamic loads and thus is sandwich stiffened for strength and rigidity. The multiwall container or tile shown on figures 4 and 5 may be designed for the shuttle for the temperature range of 810-1310 K (1000-1900°F).

The outer face of the tile consists of two layers of dimpled core and three flat foils of superalloy forming a sandwich panel. All four edges of the tile are scarfed at 30° to reduce heat transfer through the expansion gap and edge seals; and beaded edge members provide the seal. These superalloy edge members transfer loads to the inner titanium alloy sandwich and to the corner attachments. The inner sandwich consists of a single dimpled core sheet and flat face sheets. Between the outer and inner sandwich panels is a layer of low density fibrous insulation. The attachments are located at the four corners of the tile. The container including a part of the attachments is diffusion bonded into a prefabricated tile. Structural strains do not transmit loads to the tile and thermal stresses are minimized because of the simple support, slip joint attachments, which are riveted to the structure, preferably at the ring frames and spars.

Nomex felt sealing strips, which may be coated with RTV for better sealing, are bonded to the primary structure along the tile edges and compressed on installation of the tiles to inhibit hot gas flow between the tiles and structure. The diffusion bonding process seals the tile. A vent hole is located in both faces of the titanium sandwich at adjacent corners to minimize the pressure difference over the hot face of the tile. The superalloy sandwich is sealed along its edges in manufacture so a vent hole is located in the interior face. The Nomex seal strips also have a single vent hole open to the gap between tiles to allow pressure equalization within the tiles.

Each multiwall tile may be 30 cm (12 in.) square or larger to span the distance between ring frames and spars. If multiwall tiles are made

30 cm (12 in.) wide by 50 cm (20 in.) long, and if the small close-out tile shapes now used for RSI are incorporated into adjacent multiwall tiles, then the 836 m^2 (9000 ft^2) of RSI on the shuttle would require less than 6000 multiwall tiles instead of the 31,000 RSI tiles.

At the more forward locations of the shuttle and at the body flap on the lower surface a coated refractory metal outer panel is required for multiwall tiles. Figures 6 and 7 show this variation of multiwall using columbium for the forward surface where the temperatures exceed 1310 K (2000°F); a tantalum alloy would be used for the flap where the temperatures exceed 1530 K (2400°F). A waffle panel was selected rather than foil gage dimpled core sandwich to better satisfy longevity factors for coated refractory metal. These factors are listed in Table II, and they include adequate coating thickness and coating thickness uniformity, use of large edge and corner radii, elimination of faying surfaces (which are difficult to coat and inspect), avoidance of slip joints that contact and slide on the coating, availability of all surfaces for coating inspection, elimination of coated rivets or threaded fasteners, and avoidance of coating contact with incompatible materials. Tests of coated columbium heat shields to a peak temperature of 1530 K (2400°F) (ref. 15) show life of about 50 simulated shuttle cycles, and tests of coated tantalum leading edge specimens to a constant temperature of 1810 K (2800°F) (ref. 30) show no failures in 37 cycles at six minutes each. Moreover, adherence to the above longevity factors could enhance the useful life of coated refractory metals.

On the upper surfaces of the shuttle the heat load is low; consequently, the required thickness of multiwall is generally less than 1.9 cm (0.75 in.).

At this thickness three dimpled layers fill the entire tile, thus an all-metal tile results. Figures 8 and 9 show the all-metal version of multiwall. It is constructed identically to the tile shown in figures 4 and 5 except all layers are diffusion bonded together. Fabrication of titanium all-metal multiwall tiles has been successfully demonstrated by Rohr Industries, Incorporated under NASA contract (NAS1-15646). Preliminary results of this effort are described in reference 31. Figures 10 and 11 show the various layers before bonding and a finished multiwall tile. For peak temperatures less than 1015 K (1000°F) a titanium alloy is used throughout. For the more forward upper surfaces, where the peak temperature exceeds 1015 K (1000°F), a bimetal tile is used. That is, the outer layers are made of a superalloy and the inner layers that are under 1015 K (1000°F) are made of titanium alloy.

Assessment.- The metals selected for multiwall tiles are strong and ductile. Multiwall TPS contains an efficient fibrous insulation and the metallic sandwich faces are effective load-bearing insulators. Like the stand-off system, multiwall TPS may be attached to the structure at ring frames and spars and thus accommodate skin buckling of the structure. Therefore, multiwall TPS does not impose a mass penalty on the primary structure. (This feature could increase the shuttle payload by eliminating the additional stiffening used to satisfy the nonbuckling skin criteria required for RSI.)

Each tile is vented only to the local pressure. Consequently, during entry heating, the only pressure difference acting over the hot sandwich face of the tile is that resulting from local pressure changes during flight. Since the tile is vented, the actual pressure difference is the pressure

equalization lag, which is very low--estimated to be less than 690 Pa (0.10 psi). With this small pressure loading, the stresses in the hot outer sandwich are low because this sandwich is designed for a much higher pressure loading during ascent. Consequently, no significant creep should occur. Therefore, the life of multiwall TPS may exceed the 100 mission life of the shuttle.

When a shock impinges on the tile face during ascent, a high local pressure is produced that is different from that at the vent in the Nomex edge seal, which controls the pressure within the tile. The resulting pressure difference over the face sandwich may be as great as 55 kPa (8 psi), based on shuttle pressure data extrapolated between test points given in reference 32. However, in areas where shock impingements are a major factor the affected tiles may be strengthened as required by increases in gage or face sandwich thickness. The majority of tiles may be lighter since they are designed for relatively low local loads.

The Appendix gives structural analyses, but key results are given here. Inplane tensile strengths for a Rene'41 sandwich is over 22.1 MPa (3200 $lb/in.^2$) based on sandwich thickness. Through-the-thickness tensile strength (determined from tests for titanium alloy sandwich in reference 31) is about 139 kPa (20 $lb/in.^2$) based on the face area (and assumed to be equal for Rene'41 sandwich). However, air loads on the panel face are transferred to the attachments primarily through the edge seals, not through the thickness of the face sandwich, except when the pressure inside the tile is greater than outside. Analysis indicates that the through-the-thickness tensile strength may be increased to about 173 kPa (25 $lb/in.^2$) by increasing the dimple contact diameter without affecting conductivity. Further increases

in strength will increase metallic conduction proportionately. Flutter analysis indicates that the Rene'41 sandwich has a flutter dynamic pressure during transonic flight of about 1.8 MPa (38,000 psf), which greatly exceeds the 33.5 kPa (700 psf) dynamic pressure of the shuttle. The 7.6 mm (0.003 in.) thick beaded edge seals have a compressive buckling strength of about 27 MPa (40,000 lb/in.^{2}) or about 48 kPa (7.0 psi) pressure difference based on tile face area. Since most tiles should have a pressure difference of much less than 6.9 kPa (1.0 psi), the baseline attachments, shown in figure 5, are sufficient for a factor of safety greater than 3 instead of the usual factor of 1.5. Moreover, the attachments may be strengthened to suit any pressure difference acting over a tile.

Hot gas ingress is inhibited by use of sealed tiles with a single vent prohibiting flow through a tile. The Nomex felt edge seals prevent flow between the tiles and structure. The beaded edge seals provide a labyrinth seal to lateral flow along tile edges, and the tile trailing edges overlap leading edges of adjacent tiles to further inhibit inflow of hot gas.

Water ingress is minimized by the use of a single vent in the Nomex, and the vent is located to permit drainage. Should water enter the space between the tile and structure, it has to travel a tortuous path to enter the fibrous insulation since the edges of the inner sandwich panel are sealed and single vents are provided in each of its face sheets at adjacent corners.

The overlapping tile faces offer a relatively smooth surface. And since the attachments are on the inner surface where the acoustic loads should be attenuated, sonic fatigue is not expected to be critical. Multiwall TPS is prefabricated to allow handling ease and independent fabrication of the

TPS and structure, and because of the particular mechanical attachment multiwall TPS is readily installed and removed from the vehicle.

In the design of multiwall TPS, the experience and knowledge gained from metallic stand-off TPS has been utilized extensively. Many of the remaining problems with stand-off TPS have been avoided by design of the multiwall system. However, limited fabrication and test experience exists. Current fabrication effort includes a curved, all-metal titanium tile and superalloy and titanium tiles containing fibrous insulation. Additional fabrication effort is required to include the refractory metal version. The thin foils require life tests at the maximum use temperature of the metals selected, where oxidation is of concern. Hot gas flow tests are planned to verify thermal-structural performance and seal effectiveness. Figure 12 shows an array of nine titanium multiwall tiles being prepared for testing in the Langley 8-Foot High Temperature Structures Tunnel. These tests will be performed at Mach 7 with a surface temperature of 1255 K (1000°F). Sonic fatigue, thermal cycle, and water retention tests are planned, and other tests are required.

Based on its potential to satisfy all TPS design goals, multiwall TPS promises an effective reusable approach.

MULTIWALL ANALYTICAL METHODS

This section contains equations and methods of analysis which are useful in design of multiwall TPS. Both insulating and load-bearing parameters are given. The Appendix gives details of the development and use of analyses to design the multiwall tiles described in this report.

Thermal Analyses

The principal thermal analyses of interest in design of multiwall TPS are the apparent thermal conductivity of the installed fibrous insulation and of the metallic sandwich faces.

Fibrous Insulation.- The fibrous insulation is surrounded by metal edge seals and an expansion gap between tiles. Consequently, the apparent conductivity and bulk density of the fibrous insulation in multiwall tiles are greater than that of the fibrous insulation alone. The apparent conductivity is given by:

$$k_{ai} = \underbrace{k_i\,[1-(A_m+A_g)]}_{\substack{\text{insulation}\\ \text{conductivity}}} + \underbrace{k_m A_m \frac{L}{X}}_{\substack{\text{edge seal}\\ \text{conductivity}}} + \underbrace{k_g A_g \left(\frac{L}{X}\right)^2}_{\substack{\text{air gap}\\ \text{conductivity}}} + \underbrace{H_r A_g \frac{L^2}{X}}_{\substack{\text{gap radiative}\\ \text{conductivity}}} \qquad (1),$$

where: $H_r = 4\sigma F T_{ave}^3 \beta$,

$$F = \frac{1}{1/f+2(1/\varepsilon-1)},$$

and $f \cong 0.022$, $\beta \cong 1.02$, and $T_{ave} = \frac{(T_h+T_c)}{2}$.

Results of evaluating equation (1) for various fibrous insulations are given in figure 13.

Equation (1) assumes that only gaseous conduction occurs in the gap between tiles; that is, no convection is present. Hot gas flow tests are required to verify this assumption.

Metallic Insulation.- The apparent conductivity, derived for reference 3 and modified herein, of the metal face sandwiches is given by:

$$k_{am} = 1.15 \quad \underbrace{\left[k_m A_m \left(\frac{L}{1.1P}\right)\right]}_{\text{thru-metal conductivity}} + \underbrace{\frac{k_g(1-A_m)}{1-\frac{z}{L}}}_{\text{gaseous conductivity}} + \underbrace{\frac{LH_r(1-A_m)}{(j-1)}}_{\text{radiative conductivity}} \qquad (2)$$

wherein: $A_m = \frac{4ptn}{6}$, or $A_m = \pi Dtn$ (use the larger value of A_m).

The diameter of the dimple contact area, D, is governed by strength requirements, and $f = 0.7$ in the equation for F given for equation (1).

The through-metal mode of heat transfer is strongly influenced by the conductivity of the metal selected. For instance, titanium alloys have lower conductivities than superalloys. Through-metal fractional area, A_m, in the sandwich is generally less than 0.5 percent. As with the fibrous insulation, the apparent conductivity of the metal sandwich is also affected--but to a lesser degree-by edge seals and gaps. Edge effects may be calculated using equation (1) wherein k_{am} from equation (2) is used for k_i in equation (1). For the transient heating analysis discussed in this report, a factor of 1.1 times k_{am} was used to estimate edge effects.

Figure 14 shows solutions to equation (2) for various metals of construction. Also shown are results of tests with stainless steel (ref. 3) and titanium panels (ref. 31). Gaseous conduction is greater than all other heat transfer modes at temperatures less than 1255 K (1000°F). Furthermore, if the cell size within the multiwall sandwich is made too large, free convection will occur thereby increasing the heat transfer. The Grashof number should be kept less than 2000 to avoid free convection. Also, the conductivity of the gas is taken equal to that at sea level since the cell size within the sandwich is larger than the mean free path of air including the

effect of reduced pressures at high altitude. If the tile could be made vacuum leak free and evacuated to a pressure of 0.013 Pa (1×10^{-4} mmH_g), then gaseous conduction would be eliminated, and the apparent conductivity of multiwall would be reduced by about 40 percent. However, in this paper the tiles are assumed to be vented.

The radiation penetration through the sandwich is governed primarily by the number of radiation barriers. This fact has been exploited in super insulations, which consist of up to 30 foils per cm (75 foils per inch) of thickness. Low emittances for all surfaces except the aerodynamic surface are also beneficial, but at high temperatures radiation transfer dominates for achievable emittances.

Structural Analysis

The structural properties of multiwall sandwich vary from other sandwich panels in that the thin multiwall face sheets and septum sheets are assumed to be nonload-bearing for compressive loads. Compressive loads are supported by the dimpled core. Tensile loads are supported by the thin face sheet and dimpled core. Thus, the moment of inertia is calculated assuming that flat sheets on the compressive side of the panel are omitted. Recent experiments have verified this assumption, and additional experiments are planned to determine the compressive strength of the dimpled core.

Once the effective moment of inertia is determined, the bending strength of the outer sandwich may be calculated by simple beam or plate theory assuming simple support for the edges. Flutter dynamic pressure may be determined by the method of reference 33. Analysis of the beaded edge

members is based on column theory using simple end supports. However, the column length is considerably greater than the tile thickness since all four edge seals are scarfed at 30° and the bead orientation on the edge seals is parallel to the corner edges of the tile. Attachment tabs are analyzed as cantilever beams. As indicated in reference 5, preliminary analysis shows that thermal stress in multiwall tiles is small primarily because of the simple, slip joint support. Other details of analyses methods are given in the Appendix.

One advantage of a metallic TPS like multiwall is that the thermal and structural properties can be easily changed to suit local dimensional and load conditions.

APPLICATIONS TO SHUTTLE

Prformance analyses have been made for multiwall TPS for several aerospace applications. In reference 27 multiwall was studied for a hypersonic cruise missile, in reference 28 for an advanced space transport, and in reference 29 for a Mach 5 cruise airplane. In this section results of analyses of multiwall for the space shuttle are given. A 30.5 cm (12 in.) square tile is compatible with the nonbuckling skin criteria of the shuttle structure, thus a tile size of 30.5 cm (12 in.) square was selected for study to reduce the number of tiles and gap heating from that of RSI. The various body points analyzed are shown in figure 15. Heating rates and other pertinent data used for the analyses are given in Table III.

Lower Surface

The majority of the lower surface of the shuttle has a peak temperature of under 1310 K (1900°F). Multiwall tiles, figures 4 and 5, consisting of a superalloy outer sandwich and edge seals with a titanium inner panel and attachments with Microquartz insulation, have been analyzed for the lower surface at body point 1700. Results of the transient heating analyses, using the method of reference 34, are shown in figure 16. Several thicknesses of multiwall were analyzed for each body point to determine the required thickness to satisfy the peak structural temperature limit. Analysis given in the Appendix shows that the tile bows elastically by about 0.3 cm (0.12 in.) during peak heating. Unit-area masses for multiwall and RSI are given in Table IV for the various locations on the shuttle. The RSI data were taken from a Rockwell International Corporation document and supplied by the Johnson Space Center of NASA. As seen in figure 16, the peak aerodynamic temperature is less than 1200 K (1700°F) while the peak temperature of the aluminum structure is 450 K (350°F).

Masses listed in Table IV for body point 1700 show that RSI is about 2.4 kg/m^2 (0.5 lb/ft^2) lighter than multiwall. However, all RSI masses in Table IV are based on 144 kg/m^3 (9 lb/ft^3) density; whereas, the average density of RSI is greater than 144 kg/m^3 (9 lb/ft^3) because a considerable number of 322 kg/m^3 (22 lb/ft^3) RSI tiles are used on the shuttle and many tiles have a densified inner layer. The RSI masses shown for the selected body points are somewhat lower than average due to aerodynamic fairing. Multiwall TPS is about 68 percent thicker than RSI at body point 1700. This requires either a modified mold line or use of a denser Microquartz in the multiwall tiles. The denser fibrous insulation has a lower thermal conductivity thus less thickness is required, but a mass penalty would result.

At a more forward location (body point 1300), figure 17 shows that the peak temperature approaches the maximum useful temperature of superalloys (considered to be 1310 K (1900°F) for this application). The Microquartz is temperature limited to about 1172 K (1650°F) (ref. 35); therefore, a thin outer layer of Dyna-Flex, which has a maximum use temperature of about 1422 K (2100°F) is added to the multiwall tile. Again, as seen in Table IV, 144 kg/m^3 (9 lb/ft^3) RSI is shown to be lighter than multiwall TPS--about 2.4 kg/m^2 (0.5 lb/ft^2) or 25 percent.

At still more forward locations on the lower surface, a coated refractory metal (columbium alloy) outer panel would be used for multiwall tiles. A waffle panel was selected for the refractory metal panel rather than a dimpled core foil sandwich to better satisfy longevity factors for coated refractory metal. The waffle was sized to have the same moment of inertia as the superalloy panel used at body points 1300 and 1700; however, a waffle panel is heavier than the dimpled core sandwich, and a tantalum waffle (used on the body flap) is heavier than a columbium waffle. The unit mass of the refractory metal tile was estimated by calculating the mass of the refractory metal outer panel and the mass of the thicker fibrous insulations, which were taken proportional to the thickness increase of RSI. Results of these calculations are given in the section entitled "TPS Comparative Masses."

The use of dispersion strengthened superalloys could reduce dependence on refractory metals with an appreciable mass savings. However, current dispersion strengthened alloys are not available in foil gages, and the adequacy of mechanical properties and oxidation resistance for foil gages in entry environment has not been determined. Further development of dispersion strengthened alloys in thin gages warrants continued investigation

and support. However, less than 10 percent of the shuttle would require refractory metals, as seen in figure 18; and only four percent of the surface would require refractory metal should the dispersion strengthened alloys with required properties become available. Refractory metal would be required at the body flap and the most forward locations, particularly adjacent to the reinforced carbon-carbon leading edges and nose cap.

Upper Surfaces

On upper surfaces of the shuttle the peak temperature is less than 922 K (1200°F) and the heat loads are low. Consequently, the thickness of multiwall is generally less than 1.9 cm (0.75 in.). At this thickness three dimpled layers required for strength and stiffness fill the entire tile and an all-metal tile results. For peak temperatures less than 810 K (1000°F) figure 19 (body point 3554) and figure 20 (body point 3140) a titanium alloy is used throughout.

At a more forward upper surface location, figure 21 (body point 3154), a bimetal all-metal tile is used. The outer layers are made of a superalloy and the inner layers are made of a titanium alloy. At this location the thickness is greater than three dimpled layers; that is, eight dimpled layers are required. However, three layers with a fibrous insulation filler, as shown in figure 4, would be somewhat lighter. As seen in Table IV for the body points analyzed, the average mass of multiwall tiles for upper surfaces are more nearly equal to the average mass of the RSI. Also the multiwall thicknesses for these body points are equal the RSI thicknesses because the RSI is thicker than required thermally to provide an aerodynamically faired surface.

TPS Comparative Masses

Comparative masses for the RSI, stand-off TPS, and multiwall TPS were calculated and are discussed below.

The multiwall unit mass data, calculated as discussed previously for various shuttle body points, are plotted in figure 22 as a function of peak surface temperature. Also, figure 22 shows RSI unit masses for 144 kg/m^3 (9.0 lb/ft^3) density, which were increased by about 15 percent from Table IV values to give average masses based on aerodynamic fairing. The metallic systems may also require some mass increase for fairing, but their thickness can be increased at less mass increase than RSI since the metallic systems use a lower density insulation. The body points were selected to compare point designs and do not represent average mass designs. Using the modified masses and the percentage areas (based on reference 1), also plotted as a function of peak surface temperature in figure 18, the unit masses may be plotted as a function of surface area as seen in figure 23. The curves of figure 23 were graphically integrated to yield total masses of RSI, stand-off, and multiwall TPS.

The total mass of RSI (based on only 144 kg/m^3 (9 lb/ft^3) tiles) is 5455 kg (12,000 lb.), which is in agreement with Rockwell data for 144 kg/m^3 (9 lb/ft^3) RSI. The estimated installed mass for RSI, which assumes a 15 percent mass increase to account for the use of some 322 kg/m^3 (22 lb/ft^3) tiles, is 6273 kg (13,800 lb.), which is in agreement with the current estimate of the Johnson Space Center. The integrated mass of multiwall TPS using dispersion strengthened alloys--where they apply--yields a total mass of about 6590 kg (14,500 lb.). And, as shown in figure 22, the mass of the metallic

stand-off system (data from reference 22 with a 96 kg/m^2 (0.2 lb/ft^2) foil container added) is equal to the mass of multiwall TPS. Therefore, within the accuracy of the analyses performed herein, all three thermal protection systems have about equal mass. Moreover, the RSI system requires considerable additional mass for structural stiffening to satisfy the nonbuckling skin criteria; whereas, the metallic systems can be designed for a skin that is permitted to buckle. Thus, the metal systems potentially offer an increase in shuttle payload.

CONCLUDING REMARKS

This paper contains a design assessment of reusable thermal protection systems (TPS) with emphasis on their performance for space shuttle application. The systems considered are Reusable Surface Insulation (RSI, currently used for the space shuttle), metallic stand-off TPS, and multiwall TPS. Multiwall TPS is described in some detail. Analytical methods useful for design analyses are included in the Appendix.

All three thermal protection systems are shown within the accuracy of the analyses to have about equal total mass. However, the strain isolation pad used with the RSI system is not sufficient to isolate the tiles from skin buckling of the structure and considerable stiffening has been added to the shuttle primary structure to satisfy a nonbuckling skin criteria. This stiffening is not required to support structural loads, thus it logically represents a RSI TPS mass penalty, that is not included in the TPS mass comparison made above. The metallic systems can be designed to function with a buckled skin. Thus, by not requiring the added stiffeners use of metallic TPS can potentially increase the shuttle payload.

The metallic stand-off system is strong and ductile. However, it may be subject to hot gas and water ingress, and its service life may be limited to less than the shuttle 100-mission life by creep deformation in some instances. Solutions to these problems are subjects for further study, and some mass increase may result. Moreover, metallic stand-off TPS is installed as numerous small pieces and therefore not readily installed or removed from the structure. However, with more in-depth effort, metallic stand-off TPS should become a workable system.

Multiwall TPS is a relatively new approach that is based on experience gained from all reusable systems. Multiwall is strong and ductile and not subject to excessive creep. Therefore, multiwall TPS has the potential to last 100 shuttle missions or more with the exception of a small percentage of surface area requiring refractory metals, which may last over 50 missions. Multiwall TPS is potentially resistant to either hot gas or water ingress and offers a relatively smooth surface. Moreover, it may be readily installed and removed from the structure. However, limited fabrication and test experience currently exists compared to the other systems. Therefore, continued development and study of multiwall TPS is required to verify its potential and to provide the necessary data base for design.

APPENDIX

MULTIWALL TPS ANALYSES

This appendix gives the details used for the design of the 30.5 x 30.5cm (12 x 12 in.) Rene' 41-insulation-titanium multiwall TPS described in the body of this report; the procedures are the same for the other multiwall variations. Where experimental results are available or needed they are indicated. Also, where a need for an empirical correction factor is indicated, the results of tests are cited and an appropriate corrective factor is suggested. Both apparent thermal conductivity and structural analyses are given; however, no attempt was made to structurally optimize the tiles. Gage selections were made based on experience and analyses given herein.

Apparent Thermal Conductivity

Fibrous Insulation. - The apparent thermal conductivity was calculated for the various fibrous insulations, and the following analysis is typical for each fibrous insulation.

The equation for apparent thermal conductivity is:

$$k_{ai} = \underbrace{k_i\,[1-(A_m+A_g)]}_{\text{insulation conductivity}} + \underbrace{k_m A_m \frac{L}{X}}_{\text{edge seal conductivity}} + \underbrace{k_g A_g \left(\frac{L}{X}\right)^2}_{\text{air gap conductivity}} + \underbrace{H_r A_g \frac{L^2}{X}}_{\text{gap radiation conductivity}} \qquad \text{(A1)}.$$

Evaluation of each of the terms in equation (A1) are described as follows:

Insulation Conductivity: The source references for fibrous insulation, K_i, as functions of temperature and pressure, are reference 35 (for Microquartz and Dyna-Flex) and reference 22 (for TG-15000). Space Shuttle data show that the static pressure acting on the lower surface at peak entry heating is 1.07 kPa (0.155 psia). Thus, the conductivity of the fibrous insulation is based on this pressure, since the multiwall tiles are vented to the local static pressure.

Geometric symbols are given in the following figure:

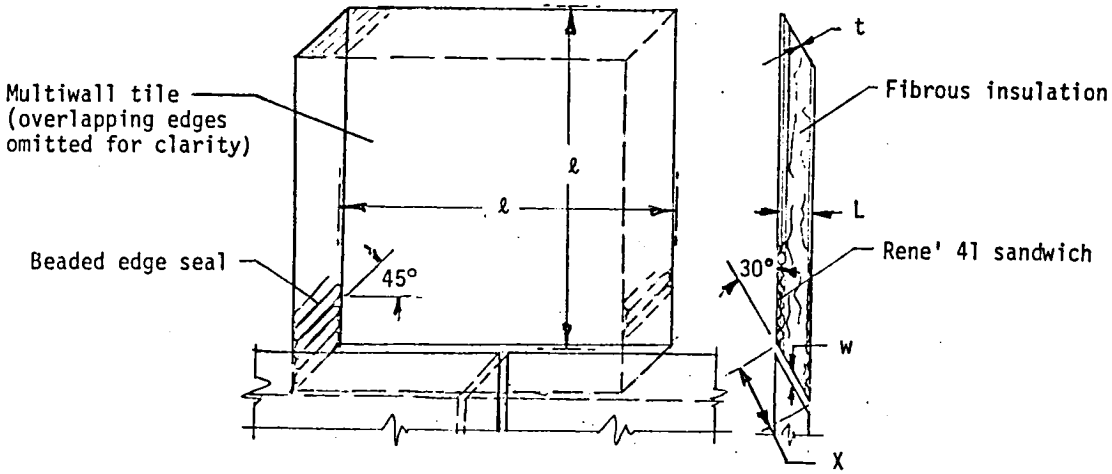

The fractional area of through metal, A_m, along the edge seals (fig. 5) is given by:

$$A_m = \frac{N\ell t}{\ell^2} = 0.0010 \qquad \text{(A2)},$$

wherein:

N (the number of edges seals per tile) = 4,

ℓ (the edge seal length) = 30.5 cm (12 in.),

t (the edge seal equivalent thickness) = 0.076 mm (0.003 in.).

The fractional area of air gaps, A_g, at body point 1700 is given by:

$$A_g = \frac{N\ell w}{\ell^2} = 0.0250 \qquad \text{(A3)},$$

wherein:

w (the average gap width) = 1.91 mm (0.075 in.).

This width is calculated as follows:

The radius of curvature of the hot face of the tile, R, (ref. 36) is given by:

$$R = \frac{L}{\alpha \Delta T} = 4.09 \text{ m (161 in.)},$$

where:

L (the tile thickness) = 5.18 cm (2.04 in.)

α (the coefficient of thermal expansion of Rene' 41 (ref. 37)) = 14.4μ cm/cmK (8.0×10^{-6} in./in. R), and

ΔT (the temperature difference between the hot and cold faces of the multiwall tile*) = 890 K (1600°F).

(*The Rene' 41 hot face sandwich is assumed to have the same temperature gradient through its thickness as the entire tile.)

The change in chord length of the tile hot face, Δc_h, is given by:

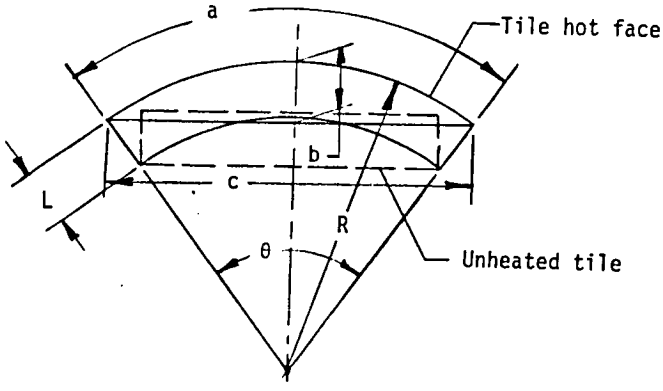

$\Delta c_h = c - \ell$ = 3.83 mm (0.151 in.)(which is the required fabricated gap width), where:

$$c = 2\,R \sin \frac{\theta}{2} = 30.483 \text{ cm } (12.001 \text{ in.})$$

$$\theta = \frac{a\ 180°}{\pi R} = 4.27°$$

$a = \Delta\ell + \ell$ = 30.493 cm (12.005 in.), and

the change in length, $\Delta\ell$, due to thermal expansion of the hot face of the tile is given by:

$\Delta\ell = \alpha\Delta T\ell = 3.94$ mm (0.155 in.)

where:

α (the coefficient of thermal expansion of Rene' 41 (taken from reference 37))= 14.4 μcm/cmK (8.0 x 10^{-6} in./in.°R),

ΔT (the difference between the peak heating hot face temperature and room temperature) = 1166 K (1639°F), (See figure 24 for the temperature distribution through the tile at peak heating.), and

ℓ (the tile length) =30.2 cm (11.85 in.).

The fabricated gap width is 3.9 mm (0.15 in.) as shown in figure 5b. At this fabricated gap width the hot face gap width is zero.

The change in cold face gap width, Δc_c, is given by:

$$\Delta c_c = c\left(\frac{R-L}{R}\right) - \ell = 0.0 \text{ cm } (0.0 \text{ in.}).$$

Thus, the cold face gap width is unchanged, or remains at 3.8 mm (0.15 in.), and the average gap width used in the calculations, w, through the tile thickness, $(\Delta c_h + \Delta c_c)/2$ is 1.90 mm (0.075 in.). Consequently, the insulation conductivity from equation (A1) is:

$$k_i\,[1-(A_m + A_g)] = 0.974\ k_i.$$

The above analysis also indicates that the tile bows, b, elasticially 2.97 mm (0.117 in.) at its center during peak heating.

Edge Seal Conductivity: The edge seal material is Rene' 41, and its thermal conductivity, k_m, is taken from reference 37; the ratio L/X = 1/2 since the edges are scarfed at 30°. Therefore, edge seal conductivity from equation (A1) is:

$$k_m A_m \frac{L}{X} = 0.005\ k_m.$$

Air Gap Conductivity: Thermal conductivity of the air in the gap, k_g, at atmospheric pressure is taken from reference 38.

Therefore, air gap conductivity from equation (A1) is:

$$k_g A_g \left(\frac{L}{X}\right)^2 = 0.00625\ k_g.$$

Gap Radiative Conductivity: To evaluate radiative conductivity in equation (A1) it is necessary to define the radiation heat transfer coefficient, H_r.

The usual equation used for H_r involving more than one surface (ref. 39) is:

$$H_r = \sigma F(T_h^2 + T_c^2)(T_h + T_c) \qquad (A4).$$

To simplify calculation of H_r, in terms of the average temperature of the hot, T_h, and cold, T_c, faces of an incremental thickness of the tile, a factor β is introduced. An incremental thickness is used for the transient heating analysis and to determine T_h and T_c values needed to evaluate β. This factor β is defined so that

$$4\beta\, T_{ave}^3 = (T_h^2 + T_c^2)(T_h + T_c),$$

where:

$$T_{ave} = \frac{(T_h + T_c)}{2},$$

then

$$\beta = \frac{(T_h^2 + T_c^2)(T_h + T_c)}{4\left(\frac{(T_h + T_c)}{2}\right)^3} = \frac{2(T_h^2 + T_c^2)}{(T_h + T_c)^2} = \frac{2\left(1 + \left(\frac{T_c}{T_h}\right)^2\right)}{\left(1 + \left(\frac{T_c}{T_h}\right)\right)^2},$$

and introduce

$$\frac{T_c}{T_h} = 1 - \left(\frac{T_h - T_c}{T_h}\right),$$

to yield

$$\beta = \frac{1 - \left(\frac{T_h - T_c}{T_h}\right) + 0.50 \left(\frac{T_h - T_c}{T_h}\right)^2}{1 - \left(\frac{T_h - T_c}{T_h}\right) + 0.25 \left(\frac{T_h - T_c}{T_h}\right)^2} \qquad \text{(A5)}.$$

Finally, using β the expression for H_r, equation (A4), becomes

$$H_r = 4\sigma F T_{ave}^{\ 3} \beta \qquad \text{(A6)},$$

where F in equation (A6)

$$F = \frac{1}{\frac{1}{f} + 2\left(\frac{1}{\varepsilon} - 1\right)} = 0.021,$$

$f = 0.022$ (ref. 38), f is a function of sin 45°w (L/X)/X = 0.0065, since radiation is parallel to the beads and the average emittance, ε is taken to be 0.5.

Equation (A5) is plotted in figure 25 as a function of $\left(\frac{T_h - T_c}{T_h}\right)$.

In the calculation of k_{ai}, for use in the transient heating analysis the incremental thickness was 8.6 mm (0.34 in.); and, during entry heating (for the average temperature incremental thickness) the time average hot face temperature, T_h, is 533 K (960°R) and the time average cold face temperature, T_c, is 436 K (785°R). Therefore, $\left(\frac{T_h - T_c}{T_h}\right) = 0.18$ and from figure 25, β =

1.02. The factor, β, may be evaluated for each incremental thickness, but the correction is so small that only the average temperature increment was used in this analysis.

Therefore; substituting given values into equation (A6) yields:

$$H_r = 0.0049 \left(\frac{T_{ave}}{1000}\right)^3 \left(\frac{kW}{m^2\text{-}K}\right), \quad \text{or} \quad 0.148 \left(\frac{T_{ave}}{1000}\right)^3 \left(\frac{Btu}{hr\text{-}ft^2\text{-}°R}\right),$$

and from equation (A1) the radiation conductivity is:

$$H_r A_g L \left(\frac{L}{X}\right) = 0.0032 \left(\frac{T_{ave}}{1000}\right)^3 \left(\frac{W}{m\text{-}K}\right), \quad \text{or} \quad \left(0.0003 \left(\frac{T_{ave}}{1000}\right)^3\right) \left(\frac{Btu\text{-}ft}{hr\text{-}ft^2\text{-}°R}\right),$$

where:

L (the tile thickness) = 0.052m (0.170 ft).

Evaluated Equation (A1): Therefore, substituting the values for the various forms of conductivity into equation (A1) yields:

$$k_{ai} = 0.974\, k_i + 0.00050\, k_m + 0.00625\, k_g + 0.0032 \left(\frac{T_{ave}}{1000}\right)^3 \left(\frac{W}{m\text{-}K}\right),$$

or

$$k_{ai} = 0.974\, k_i + 0.0005\, k_m + 0.00625\, k_g + 0.0003 \left(\frac{T_{ave}}{1000}\right)^3 \left(\frac{Btu\text{-}ft}{hr\text{-}ft^2\text{-}°R}\right).$$

Results, from these equations are given in figure 13 for various fibrous insulations. An examination of the results indicates that at low temperatures with Rene' 41 edge seals the apparent conductivity, k_{ai}, is essentially equal

to the conductivity of the fibrous insulation, k_i, and at high temperature k_{ai} = 1.10 k_i due to increased heat transfer in the gaps. Thus, the joint design is thermally efficient. Moreover, k_{ai} = 1.1 k_i is considered adequate for preliminary transient heating analysis and this value was used in this study. However, solutions to equation (1) with the columbium edge seals, which are thicker and have a higher conductivity than Rene' 41 edge seals (particularly at low temperatures), indicate that k_{ai} = 1.4 k_i for preliminary transient heating analyses. Possibly, the columbium edge seals should be chemically milled from 0.15 mm (0.006 in.) thick at the hot edge to 0.08 mm (0.003 in.) thick at the cold edge, rather than the constant 0.13 mm (0.005 in.) thickness shown in figure 7.

Metal Sandwich. - The equation for apparent thermal conductivity for the metal sandwiches in multiwall TPS was derived for reference 3 and modified herein and is given by:

$$k_{am} = 1.15 \left[\underbrace{k_m A_m \left(\frac{L}{1.1P}\right)}_{\text{through-metal conductivity}} + \underbrace{\frac{k_g(1-A_m)}{\left(1 - \frac{z}{L}\right)}}_{\text{gaseous conductivity}} + \underbrace{\frac{LH_r(1-A_m)}{(j-1)}}_{\text{radiative conductivity}} \right] \qquad \text{(A7)}$$

In the derivation of equation (A7), k_{am} is proportional to the conductivities of the through metal, enclosed air, and internal radiation. Analysis of the results of tests of a stainless steel sandwich (ref. 3) indicates that a proportionality constant of 1.15 will give a best fit curve when the view factor, f, is taken to be 0.7. Later tests, performed by Rohr Industries, Incorporated with a similar sandwich but in titanium alloy, gave results that agree with equation (A7) for the same view factor. Figure 14 shows the calculated curves and test results; excellent agreement is indicated.

The apparent thermal conductivity of Rene' 41 sandwich (fig. 5) is calculated as follows:

Through-Metal Conductivity: The source references for thermal conductivity of metal, k_m, used for multiwall TPS are reference 37 (titanium and superalloys) and reference 40 (columbium and tantalum). No source reference is known for conductivity of dispersion strengthened alloys.

Geometry symbols are given in the following figure:

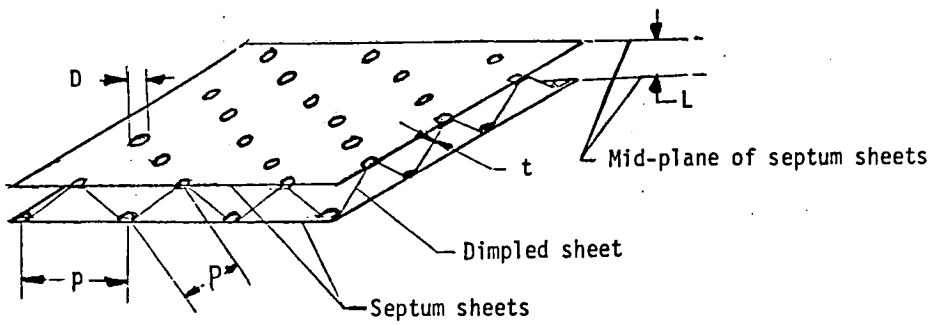

The fractional area of through-metal, A_m, is given by:

$$A_m = \frac{4ptn}{6} = 0.00424 \qquad \text{(A8)},$$

or

$$A_m = \pi Dtn = 0.001696 \text{ (Use the larger value for } A_m) \qquad \text{(A9)}.$$

Equation (A8) is used for dimple contact diameters, D, less than

$$D = \sqrt{\frac{8ptn}{3\pi}} \qquad \text{(A10)},$$

and equation (A9) is used for diameters equal to or greater than the value given by equation (A10).

Equation (A8) was derived by the method of curvilinear squares to approximate the through-metal fractional area for dimple crests that either have very small contact areas or no contact area; that is, it is not necessary

for a dimpled sheet to contact the septum sheets to have through-metal conduction. If no contact exists heat will transfer through the air by conduction and by radiation to the crest region, then conduct within the dimpled sheet from hot to cold crests. The following figure shows (for a contact diameter of D = 0) the curvilinear square approach to deriving equation (A8):

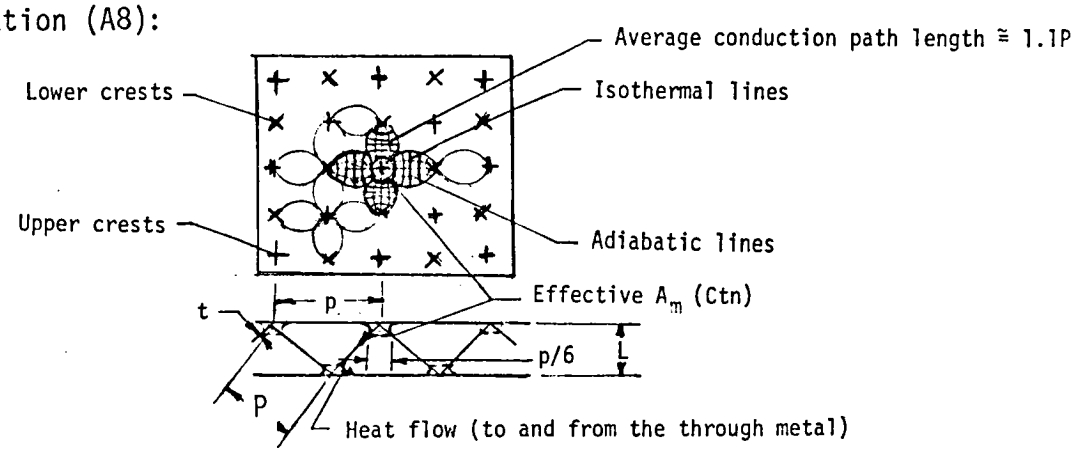

The effective dimple contact diameter is the largest diameter where heat flow is radial in the dimple sheet near the crest. The circumference, C, of the effective diameter,

$$C = \frac{4p}{6} \quad ,$$

was approximated by a square with sides equal to p/6.

The dimpled sheets are made from 0.08 mm (0.003 in.) thick foil. After forming their thickness is reduced to t = 0.06 mm (0.00225 in.). The diagonal pitch of the dimples, p, is 1.8 cm (0.707 in.), and the number of dimples per unit area, n, is 0.62/cm^2 (4/in.^{2}). The dimple contact diameter, D, is 0.15 cm (0.060 in.). The ratio L/P is 1/2 where P is measured along the diagonal pitch of the dimples; that is, along the conduction path between upper and lower dimple crests. Therefore, the through metal conductivity from Equation (A7) is:

$$k_m A_m \left(\frac{L}{1.1P}\right) = 0.00193\ k_m.$$

Gaseous Conductivity: The gaseous conductivity for incremental thickness L is the conductivity of air, k_g, at atmospheric pressure taken from reference 38, corrected for the presence of the metal in the thickness L, which is 4.33 mm (0.1705 in.). The dimpled sheet occupies (normal to the septum sheets) the fractional area of through metal, A_m, and the dimpled sheet plus half the thickness of the two septum sheets have a total thickness, z, (parallel to the septum sheets) of 0.11 mm (0.0045 in.). That is, not all of the thickness, L, is air. An incremental thickness of sandwich rather than the total thickness of the sandwich is used to calculate the apparent thermal conductivity to permit use of tile faces that are thicker than the septum sheets without affecting the calculation of the apparent conductivity of the sandwich.

Therefore, the gaseous conductivity from equation (A7) is:

$$\frac{k_g(1-A_m)}{(1 - \frac{z}{L})} = 1.023\ k_g.$$

Radiative Conductivity: The radiative heat transfer through the metal sandwich is calculated as an equivalent thermal conductivity. However, it is first necessary to evaluate the radiation heat transfer coefficient acting over thickness L.

The radiation heat transfer coefficient is:

$$H_r = 4\sigma F T_{ave}^{3} \beta = 0.0821 \left(\frac{T_{ave}}{1000}\right)^3 \left(\frac{kW}{m^2\text{-}K}\right), \text{ or } \left(2.48\left(\frac{T_{ave}}{1000}\right)^3\right) \left(\frac{Btu}{hr\text{-}ft^2\text{-}^\circ R}\right)$$

wherein:

$$F = \frac{1}{\frac{1}{f} + 2\left(\frac{1}{\varepsilon} - 1\right)} = 0.362.$$

The view factor, f, is 0.7, and the average emittance, ε, is taken to be 0.6. The average temperature of the hot and cold faces throughout the entry trajectory are: T_h = 758 K (1365°R) and T_c = 753 K (1355°R), respectively. Then, from figure 25, $\beta \cong 1.0$.

The dimpled sheet devides the thickness, L, into two equal radiation spaces; that is, the dimpled sheet provides a radiation barrier between two septum sheets. Thus the radiation coefficient must be devided by the number of spaces in thickness L or the total number of sheets minus one sheet, (j-1) = 2, in thickness L, which is 0.043 cm (0.0142 ft.).

Therefore, the radiative conductivity from equation (A7) is:

$$\frac{LH_r(1-A_m)}{(j-1)} = 0.186 \left(\frac{T_{ave}}{1000}\right)^3 \left(\frac{W}{m\text{-}K}\right), \text{ or } 0.0176\left(\frac{T_{ave}}{1000}\right)^3 \left(\frac{Btu\text{-}ft}{hr\text{-}ft^2\text{-}°R}\right).$$

Evaluated Equation (A7): Therefore, substituting the values for the various forms of conductivity into equation (A7) yields:

$$k_{am} = 1.15 \left[0.00193\, k_m + 1.023\, k_g + 0.186 \left(\frac{T_{ave}}{1000}\right)^3\right] \left(\frac{W}{m\text{-}K}\right),$$

or

$$k_{am} = 1.15 \left[0.00193\, k_m + 1.023\, k_g + 0.0176 \left(\frac{T_{ave}}{1000}\right)^3\right] \left(\frac{Btu\text{-}ft}{hr\text{-}ft^2\text{-}°R}\right).$$

Evaluations of k_{am} from this equation are given in figure 14.

Structural Analyses

Structural analyses of multiwall TPS include bending and tensile strengths of the outer sandwich, flutter resistance of the outer sandwich,

edge seal strength, and attachment strength. Properties of structural materials selected for multiwall TPS tiles are given in Table V.

Bending Strength. - Bending strength of the outer sandwich of figure 5 is calculated assuming that flat sheets can not support a compressive load. Compressive load is supported by the dimpled sheet and the tensile load is supported by the flat sheet that is in tension. For a single dimpled sheet sandwich, the moment of intertia per unit of width is:

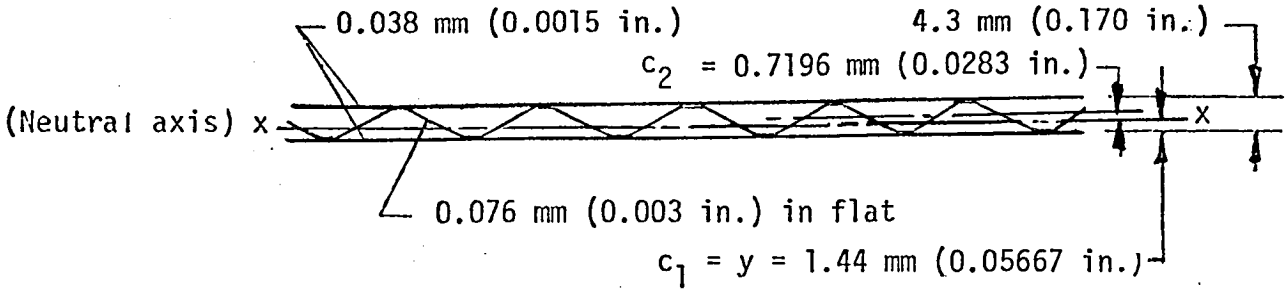

A	y	Ay
0.00762cm^2/cm(0.003in.^{2}/in.)	0.216cm(0.085in.)	0.00165cm^3/cm(0.000255in.^{3}/in.)
0.00380cm^2/cm)0.0015in.^{2}/in.)	0	0
Σ=0.0014cm^2/cm(0.0045in.^{2}/in.)	----------	0.00165cm^3/cm(0.000255in.^{3}/in.)

Ay^2	Io
0.000356cm^4/cm(0.000021675in.^{4}/in.)	------
0	------
Σ=0.000356cm^4/cm(0.000021675in.^{4}/in.)	------

where:

$$\bar{y} = \frac{\Sigma Ay}{\Sigma A} = 1.44 \text{ mm } (0.05667 \text{ in.}),$$

and

$$I_x = \Sigma Ay^2 - \Sigma A(\bar{y})^2 = 0.000119 \text{ cm}^4/\text{cm } (0.000007225 \text{ in.}^4/\text{in.}).$$

Experiments of dimpled sheet sandwich with foil faces indicate that the effective moment of inertia is somewhat greater than the calculated value, thus the calculated value is used.

The bending stress is given by:

$$\sigma = \frac{Mc}{I} .$$

For a unit width strip acting as a beam through the center of the sandwich,

$$M = \frac{p\ell^2}{8} = 80.1 \frac{\text{m-N}}{\text{m}} \quad (18 \frac{\text{in.-lb}}{\text{in}}).$$

(Based on an ultimate load of 6.89 kPa (1.0 psi) as discussed below.)

Shuttle wind tunnel pressure data (Ref. 32) during transonic ascent flight are available at 1.5 m (5 ft.) increments of length, and indicates that most of the lower surface has a local pressure difference of 10.3 kPa (1.5 psi) in a 1.5 m (5 ft.) length or an average pressure difference of 2.07 kPa (0.3 psi) in a 0.3 m (1 ft.) length. If one end of the tile is vented to either end of the pressure difference, the load is $\pm$2.07 kPa ($\pm$0.3 psi) acting on the outer face sandwich. Since shuttle data on 0.3 m (1 ft.) increments of length are not available, an ultimate pressure difference, p = $\pm$6.89 kPa ($\pm$1.0 psi), is selected as the design load.

The bending stress then is:

$$\sigma = \frac{Mc_2}{I} = 486 \text{ MPa } (70{,}500 \text{ lb/in.}^2) \text{ (Compression)},$$

and

$$\sigma = \frac{Mc_1}{I} = 972 \text{ MPa } (141{,}000 \text{ lb/in.}^2) \text{ (Tension)}.$$

These stresses for a single dimple layer Rene' 41 sandwich are not acceptable since the tensile stress exceeds the material ultimate tensile strength, so a double dimpled layer sandwich is used.

For a double dimple layer sandwich the moment of intertia per unit of width is:

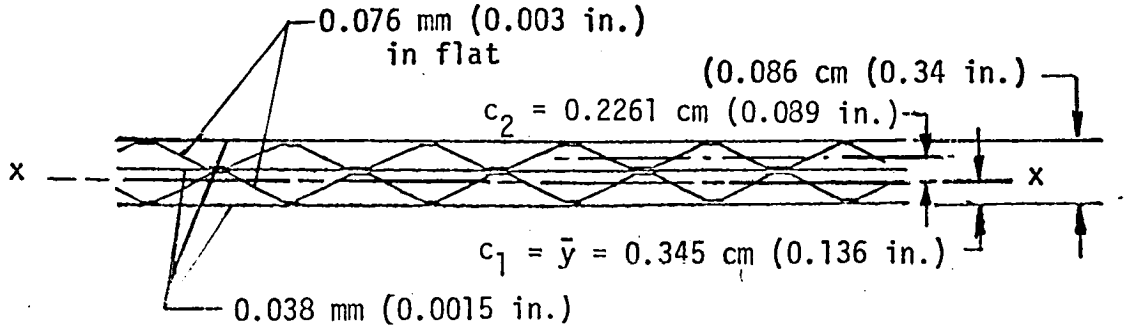

A	y	Ay
0.00762cm^2/cm(0.003in.^{2}/in.)	0.648cm(0.225in.)	0.004938cm^3/cm(0.000765in.^{3}/in.)
0.00762cm^2/cm(0.003in.^{2}/in.)	0.216cm(0.085in.)	0.001646cm^3/cm(0.000255in.^{3}/in.)
0.00381cm^2/cm(0.0015in.^{2}/in.)	0	0
Σ=0.01905cm^2/cm(0.0075in.^{2}/in.)	-----	0.00658cm^3/cm(0.00102in.^{3}/in.)

Ay^2	I_o
0.00320cm^4/cm(0.000195in.^{4}/in.)	------
0.00036cm^4/cm(0.000217in.^{4}/in.)	------
0	
Σ=0.00356cm^4/cm(0.0002168in.^{4}/in.)	------

wherein:

$$\bar{y} = \frac{\Sigma Ay}{\Sigma A} = 0.345 \text{ cm } (0.136 \text{ in.}),$$

and

$$I_x = \Sigma Ay^2 - \Sigma A(\bar{y})^2 = 0.00128 \text{ cm}^4/\text{cm } (0.0000781 \text{ in.}^4/\text{in.}).$$

Then:

$$\sigma = \frac{Mc_2}{I} = 141.3 \text{ MPa } (20{,}500 \text{ lb/in.}^2) \text{ (Compression)},$$

and

$$\sigma = \frac{Mc_1}{I} = 215.7 \text{ MPa } (31{,}300 \text{ lb/in.}^2) \text{ (Tension)}$$

This tensile stress is within the Rene' 41 allowable; however, tests are required to determine the compressive buckling strength of the dimpled sheet in a two dimple layer sandwich.

Inplane Tension. - The sandwich ultimate tensile strength, σ_{tu}, is based on an assumed ultimate tensile strength, σ_u, of 827.4 MPa (121,000 lb/in^2) for foil gage Rene' 41.

Therefore:

$$\sigma_{tu} = \frac{\rho_{mw}}{\rho_m} \sigma_u = 22 \text{ MPa } (3200 \text{ lb/in.}^2),$$

wherein:

ρ_{mw} (Density of Rene' 41 multiwall sandwich) = 216 kg/m^3 (13.5 lb/ft^3),

and

ρ_m (Density of Rene' 41) = 8.25 Mg/m^3 (515 lb/ft^3).

Flutter Analysis. - Flutter analysis for the outer Rene' 41 sandwich was performed using the method of reference 33. The geometry parameter, GP, is:

$$GP = \frac{a}{b} \sqrt{\frac{D_{12}}{D_1}}$$

$a = b = \ell$ (a, b, and ℓ are the tile edge lengths),

$D_{12} = \sqrt{D_1 D_2}$ (D_{12} is the shear stiffness parameter).

and

$D_1 = D_2$ (D_1 and D_2 are the bending stiffness parameters).

Therefore: $GP = 1$

The dynamic pressure at which flutter will exist is given as follows: Referring to reference 33, the FP at which flutter occurs is 4×10^{-3} for $GP = 1$, and for a single dimple layer sandwich the flutter q is:

$$q = \frac{D_1 \, f(M)}{FP \, \ell^3} = 166.1 \text{ kPa (3470 psf)},$$

where

$D_1 = EI/(1-\nu^2) = 25.2$ N-m^2/m (222.3 lb-in.^{2}/in.)

E (The modulus of elasticity of Rene' 41 (ref. 37))=192.5 GPa (28×10^6psi)

ν (Poisson's ratio of Rene' 41 (ref. 37)) = 0.3,

$f(M) = \sqrt{M^2 - 1} = 0.75$ (at Mach = 1.4),

and

$\ell = 30.5$ cm (1.0 ft.).

For the double dimple layer sandwich the flutter q is:

$$q = \frac{D_1 \, f(M)}{FP \, \ell^3} = 1.79 \text{ MPa (37,500 psf)},$$

where $D_1 = EI/(1-\nu^2) = 272.4$ N-m^2/m (2403 lb-in^2/in.).

Each of the above flutter dynamic pressures greatly exceed the shuttle dynamic pressure during transonic flight of 33.5 kPa (700 psf). However, the above analysis is based on the assumption that the Rene' 41 sandwich is inplane isotropic. Bending tests (with various orientations of the dimple pattern) of sandwich panels are required to verify this assumption.

Edge Seal Strength. - The edge seals support the outer sandwich panel; and the edge seals are beaded to provide effective columns.

The force acting on the panel face due to the 6.89 kPa (1.0 psi) pressure load is:

$$F = p\ell^2 = 641 \text{ N } (144 \text{ lb }).$$

F expressed in terms of unit length of edge support, F_p, is:

$$F_p = \frac{F}{4\ell} = 0.339 \text{ N/m } (3 \text{ lb/in.}).$$

This force may be represented by a compressive force, F_c, acting axially along the beads in the edge seals, and by shear forces, F_s. The following figure shows this system of forces:

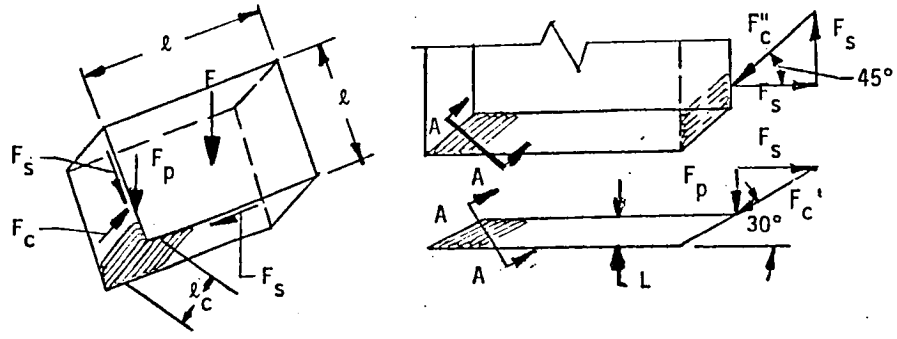

A vector diagram of the system of forces, F_p, F_s, and F_c is given as follows wherein the primed components of F_c, shown above, are included.

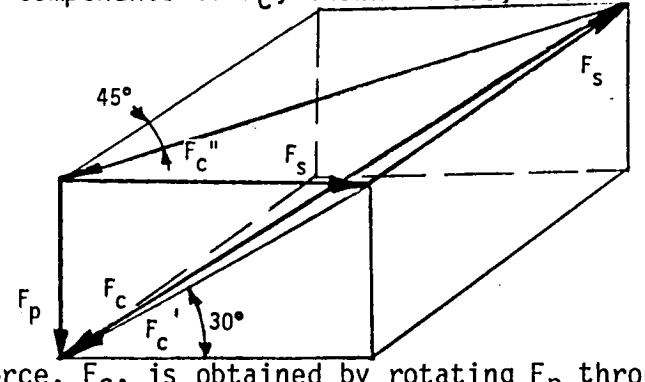

The compressive force, F_c, is obtained by rotating F_p through the 30° scarf angle and the 45° bead angle, thus

$$F_c = \frac{F_p}{\sin 30^\circ \sin 45^\circ} = 0.958 \text{ N/m } (8.48 \text{ lb/in.}),$$

and the shear force, F_s, is:

$$F_s = \frac{F_p}{\tan 30^\circ} = 0.585 \text{ N/m } (5.2 \text{ lb/in.}),$$

and since shear is reacted only by edge seals that are parallel to the shear force, a factor of 2 is required to yield the total shear, F_{st}, per unit length of edge seal:

$$F_{st} = 2 F_s = 1.17 \text{ N/m } (10.39 \text{ lb/in.}).$$

The compressive stress, σ_c, in the edge seal perpendicular to the beads is:

$$\sigma_c = \frac{F_c}{\bar{t}} = 19.3 \text{ MPa } (2800 \text{ lb/in.}^2).$$

where

$\bar{t}$ (the equivalent thickness or unit area of the edge seal) = 0.00762 cm^2/cm (0.003 $\text{in.}^2/\text{in.}$).

The shear stress, σ_s, in the edge seal is:

$$\sigma_s = \frac{F_{st}}{\bar{t}} = 24.1 \text{ MPa } (3500 \text{ lb/in.}^2).$$

The buckling strength, σ_{cr}, of the beads is given by:

$$\sigma_{cr} = \frac{\pi^2 E}{\left(\frac{\ell_c}{\rho}\right)^2} = 2.86 \text{ MPa } (41{,}500 \text{ lb/in.}^2),$$

where:

$$\ell_c = \frac{L}{\sin 30^\circ \sin 45^\circ} = 14.7 \text{ cm } (5.77 \text{ in.}),$$

and

$$L = 5.18 \text{ cm } (2.04 \text{ in.}).$$

The radius of gyration, ρ, is:

$$\rho = \sqrt{\frac{I}{A}} = 1.796 \text{ mm } (0.0707 \text{ in.}),$$

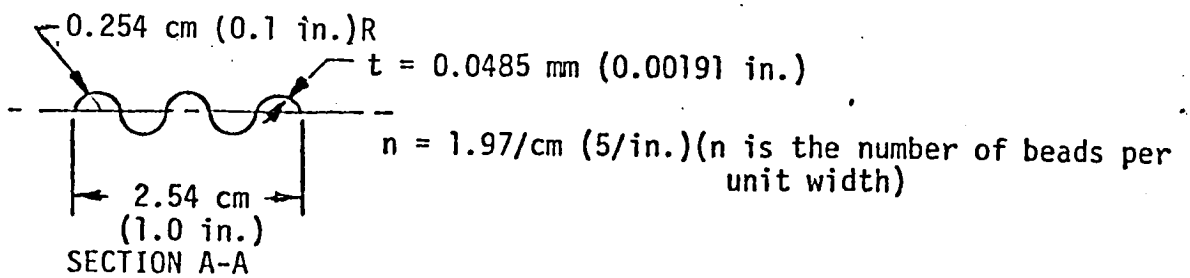

where:

$$I = \pi R^3 t \ (n/2) = 0.000246 \text{ cm}^4/\text{cm } (1.5 \times 10^{-5} \text{ in.}^4/\text{in.}),$$

and

$$A = \bar{t} = 0.00762 \text{ cm}^2/\text{cm } (0.003 \text{ in.}^2/\text{in.}).$$

The effect of interaction between shear and compression should be negligible, because the shear stress, σ_s is relatively low compared with the buckling strength, σ_{cr}. Therefore, the edge seals should support the compressive load since the buckling strength, σ_{cr}, is much greater than the applied compressive stress σ_c.

Attachment Strength. - The pressure difference load is supported at the four corners of the tile by attachments to the structure. Analyses of the attachments are given as follows:

The tabs and the tile clips with doublers are diffusion bonded to the inner titanium sandwich, but the dimple contact areas in this sandwich have a through-the-thickness tensile strength (determined by tests) of about 137 kPa (20 lb/in.^{2}) based on sandwich face area. The tab and tile clip doubler areas, A, are about 38.7 cm^2 (6 in.^{2}) each, and there are two tabs and two tile clip doublers per tile.

Thus, the tensile stress, σ_t, in the sandwich is:

$$\sigma_t = \frac{F}{4A} = 41.4 \text{ kPa } (6 \text{ lb/in.}^2).$$

Therefore, the attachment load will not fail the dimpled sandwich. Actually, much of the load will be transferred through the edge seals--not through the inner sandwich.

The tabs extend under a structural clip riveted to the structure as shown below:

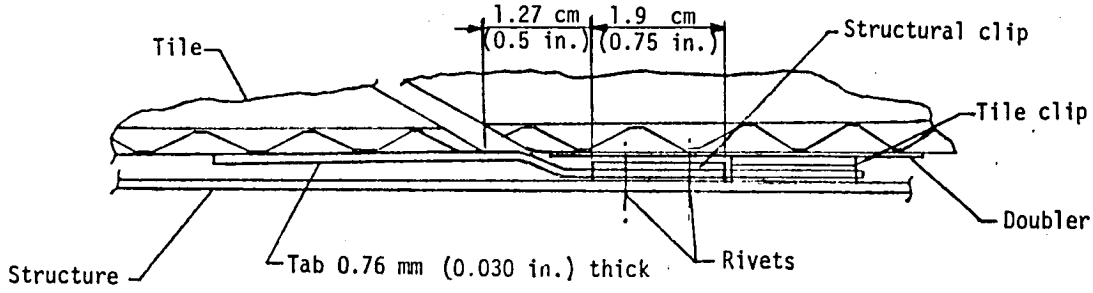

Since the tab is effectively clamped on both ends by the tile and clips, bending of the tab is analyzed as a cantilever beam of length = 6.35 mm (0.25 in.), and the load is F/4. The following figure shows the effective length of the cantilever tab between the tile and structural clip.

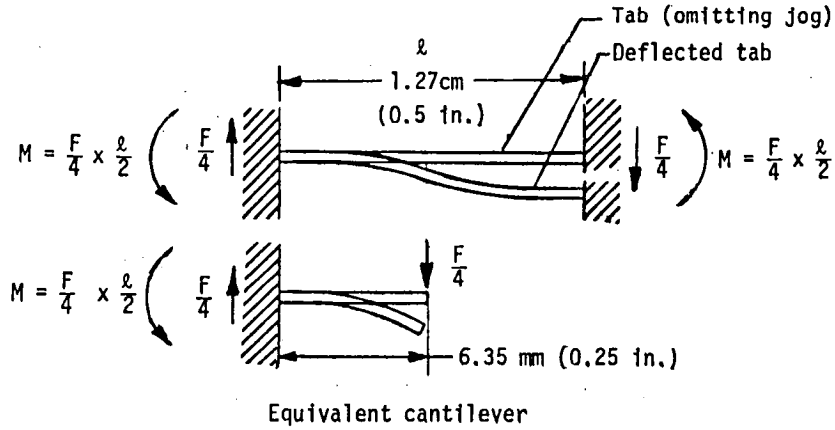

Equivalent cantilever

The bending stress is:

$$\sigma = \frac{Mc}{I} = 276 \text{ MPa } (40{,}000 \text{ lb/in.}^2).$$

This stress is well within the allowables of the titanium alloy selected for the tab. Considering the low magnitude of the load transmitted by the tile through the clips and rivets, stresses in the clips and rivets are negligible.

The structural analyses given in this appendix indicate that the tile design shown in figure 5 is capable of supporting the 6.9 kPa (1.0 psi) ultimate design load. Actually, were the panel optimized for the load, mass could be saved. That is, the tile is overdesigned and the next section discusses the ultimate pressure load that would cause tile failure.

Multiwall Tile Ultimate Strength

The following analyses determine the maximum pressure load, p_m, that can be supported by the tile shown in figure 5.

Sandwich Bending Strength. - A major unknown is the compressive strength of the dimpled sheet in a sandwich. For the purpose of this analysis it is assumed that the dimpled layer in the outer Rene' 41 sandwich can support a compressive stress equal to half the yield strength. Assuming the yield strength is 689 MPa (100,000 lb/in.^{2}) for solution-treated-and-aged foil, then the maximum moment carrying capability, M_m, for a double dimpled layer is given by:

$$M_m = \frac{\sigma I}{c_2} = 230 \frac{m\text{-}N}{m} \text{ (51.8 in.-lb/in.)},$$

and the maximum pressure load is:

$$p_m = \frac{M_m}{M} \times p = 19.7 \text{ kPa } (2.85 \text{ psi}) \text{ ultimate.}$$

Edge Seal Strength. - As the column load in the beads of the edge seal is increased, the shear load also increases, thus the interaction of shear and compression will become significant. Assuming that the interaction reduces the buckling strength to $\sigma_{cr}/2$, the pressure that can be supported by the edge seals is determined as follows:

$$\sigma_c = \frac{\sigma_{cr}}{2} = 143 \text{ MPa } (20{,}750 \text{ lb/in.}^2),$$

$$F_p = F_c \sin 30° \sin 45° = \sigma_c \bar{t} \sin 30° \sin 45° = 2.49 \text{ n/m } (22 \text{ lb/in.}),$$

$$F = 4\ell F_p = 4.71 \text{ kN } (1060 \text{ lb.}),$$

therefore

$$p_m = \frac{F}{\ell^2} = 51 \text{ kPa } (7.4 \text{ psi}).$$

Attachment Strength. - The load the tab can support in bending is given as follows for a titanium alloy with a yield strength of 827 MPa (120,000 lb/in.^{2}):

$$p_m = \frac{\sigma_y}{\sigma} \times p = 20.7 \text{ kPa } (3 \text{ psi}).$$

Therefore, the above analyses indicate that the tile, as designed, can support an ultimate pressure load of 19.7 kPa (2.85 psi), which is more than twice the design ultimate pressure, and the edge seals and attachments can support greater loads.

REFERENCES

1. Strouhal, George; and Tillian, Donald J.: Testing the Shuttle Heat-Protection Armor. Astronautics & Aeronautics, January 1976, pp. 57-65.

2. Bohon, Herman L.; Shideler, John L; and Rummler, Donald R.: Radiative Metallic Thermal Protection Systems: A Status Report. Journal of Spacecraft and Rockets, Vol. 14, No. 10, pp. 626-631, October 1977.

3. Jackson, L. Robert; Davis, John G.; and Wichorek, Gregory R.: Structural Concepts for Hydrogen Fueled Hypersonic Airplanes. NASA TN D-3162, 1966.

4. Hirsch, Richard A.: Development of Techniques and Fabrication of a Structural Model for Research of Strucutres for Hypersonic Aircraft. NASA CR-66211, 1966.

5. Jackson, L. Robert: Multiwall TPS. Recent Advances in Structures for Hypersonic Flight. NASA CP-2065, pp. 671-706, September 1978.

6. Ransone, Philip O.; and Morrison, J. D.: The Effects of Environmental Exposure on Reusable Surface Insulations for Space Shuttle. NASA TM X-3252, October 1975.

7. Ransone, Philip O.; Morrison, J. D.; and Minster, John E.: Environmental Effects on Space Shuttle Reusable Surface Insulation Coated with Reaction Cured Glass. NASA TM 80071, August 1979.

8. Ransone, Philip O.; Morrison, J. D; and Minster, John E.: Effect of 25 Cycles of Launch Pad Exposure and Simulated Mission Heating on Space Shuttle Reusable Surface Insulation Coated with Reaction Cured Glass. NASA TM 80160, September 1979.

9. Greenshields, David H.: Orbiter Thermal Protection System Development. Proceedings of Fourteenth Space Congress, Space Technology for Better Living, Cocoa Beach, Florida, April 27-29, 1977.

10. Deveikis, W. D.; Miserentino, R.; Weinstein, I.; and Shideler, J. L.: Aerothermal Performance and Structural Integrity of a Rene'41 Thermal Protection System in a Mach 6.6 Stream. NASA TN D-7943, 1975.

11. Sawyer, J. W.: Aerothermal and Structural Performance of a Cobalt-Base Superalloy Thermal Protection System at Mach 6.6. NASA TN D-8415, 1977.

12. Eidenoff, H. L.; and Rose, L.: Thermal-Structural Evaluation of TD-Ni2O-Cr Thermal Protection System Panels. NASA CR-132487, 1974.

13. Johnson, R., Jr.; and Kilpatrick, D. H.: Evaluation of Dispersion Strengthened Nickel Based Alloy Heat Shields for Space Shuttle Application. NASA CR-2614, March 1976.

14. Black, W. E.: Summary Report of Evaluation of Coated Columbium Alloy Heat Shields for Space Shuttle Thermal Protection System Applications. NASA CR-2824, April 1977.

15. Rummler, D. R.; and Black, W. E.: Evaluation of Coated Columbium for Thermal Protection Systems Application. AIAA Paper No. 75-187, Denver, Colorado, April 1975.

16. Stein, Bland A.; Bohon, Herman L.; and Rummler, Donald R.: An Assessment of Radiative Metallic Thermal Protection Systems for Space Shuttle. NASA TM X-2570, 1972.

17. Klarstrom, D. L.: Thermomechanical Processing of HAYNES Alloy No. 188 Sheet to Improve Creep Strength. NASA CR-3013, August 1978.

18. Davis, J. W.; and Cramer, B. A.: Prediction and Verification of Creep Behavior in Metallic Materials and Components for the Space Shuttle Thermal Protection System. NASA CR-2685, July 1976.

19. Sawyer, J. W.: Pressure and Heating-Rate Distributions on a Corrugated Surface in a Supersonic Turbulent Boundary Layer. NASA TP-1024, 1977.

20. Brandon, H. J.; Britt, A. H.; and Dunavant, J. C.: Aerothermodynamic Assessment of Corrugated Panel Thermal Protection Systems. AIAA Paper No. 78-841, Palo Alto, California, May 1978.

21. Brandon, H. J.; Britt, A. H.; Kipp, H. W.; and Masek, R. V.: Aerothermodynamic Assessment of Corrugated Panel Thermal Protection Systems. NASA CR-145317, 1978.

22. Varisco, A.; Bell, P.; and Walter, W.: Design and Fabrication of Metallic Thermal Protection Systems for Aerospace Vehicles. NASA CR-145313, February 1979.

23. Baer, J. W.; and Black, W. E.: Evaluation of Coated Columbium Alloy Heat Shields for Space Shuttle Thermal Protection System Application. Vol. III, NASA CR-112119-3, March 1974.

24. Ratay, R. T.; and Fischer, W. E.: Development of a Reusable Metallic Thermal Protection System for Lifting Reentry Vehicles. Grumman Aerospace Corporation Report No. ADR 02-04-7011, April 1970.

25. Shyprykevich, P.: Experimental Investigation of Orthotropic Panel Flutter of Arbitrary Yaw Angles, and Comparison with Theory. NASA CR-2265, 1973.

26. Rucker, Carl E.; Randle, Robert E.: Testing of Space Shuttle Thermal Protection System Panels Under Simulated Reentry Thermal Acoustic Conditions. AIAA/NASA/ASTM/IES Seventh Space Simulation Conference, Los Angeles, California, November 12-14, 1973.

27. Hunt, J. L.; Lawing, P. L.; Marcum, D. C.; and Cubbage, J. M.: Conceptual Design of Hypersonic Airbreathing Missiles. AIAA Paper No. 78-6, Huntsville, Alabama, January 1978.

28. Taylor, A. H.; and Jackson, L. R.: Thermostructural Analysis of Three Structural Concepts for Reusable Space Vehicles. AIAA Paper No. 79-0874, May 1979.

29. Taylor, A. H.; and Jackson, L. R.: Thermostructural Analysis of Structural Concepts for Hypersonic Cruise Vehicles. AIAA Paper No. 80-0407, Pasadena, California, January 1980.

30. Wilhelm, K. A.; et al: Hypersonic Cruise Vehicle Wing Structure Evaluation. Volume I, NASA CR-66897-1, February 1970.

31. Blair, W.: Design and Fabrication of Titanium Multiwall Thermal Protection System (TPS) Test Panels. NASA CR-159241, 1980.

32. Chee, E.: Results of a Pressure Loads Investigation on a 3% Scale Model (47-OTS) of the Integrated Space Shuttle Vehicle Configuration 5 in the NASA Ames Research Center 11 x 11 Foot Leg of the Unitary Plan Wind Tunnel (IA81A), Vol. 2 of 7, NASA CR-141837, November 1975.

33. Laurenson, R. M.; and McPherson, J. I.: Design Procedures for Flutter-Free Surface Panels. NASA CR-2801, March 1977,

34. Garrett, L. B.; and Pitts, J. I.: A General Transient Heat Transfer Computer Program for Thermally Thick Walls. NASA TM X-2058, 1970.

35. Black, W. E.: Lightweight Radiative Heat Shield Development. General Dynamics, Convair Division Report No. GDC-ERR-AN-1133, December 1967.

36. Roark, R. J.: Formulas for Stress and Strain. McGraw-Hill Book Company, 1954.

37. U. S. Department of Defense: Metallic Materials and Elements for Aerospace Vehicle Structures. Mil-HDBK-5A, 1966.

38. McAdams, William H.: Heat Transmission. McGraw-Hill Book Company, Inc., 1954.

39. Jakob, Max: Elements of Heat Transfer and Insulation. John Wiley and Sons, Inc., 1952.

40. U. S. Department of Defense: Aerospace Structural Metals Handbook, December 1978.

41. Wittenburger, J. Daniel: Tensile and Creep Properties of the Experimental Oxide Dispersion Strengthened Iron-Base Sheet Alloy MA-956E at 1365K. Metallurgical Transactions, January 1978, pp. 101-110.

- Thermal protection (limit temperature of structure)
  - Resistant to hot gas ingress
  - Smooth surface (avoid local heating and laminar turbulent transition)
- Low mass
  - Load bearing
  - Resistant to flutter
  - Compatible with strains and skin buckling of structure
  - Resistant to water retention
- Short turnaround time
  - Easily inspected
  - Installation and removal ease (prefabricated)
  - Easily maintained
- Low life cycle cost
  - Readily fabricated
  - Durability
  - Reusable, long life

Table I.- TPS design goals.

Adequate and uniform thickness of coating
Large edge and corner radii
No faying surfaces
No sliding on coated surfaces
All surfaces visible after coating
No coated rivets or threaded fasteners
No contact with incompatible materials

Table II.- Factors for coated refractory metal design that promote longevity.

Body point / Time, sec	Heating rate, kW/m^2				
	3554	3140	3154	1700	1300
0	0.12246	0.39801	0.76470	2.30441	3.56177
50	0.19588	0.63747	1.22547	3.70159	5.70843
100	0.33695	1.09756	2.11091	6.38994	9.85445
150	0.61171	1.99243	3.83381	11.63806	17.94799
200	1.16236	3.78466	7.28549	22.17016	34.19022
250	2.20874	7.18426	13.72219	42.13555	64.98052
300	3.71555	12.06751	23.24695	70.61881	108.90671
350	4.71256	15.28268	29.44362	88.73261	136.84136
400	4.99356	16.55910	31.21077	97.53739	150.32624
450	5.03589	17.13699	32.32923	100.58573	155.00861
500	5.05621	17.89647	32.38585	99.89163	153.93035
550	5.02704	18.41523	32.14264	98.14104	151.22463
600	5.03113	19.21147	32.07125	96.72787	149.04176
650	5.45229	20.16978	32.21504	90.12218	138.98212
700	6.16217	20.02610	32.47755	82.34891	127.14682
750	6.69455	18.13321	31.07072	71.43742	110.44767
800	7.18301	14.33719	29.48379	61.16317	94.69685
850	7.27130	12.62281	27.80902	54.97308	85.16346
900	7.10629	12.17975	26.01123	50.73003	78.59398
950	6.80940	11.38418	24.40035	43.12620	70.36380
1000	6.56835	10.32759	21.66013	40.48971	62.74703
1050	6.11268	9.43738	19.18399	35.23456	56.74500
1100	5.33403	8.39202	16.56954	35.99789	51.07050
1150	4.93500	7.11060	13.82512	88.08345	45.39600
1200	3.97215	5.92554	10.98935	112.22277	30.31579
1250	3.41298	3.95365	8.31643	85.31724	22.72036
1300	3.09601	2.59085	5.97264	67.43655	32.90892
1350	4.02867	1.28834	4.29980	50.16258	51.06517
1400	6.17998	0.79443	3.40243	43.96001	48.90046
1450	5.43197	0.53193	6.40027	27.55356	30.70767
1500	3.79261	0.31618	4.00064	18.50965	20.64882
1550	1.95135	0.15151	7.38661	10.25473	11.45636
1600	0.58992	0.04574	3.59718	3.79738	4.25054
1650	0.06083	0.00477	0.63986	0.61489	0.68922
1700	-0.05391	0.00454	0.00000	0.00000	0.00000
Structure thickness, cm **	0.386	0.386	0.536	0.442	0.394

*Based on a surface temperature of 273 K.
**Initial temperature of structure is 311 K,
Structure thickness includes skin and stringers.

Table III.- Data used to analyze transient heating for space shuttle body points (SI units).

Body point / Time, sec	Heating rate, Btu/sec.-ft.^{2}*				
	3554	3140	3154	1700	1300
0	0.01079	0.03507	0.06738	0.20350	0.31384
50	0.01726	0.05617	0.10798	0.32616	0.50299
100	0.02969	0.09671	0.18600	0.56304	0.86831
150	0.05390	0.17556	0.33781	1.02547	1.58146
200	0.10242	0.33348	0.64195	1.95349	3.01262
250	0.19462	0.63303	1.21911	3.71271	5.72566
300	0.32739	1.06331	2.04837	6.22247	9.59615
350	0.41524	1.34661	2.59438	7.81854	12.05757
400	0.44000	1.45908	2.75009	8.59436	13.24577
450	0.44373	1.51000	2.84865	8.86296	13.65835
500	0.44552	1.57692	2.85363	8.80180	13.56334
550	0.44295	1.62263	2.83220	8.64755	13.32493
600	0.44331	1.69279	2.82591	8.52303	13.13259
650	0.48042	1.77723	2.83858	7.94098	12.24620
700	0.54297	1.76457	2.86171	7.25605	11.20335
750	0.58988	1.59778	2.73775	6.29460	9.73193
800	0.63292	1.26330	2.59792	5.38930	8.34407
850	0.64070	1.11224	2.45035	4.84387	7.50405
900	0.62616	1.07320	2.29194	4.47000	6.92519
950	0.60000	1.00310	2.15000	3.80000	6.20000
1000	0.57876	0.91000	1.90855	3.56769	5.52886
1050	0.53861	0.83156	1.69014	3.10464	5.00000
1100	0.47000	0.73945	1.46000	3.17190	4.50000
1150	0.43484	0.62654	1.21818	7.76134	4.00000
1200	0.35000	0.52212	0.96831	9.88834	2.67123
1250	0.30073	0.34837	0.73279	7.51760	2.00197
1300	0.27280	0.22829	0.52627	5.94207	2.89972
1350	0.35498	0.11352	0.37887	4.42000	4.49953
1400	0.54454	0.07000	0.29980	3.87347	4.30879
1450	0.47863	0.04687	0.56395	2.42784	2.70576
1500	0.33418	0.02786	0.35251	1.63095	1.81944
1550	0.17194	0.01335	0.65086	0.90358	1.00946
1600	0.05198	0.00403	0.31696	0.33460	0.37453
1650	0.00536	0.00042	0.05638	0.05418	0.06073
1700	-0.00475	0.00040	0.00000	0.00000	0.00000
Structure thickness, in.**	0.152	0.152	0.211	0.174	0.155

*Based on a surface temperature of 0^{o}F.
**Initial temperature of structure is 100^{o}F, and
Structure thickness includes skin and stringers.

Table III.- Data used to analyze transient heating for space shuttle body points (U.S.Customary units).

Body point number	Location on shuttle	Peak temperature, K (°F)	RSI mass,* kg/m^2 (lb/ft^2)	Multiwall mass, kg/m^2 (lb/ft^2)
3554	Upper side over wing	632 (677)	2.68 (0.55)	2.29 (0.47)
3140	Top center near nose	806 (990)	2.98 (0.61)	4.20 (0.86)
3154	Upper side near nose	903 (1166)	5.08 (1.04)	5.91 (1.21)
1700	Lower Center under wing	1178 (1660)	5.76 (1.18)	8.10 (1.66)
1300	Lower center near nose	1311 (1900)	7.76 (1.59)	10.25 (2.10)

* Based on only 144 kg/m^3 (9 lb/ft^3) density RSI

Table IV. - Comparative masses for RSI and multiwall TPS point designs.

Property[1] \ Metal	Ti-6Al-4V (Ref. 37)	Ti-6Al-2Sn 4Zr-2Mo (Ref. 40)	Inconel 718 (Ref. 40)	Rene '41 (Ref. 37)	HS 188 (Ref. 40)	ODS[2] MA-956E (Ref.41)	Cb 752 (Ref. 40)	Ta-10W (Ref. 40)
Tensile ultimate, Pa	924	1138	1069	1172	917	552	445	612
Tensile yield, Pa	869	1055	848	896	490	517	517	519
Modulus, G Pa	110	110	193	218	228	193	94	174
Poisson's ratio	0.323	0.325	0.30	0.306	0.3	0.3[4]	0.3	0.3
[3]Expansion, μcm/cmK	9.9	9.9	18.0	14.4	17.1	19.8[4]	8.1	7.2
Density, kg/m^3	2.56	2.63	4.76	4.77	5.29	4.64[4]	5.22	9.72

1. Properties for sheet material, foil properties are assumed to be 80 percent of sheet values.
2. ODS (Oxide dispersion strengthened).
3. Values for hot use temperature.
4. Estimated based on material chemistry.

Table V.- Room temperature properties of structural materials selected for design of multiwall TPS (SI units).

Property[1] \ Metal	Ti-6Al-4V (Ref. 37)	Ti-6Al-2Sn 4Zr-2Mo (Ref. 40)	Inconel 718 (Ref. 40)	Rene '41 (Ref. 37)	HS 188 (Ref. 40)	ODS[2] MA-956E (Ref. 41)	Cb 752 (Ref. 40)	Ta-10W (Ref. 40)
Tensile ultimate, ksi	134	165	155	170	133	80	64.5	88.7
Tensile yield, ksi	126	153	123	130	71	75	54.2	75.2
Modulus, 10^6 psi	16.0	16.0	28.0	31.6	33.0	28	13.6	25.3
Poisson's ratio	0.323	0.325	0.30	0.306	0.3	0.3[4]	0.3	0.3
[3]Expansion, 10^{-6} in./in.-°R	5.50	5.50	10.0	8.0	9.5	11.0[4]	4.5	4.0
Density, lb/in.^{3}	0.160	0.164	0.297	2.298	0.330	0.29[4]	0.326	0.607

1. Properties for sheet material, foil properties are assumed to be 80 percent of sheet values.
2. ODS (Oxide dispersion strengthened).
3. Values for hot use temperature.
4. Estimated based on material chemistry.

Table V.- Room temperature properties of structural metals selected for design of multiwall TPS (U.S. Customary units).

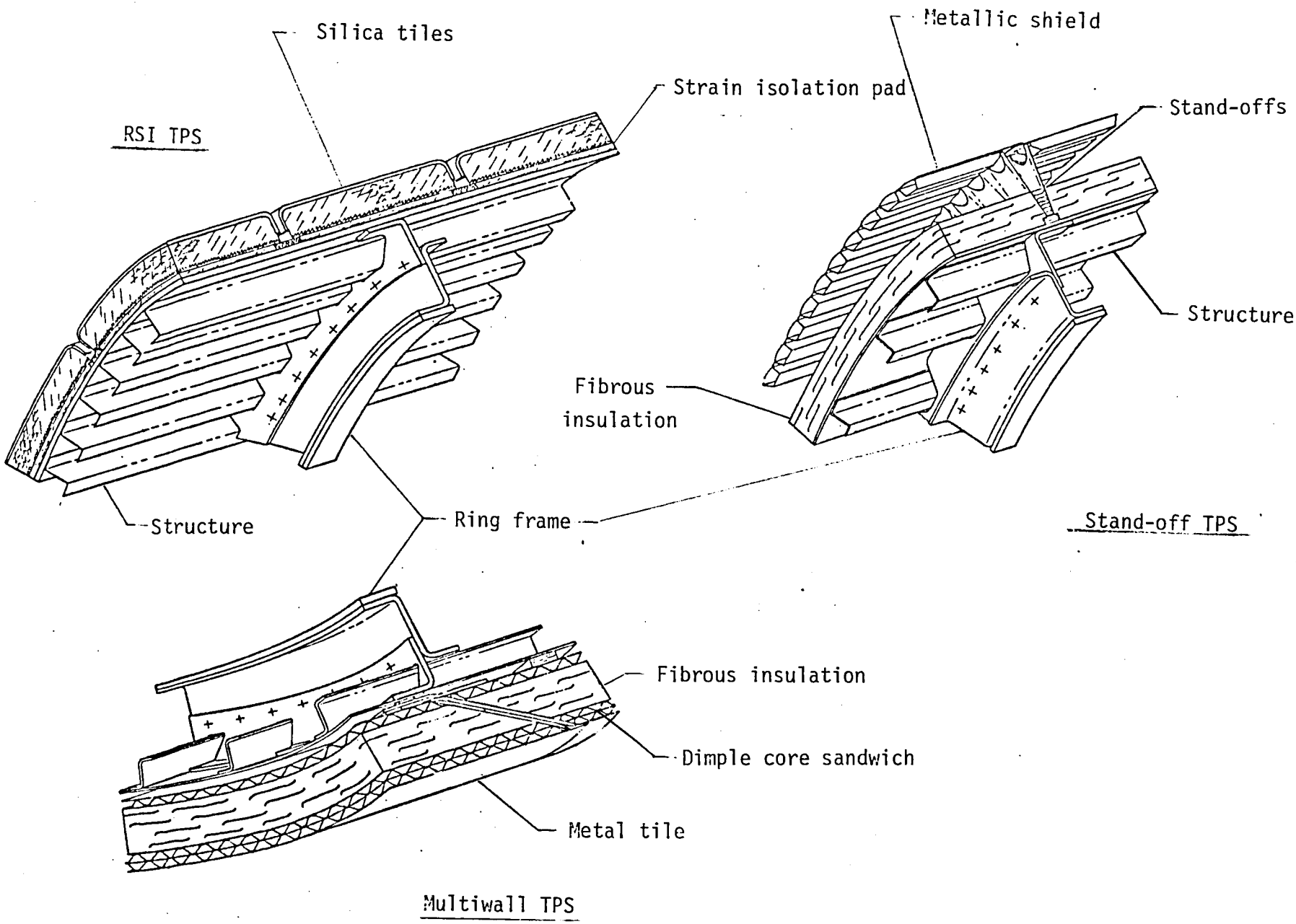

Figure 1.- Reusable surface insulation (RSI) TPS, metallic stand-off TPS and Multiwall TPS.

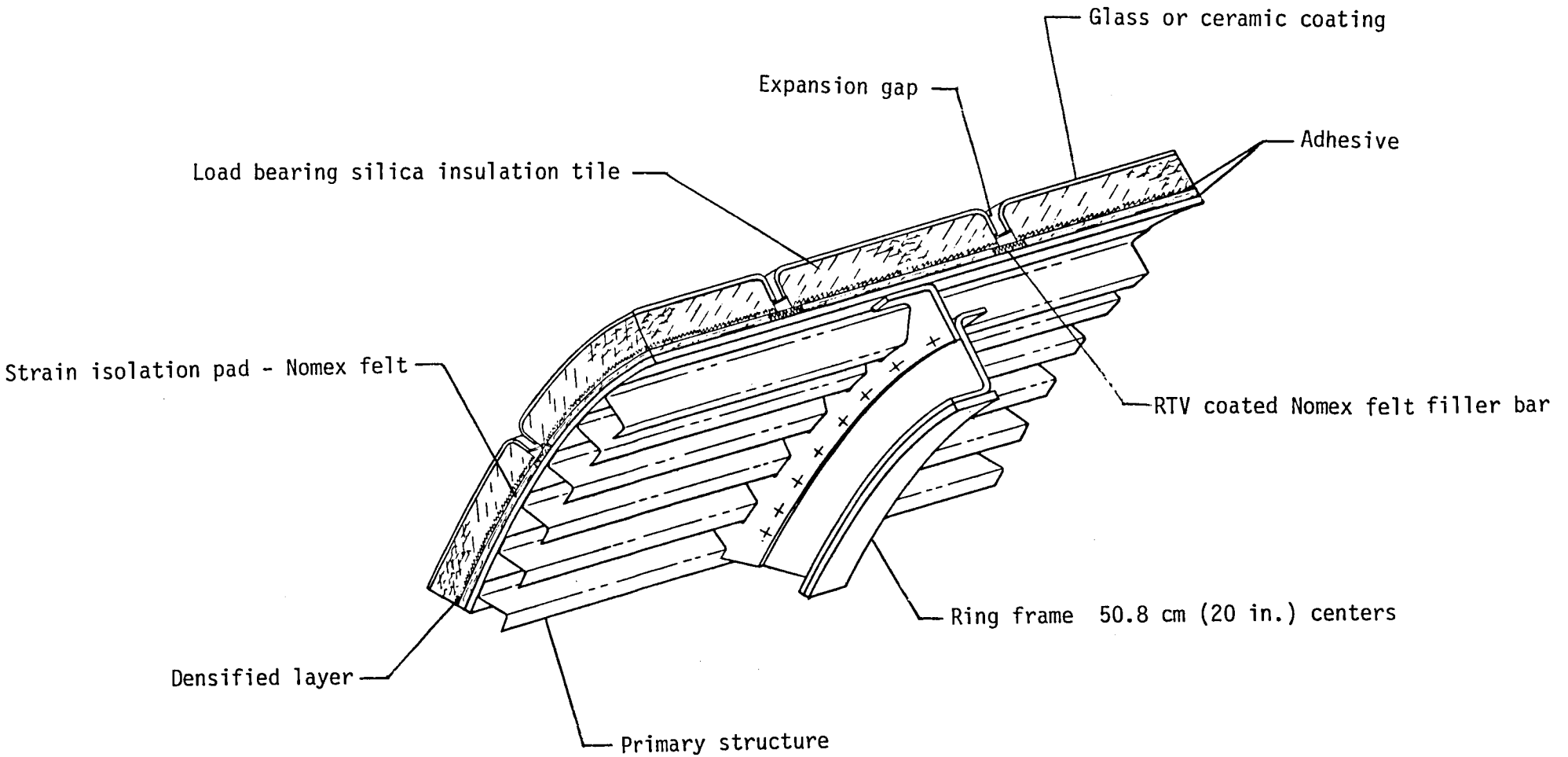

Figure 2.- Reusable Surface Insulation (RSI) thermal protection system. Typical sizes are 15 cm (6 in.) square for HRSI and 5.08 to 20.4 cm (2 in.) to (8 in.) square for LRSI.

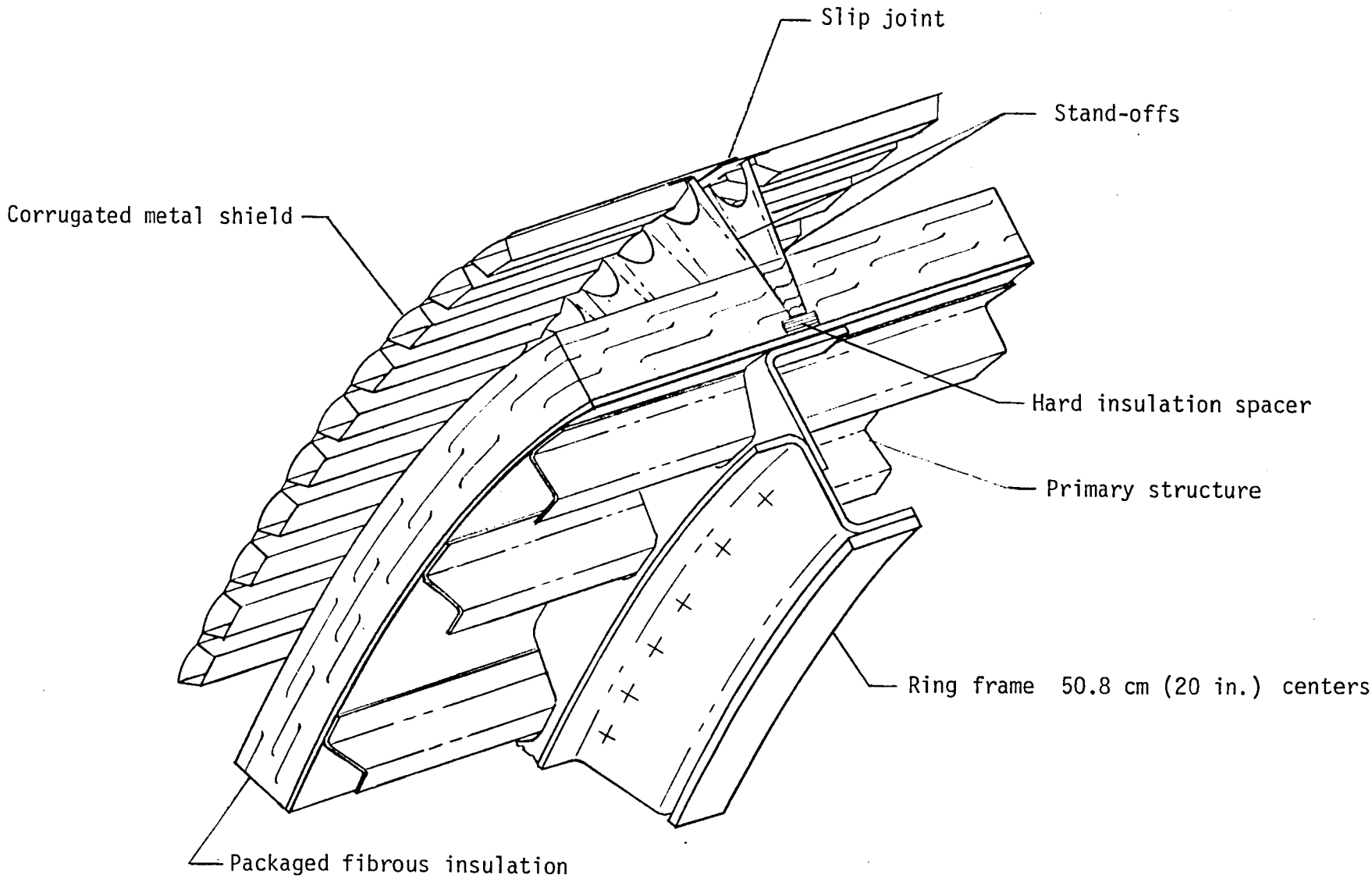

Figure 3.- Metallic stand-off TPS.
Typical sizes are 50.8 cm (20 in.) square.

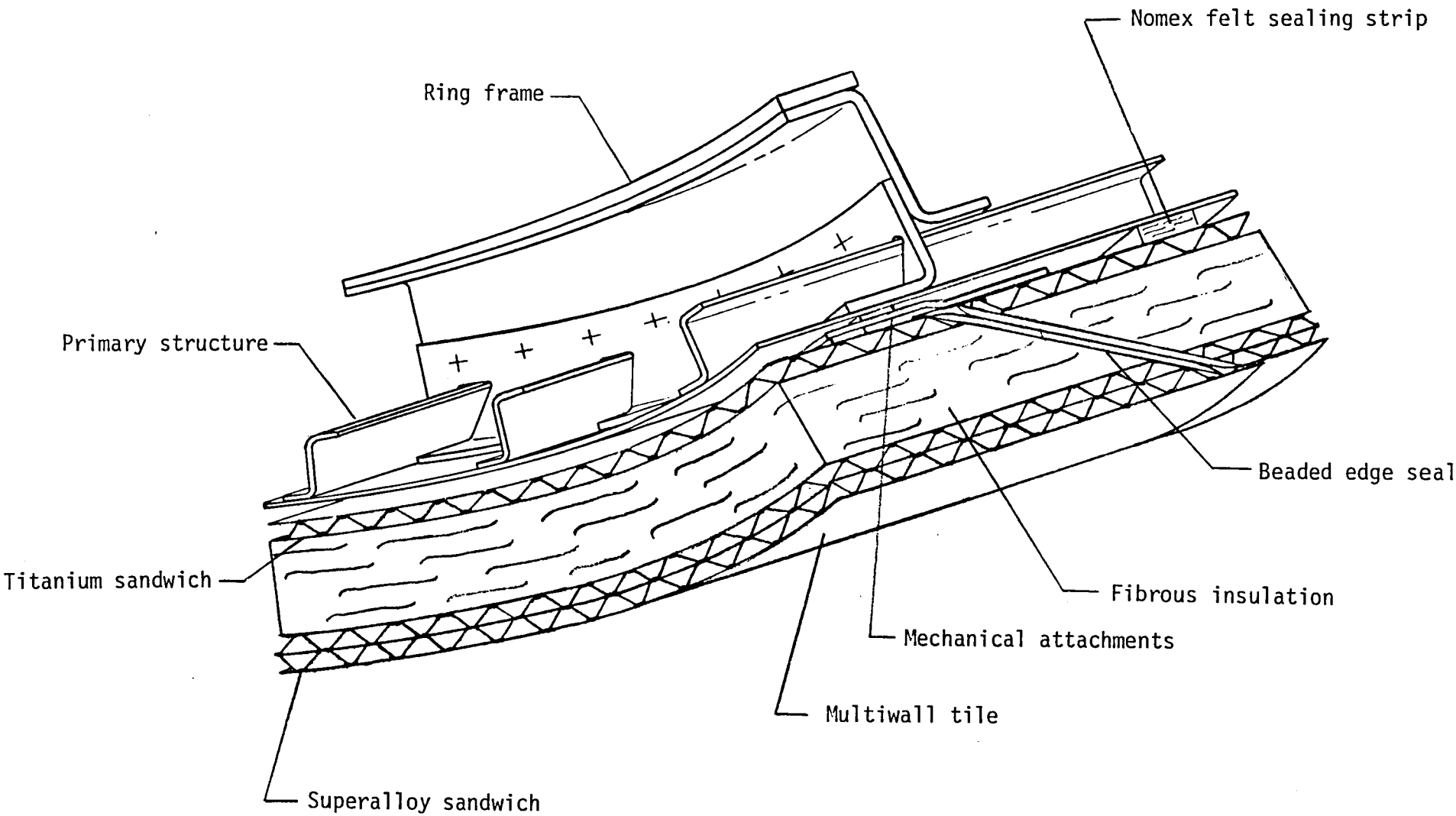

Figure 4.-Superalloy multiwall thermal protection system for the temperature range of 800 to 1300 K (1000 to 1900°F). Typical sizes range from 30.5 x 30.5 cm (12 x 12 in.) to 50.8 x 50.8 cm (20 x 20 in.).

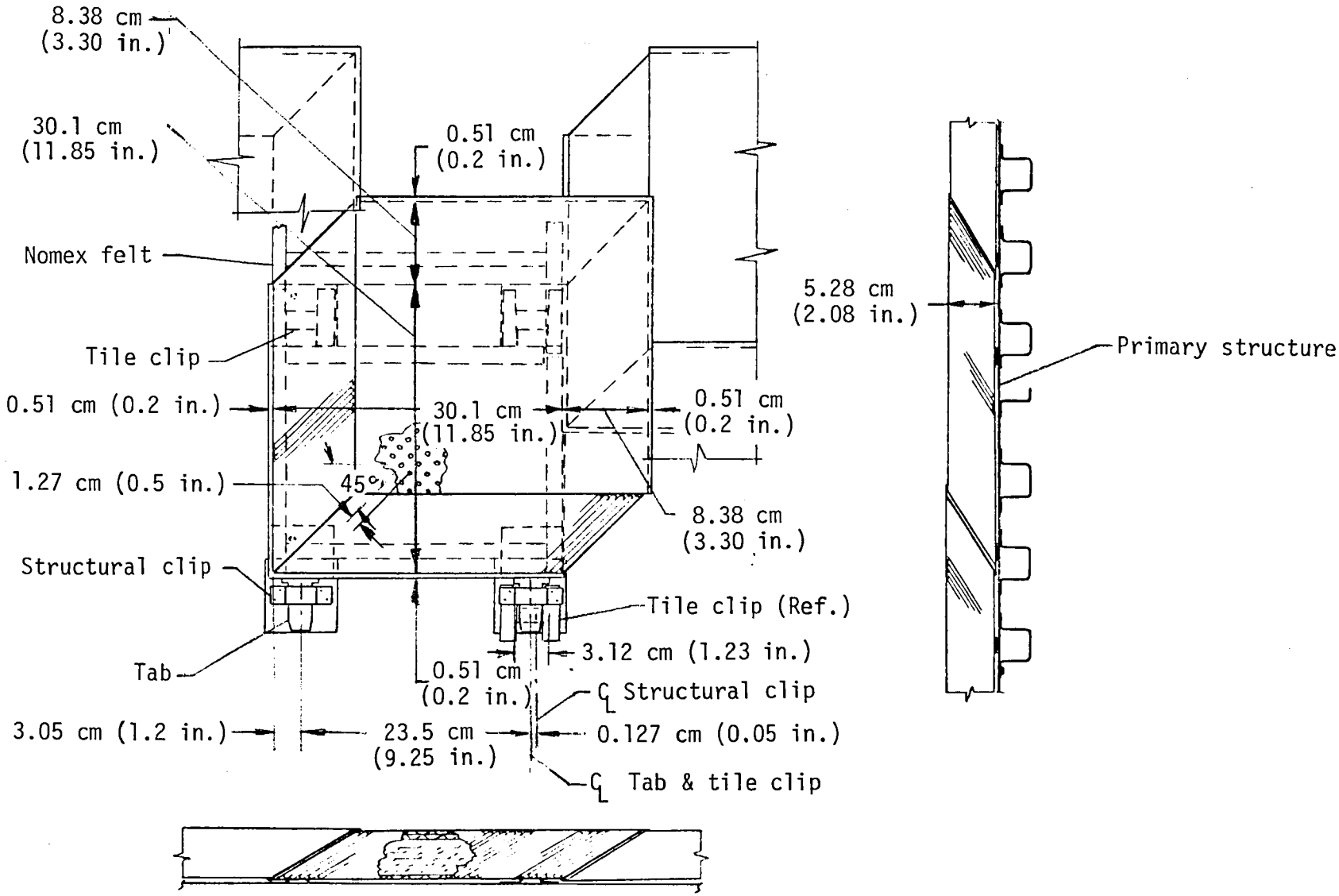

a) Multiwall tile assembly and installation.

Figure 5.- Multiwall TPS details.

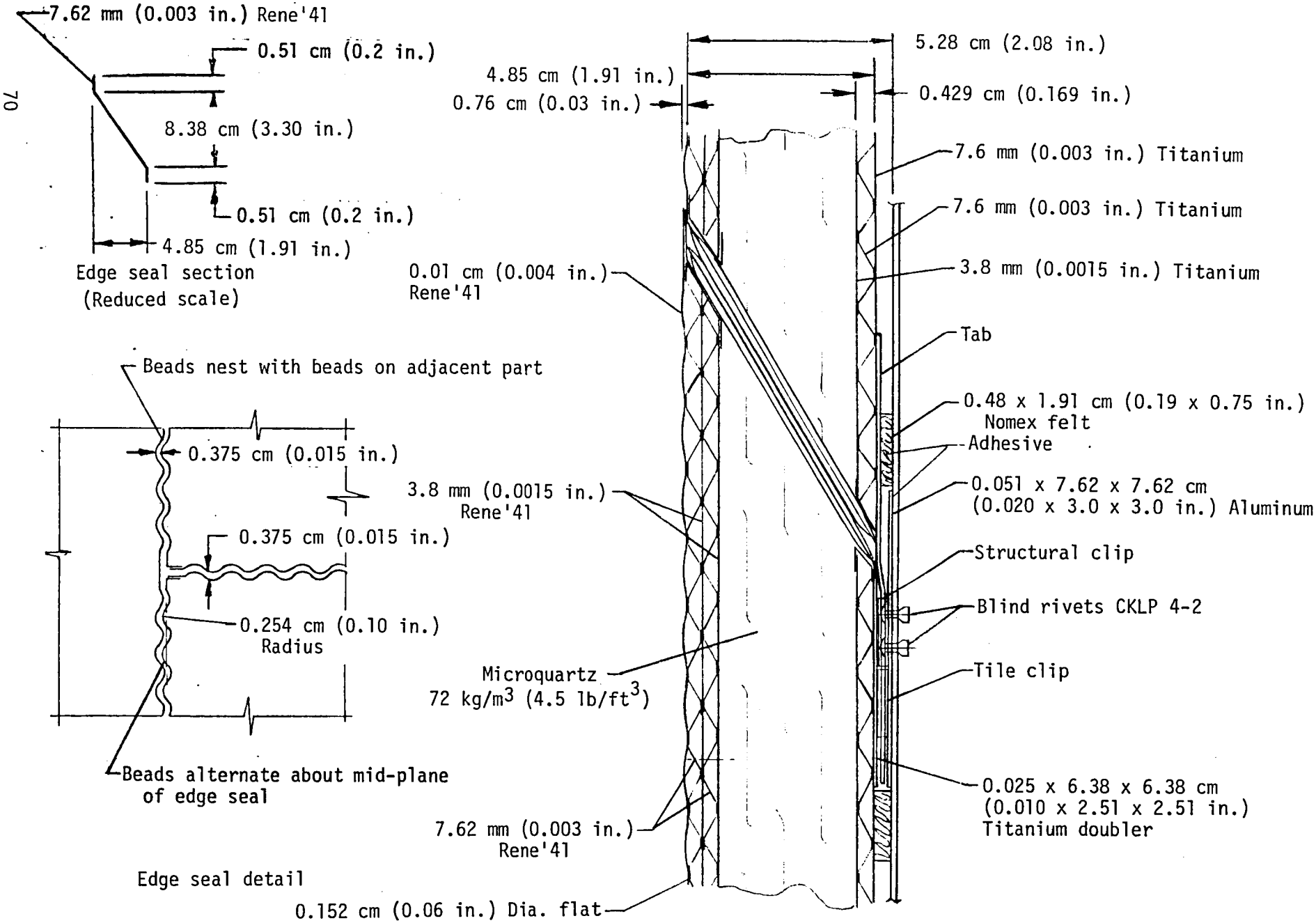

b) Multiwall tile construction.

Figure 5.- Continued.

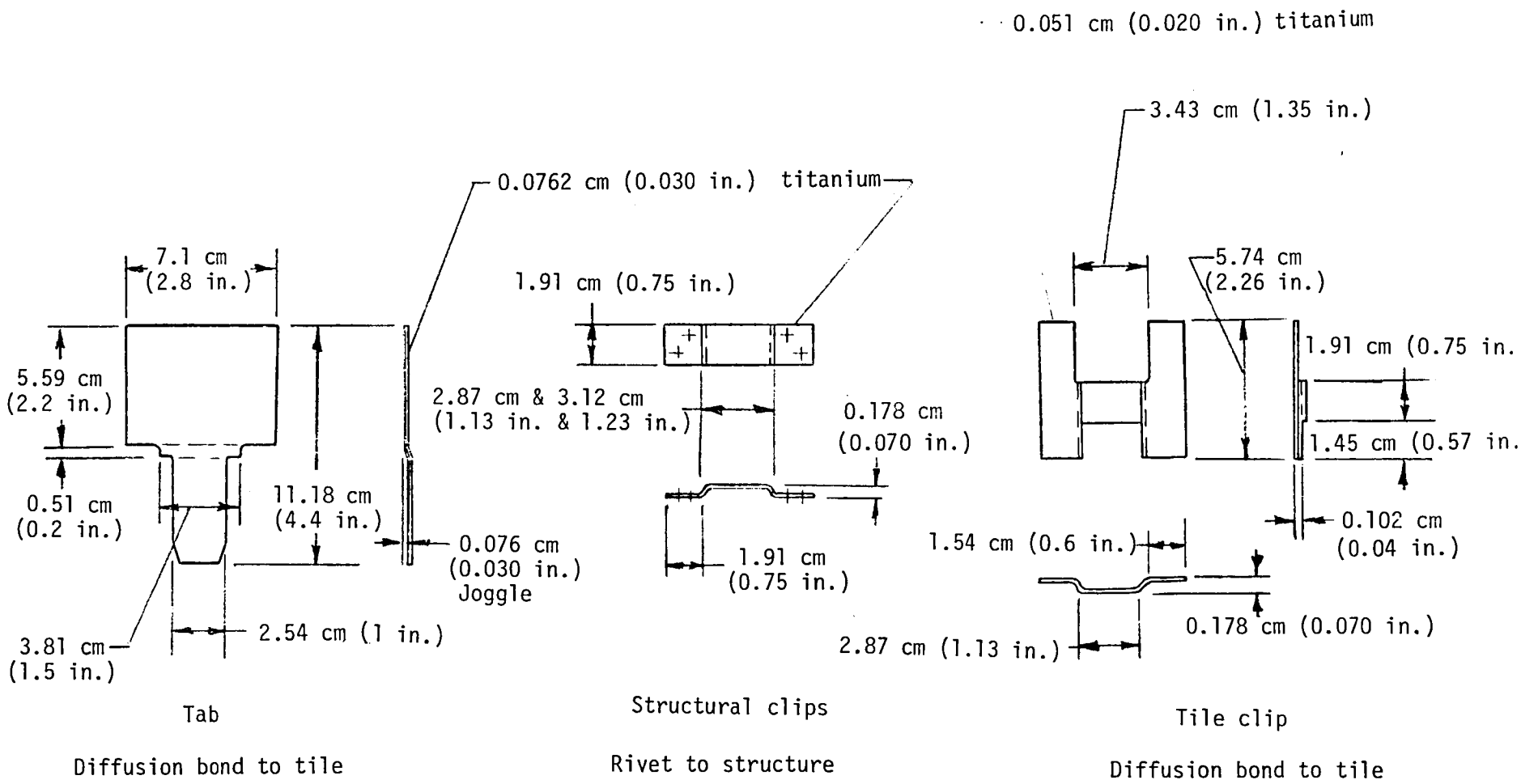

c) Multiwall tile attachments.

Figure 5.- Concluded.

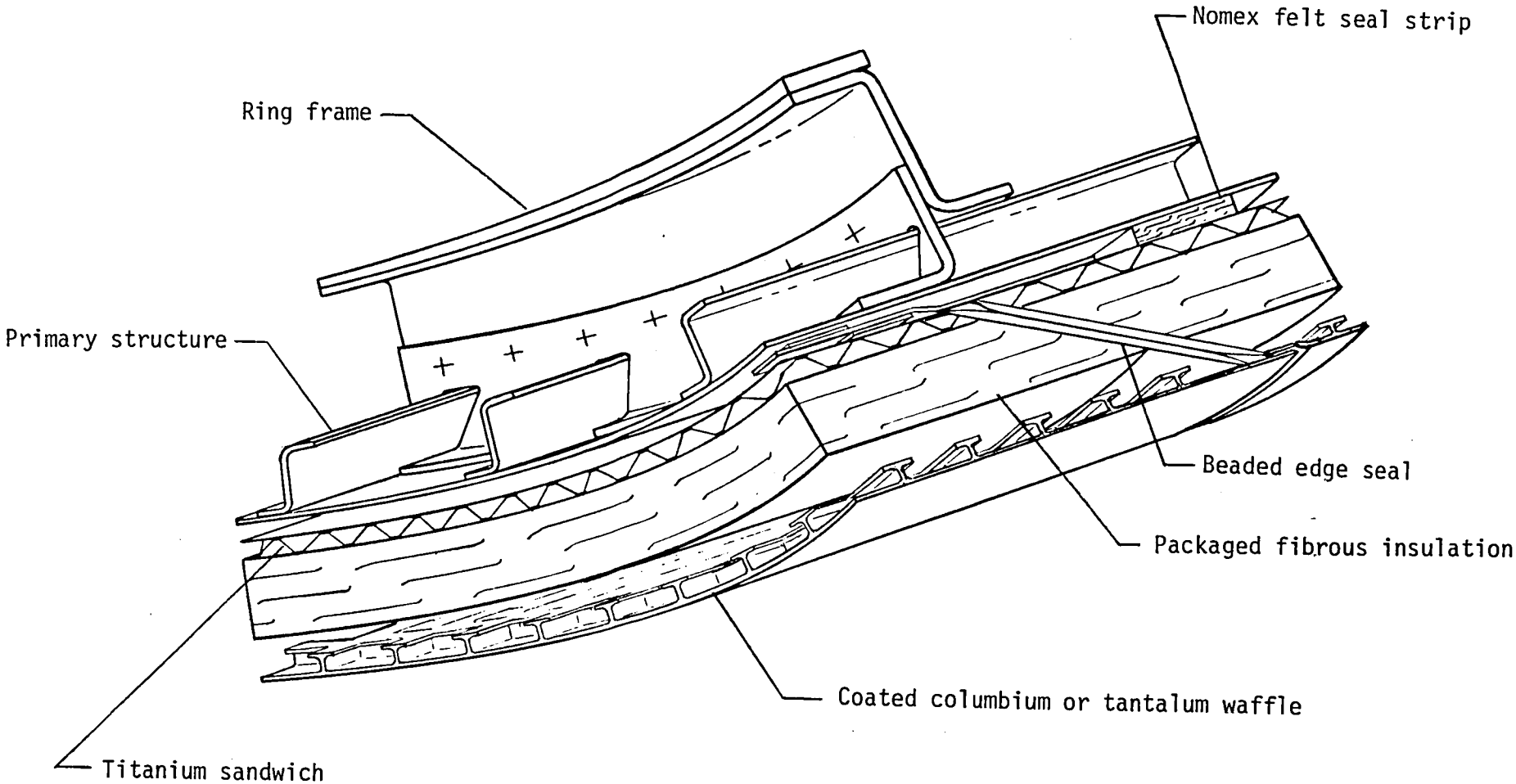

Figure 6.- Coated refractory metal multiwall TPS for temperature range of 1475 to 1650 K (2200 to 2500 °F) and 1650 to 1800 K (2500 to 2800 °F) for coated columbium and coated tantalum, respectively. Typical sizes range from 30.5 x 30.5 cm (12 x 12 in.) to 50.8 x 50.8 cm (20 x 20 in.).

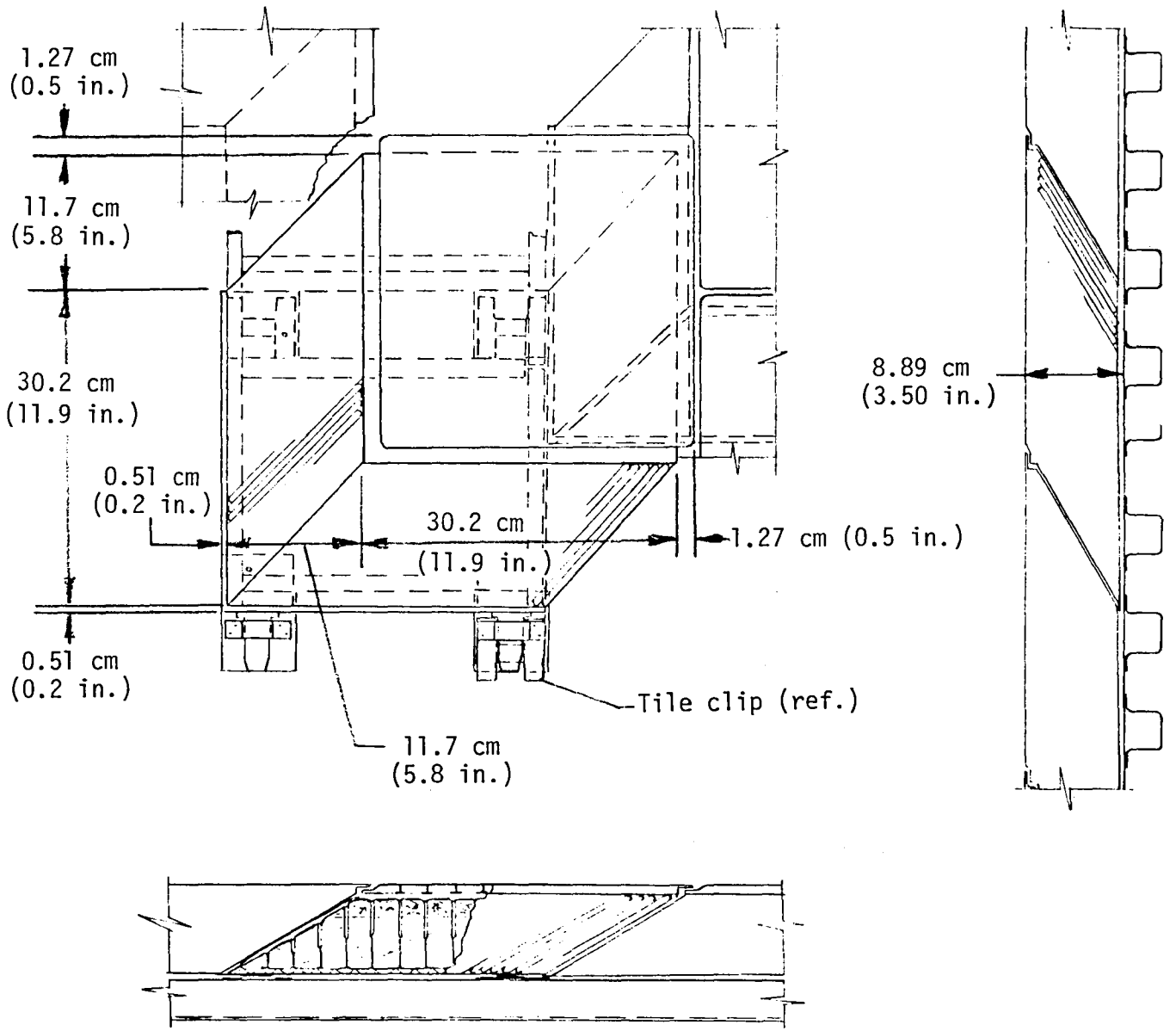

a) Multiwall tile assembly and installation.

Figure 7.- Refractory metal multiwall TPS details.

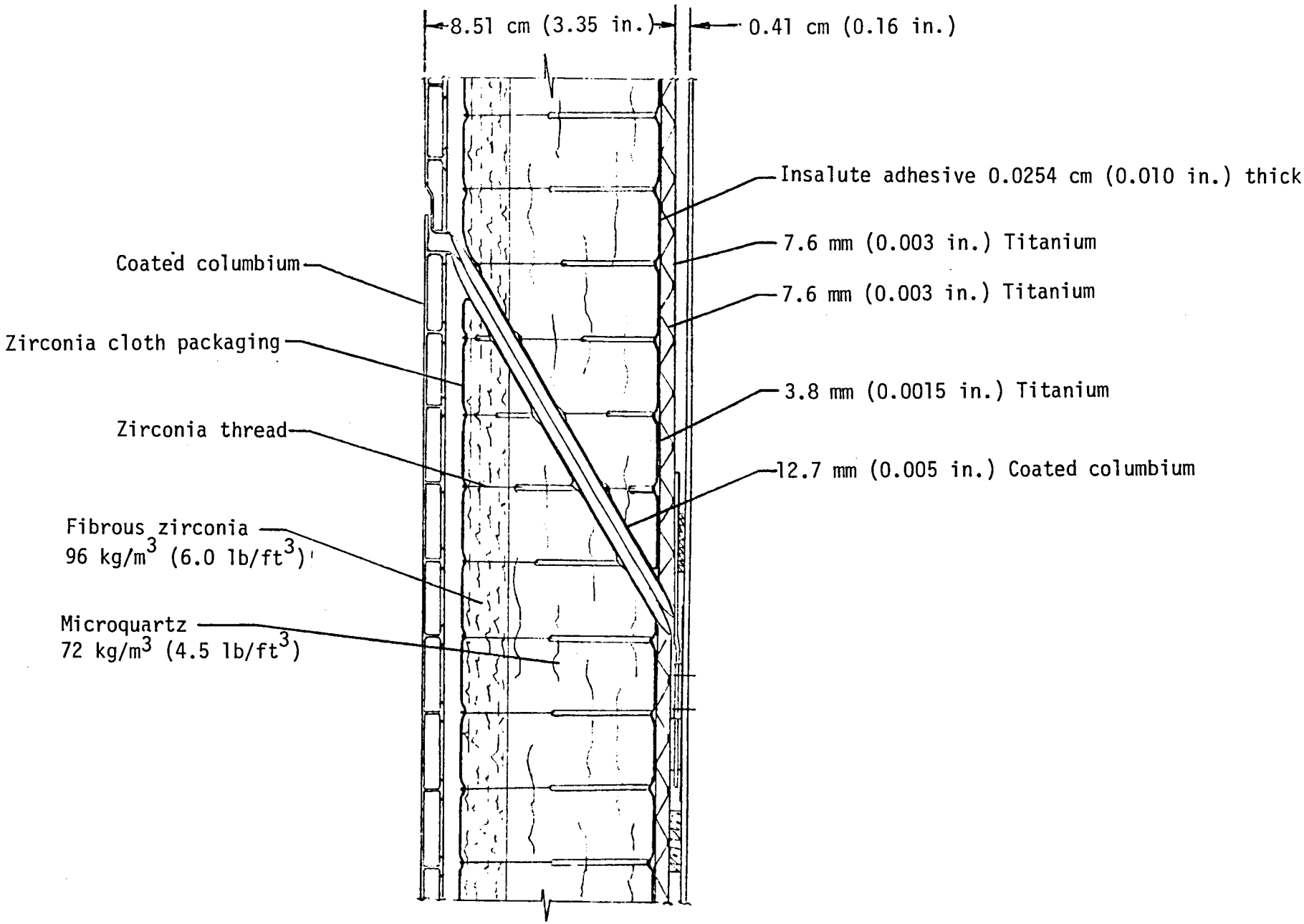

b) Multiwall tile construction.

Figure 7.- Continued.

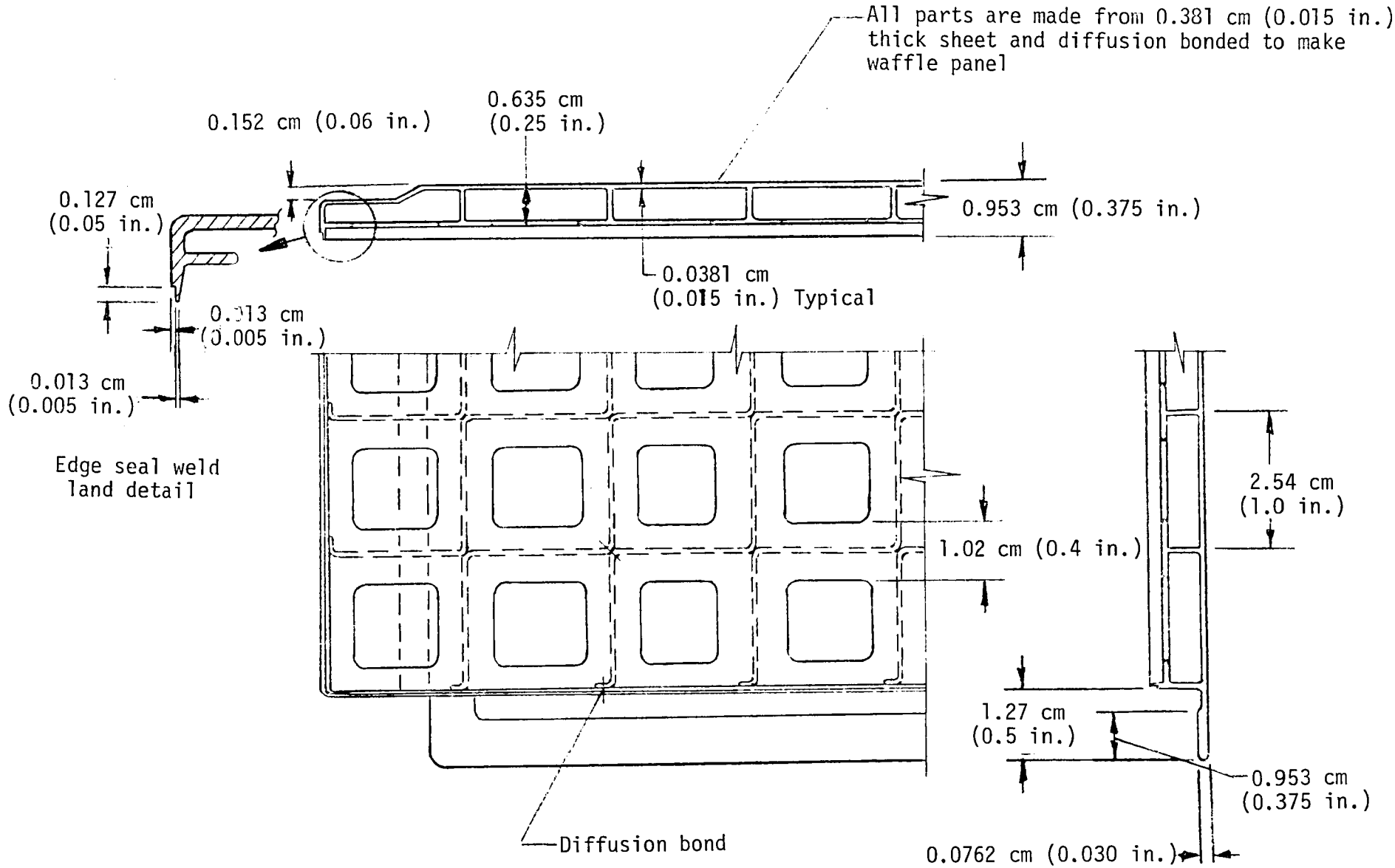

c) Refractory metal waffle details.

Figure 7.- Concluded.

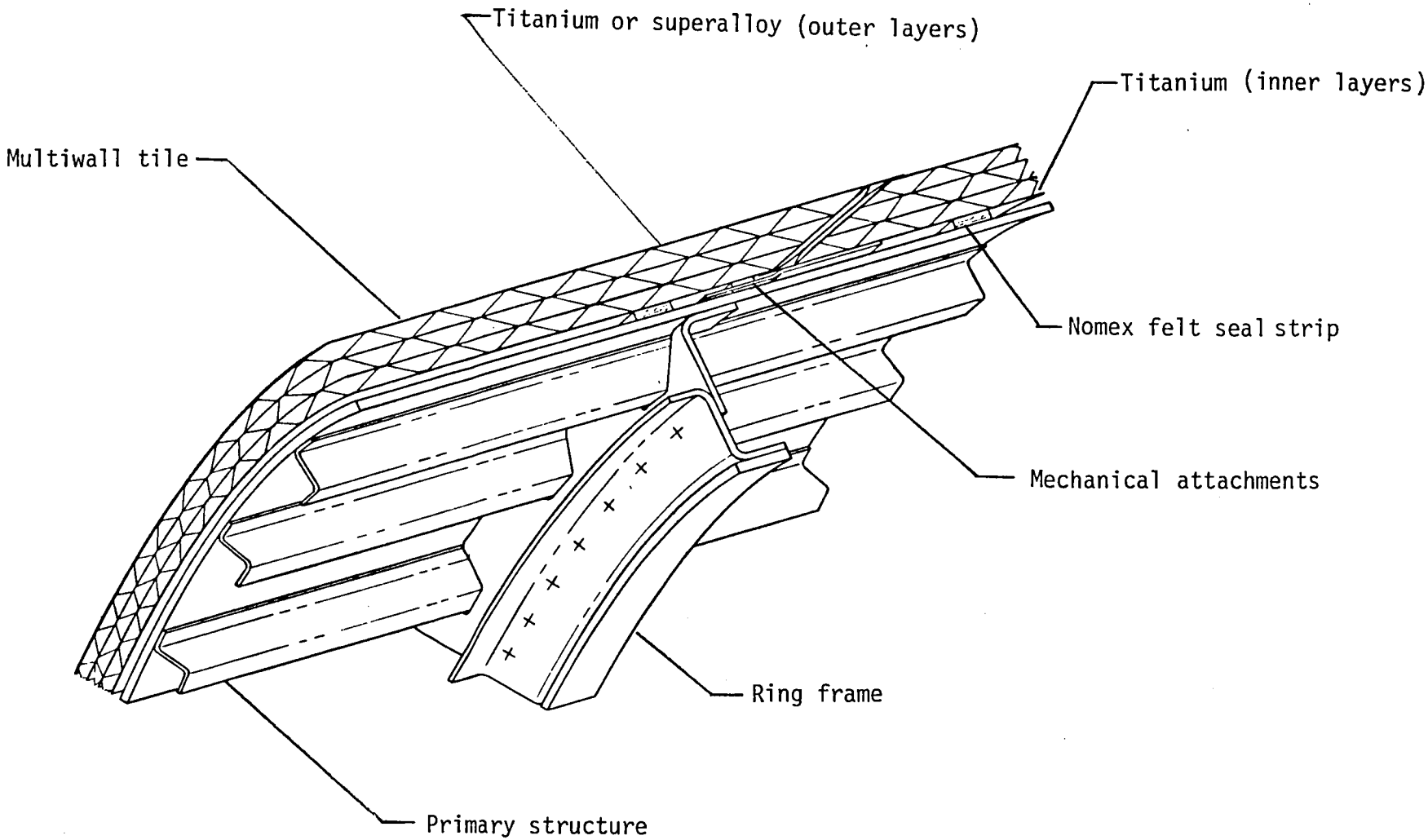

Figure 8.- All-metal multiwall TPS for temperature range 420 to 925 K (300 to 1200 °F).
Typical sizes range from 30.5 x 30.5 cm (12 x 12 in.) to 50.8 x 50.8 cm (20 x 20 in.).

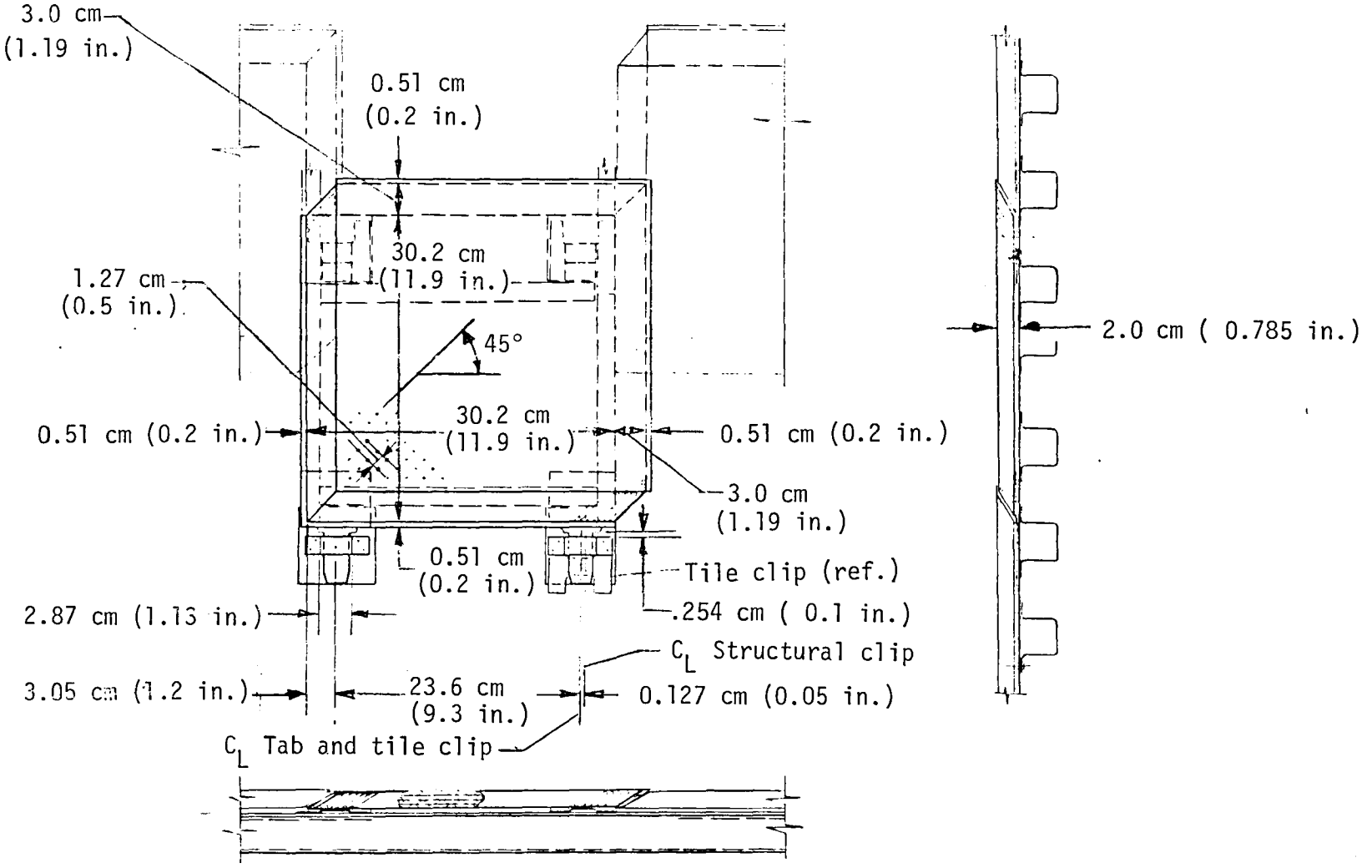

a) Multiwall tile assembly and installation.

Figure 9.- All-metal multiwall TPS details

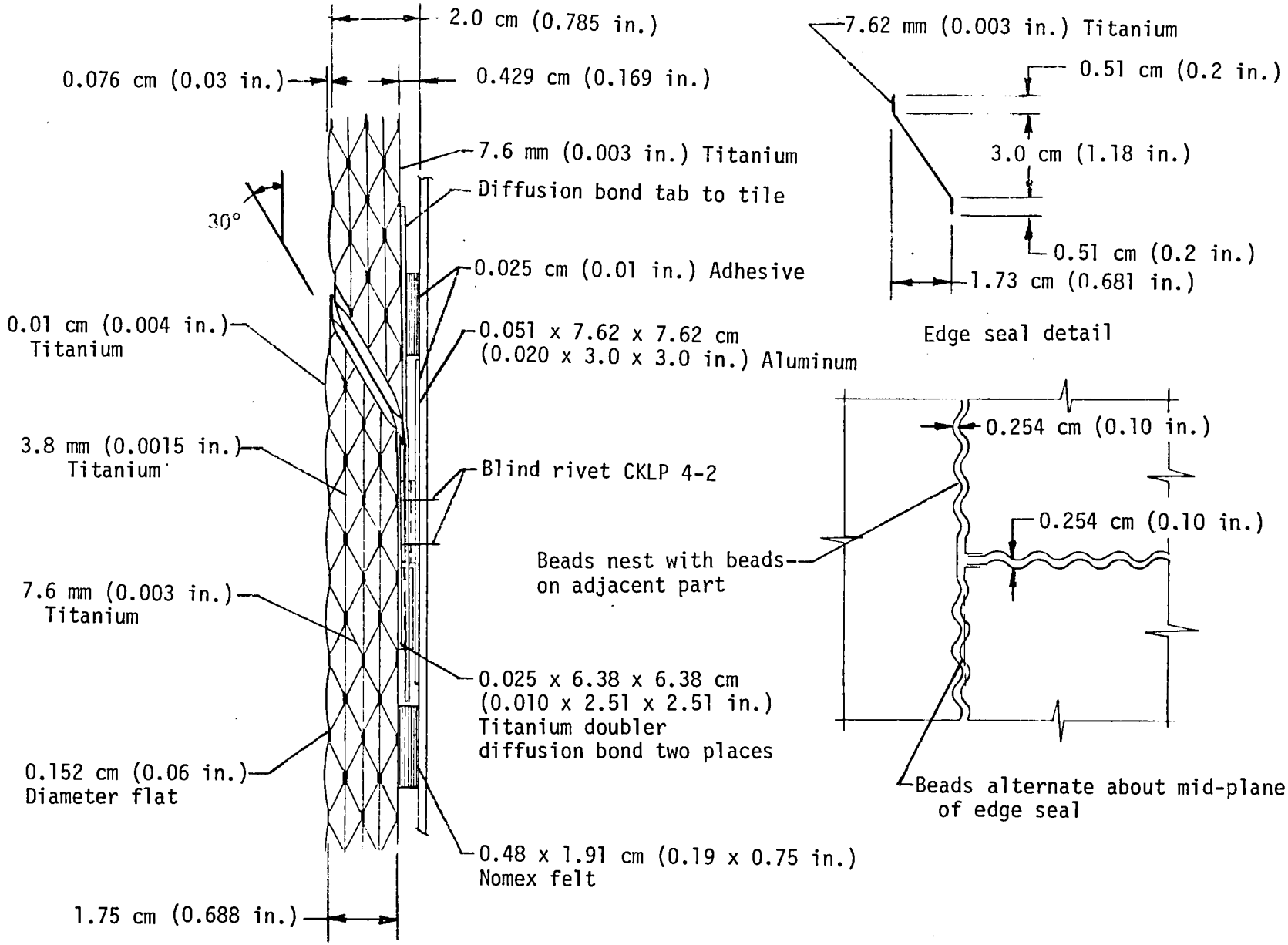

b) Multiwall tile construction.

Figure 9.- Concluded.

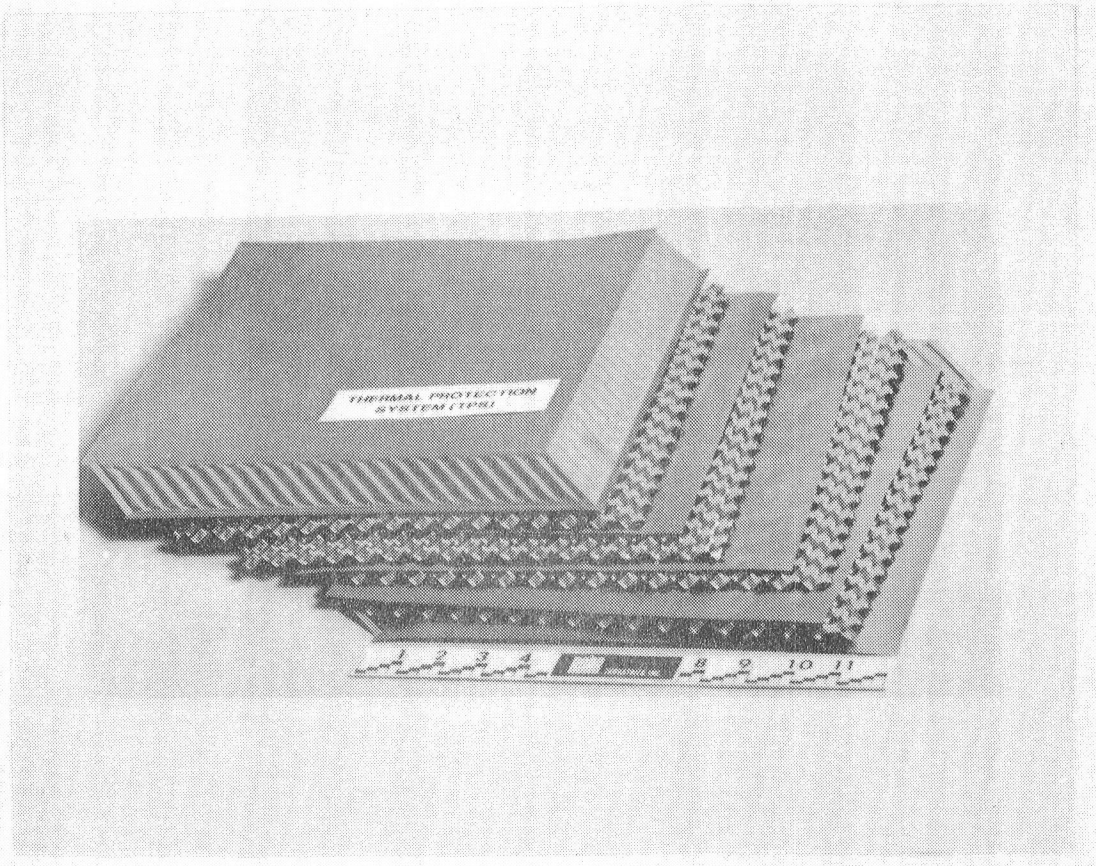

Figure 10.- Components of an all-metal multiwall tile (Ref. 31).

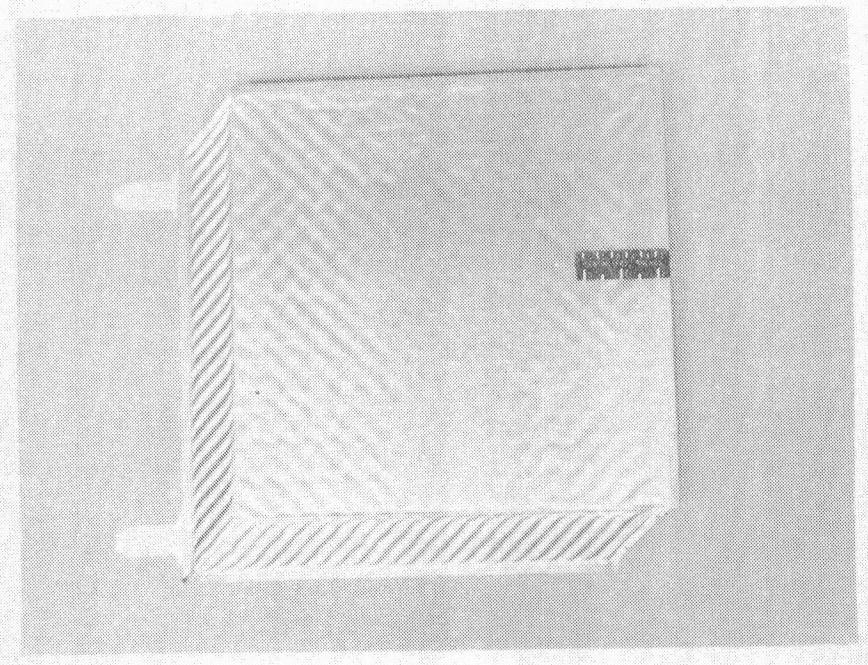

Figure 11.- All-metal multiwall tile after diffusion bonding.

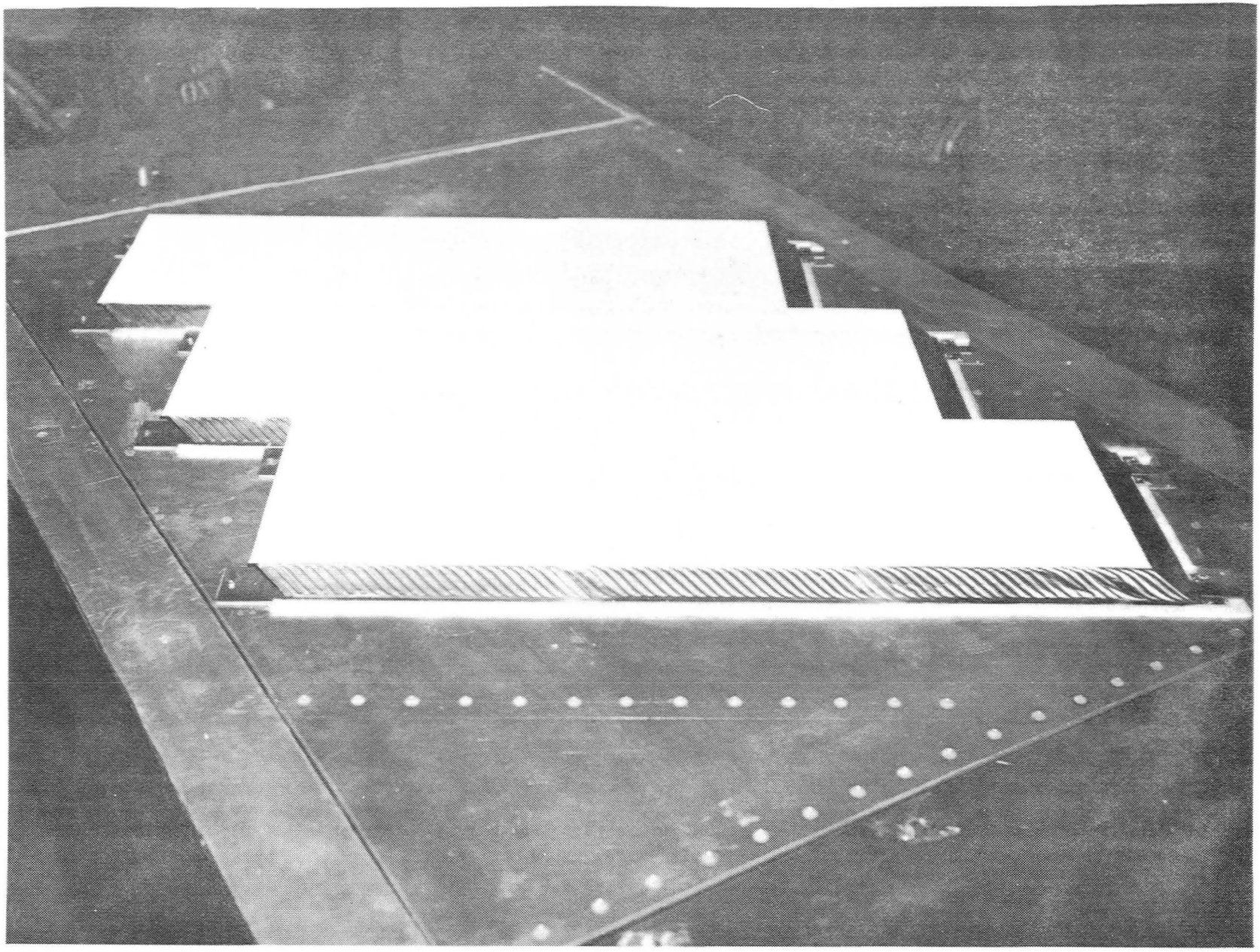

Figure 12.- Nine tile array of all-metal multiwall TPS.

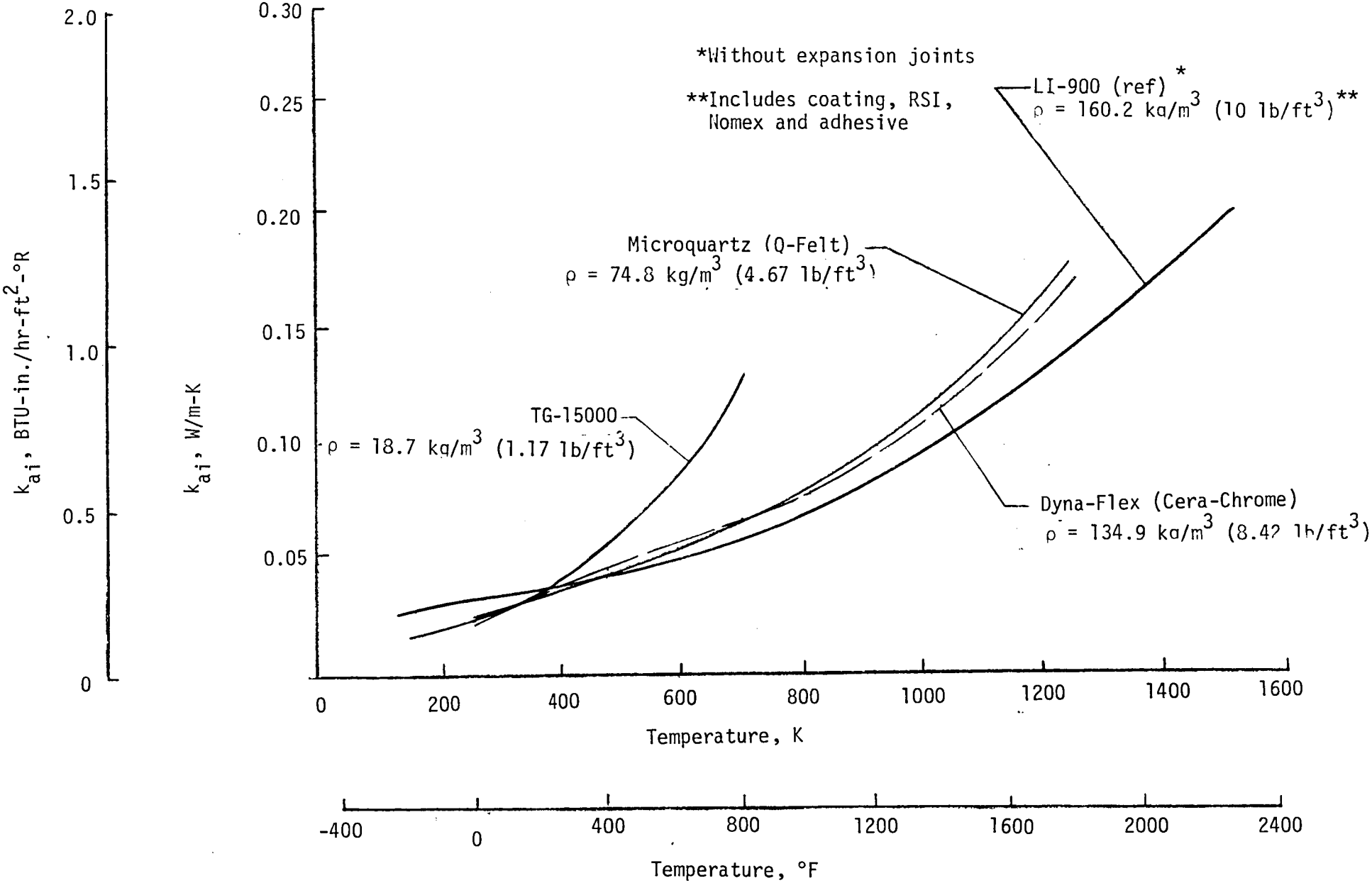

Figure 13.- Apparent thermal conductivities and bulk densities including Rene' 41 edge seal effects for various insulations from equation (1) at a pressure of 1058 Pa (0.155 psia).

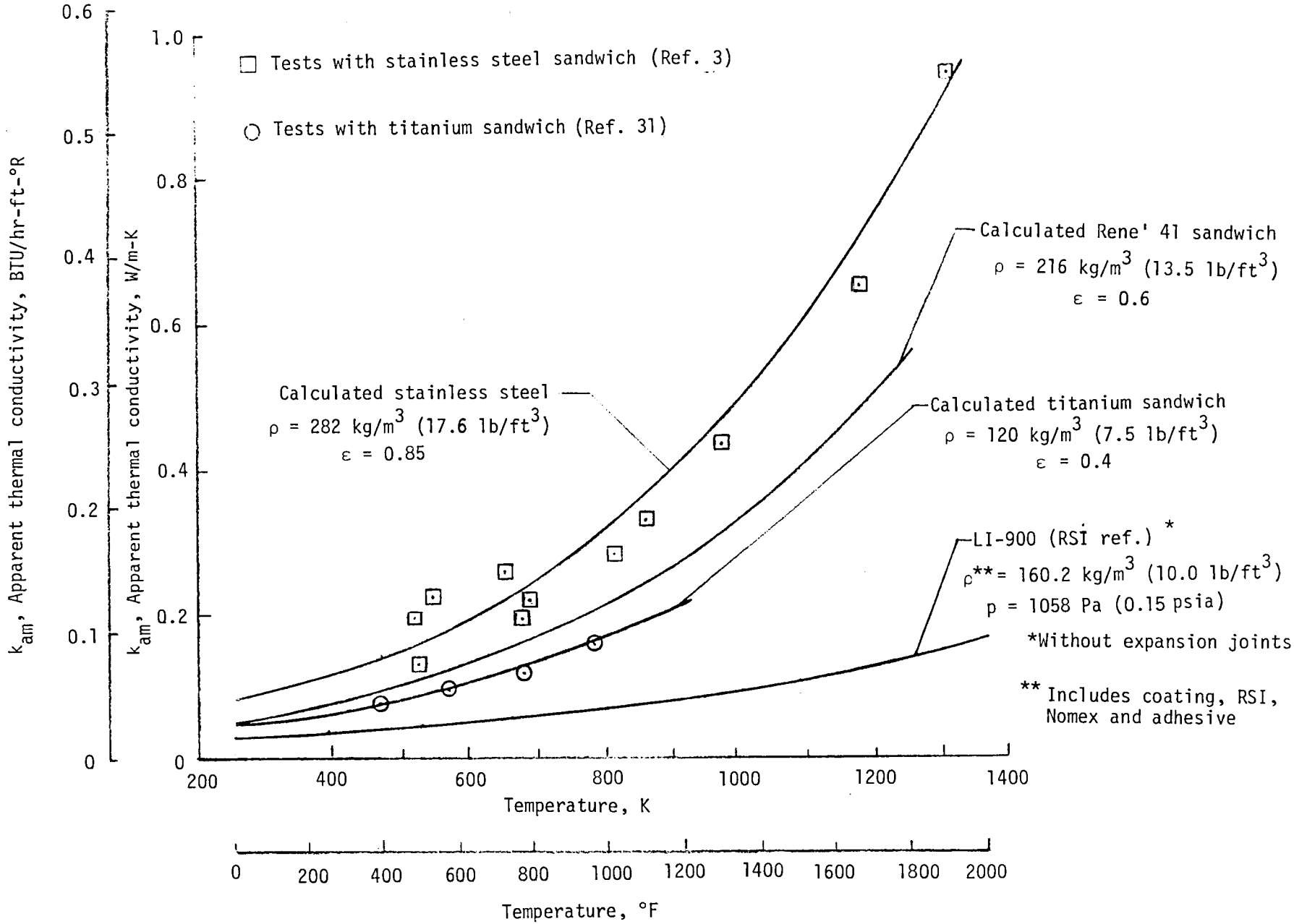

Figure 14.- Comparison of experimental and calculated thermal conductivity of metal sandwich from equation (2).

RCC = Reinforced carbon-carbon

HRSI = High temperature RSI (Entire lower surface)

LRSI = Low temperature RSI

FRSI = Flexible RSI
(RTV coated Nomex felt)

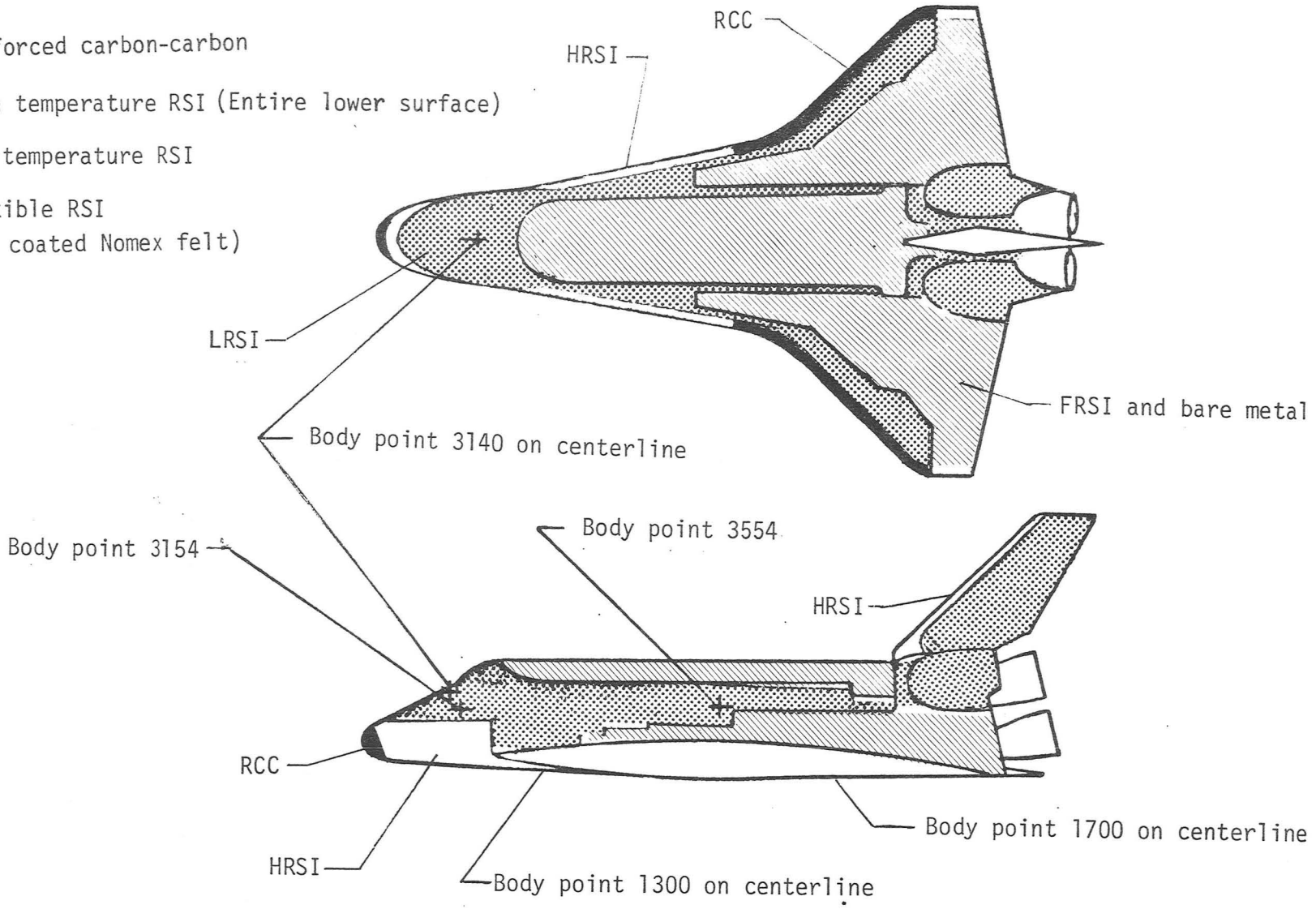

Figure 15.- Location of RSI and body points on the space shuttle.

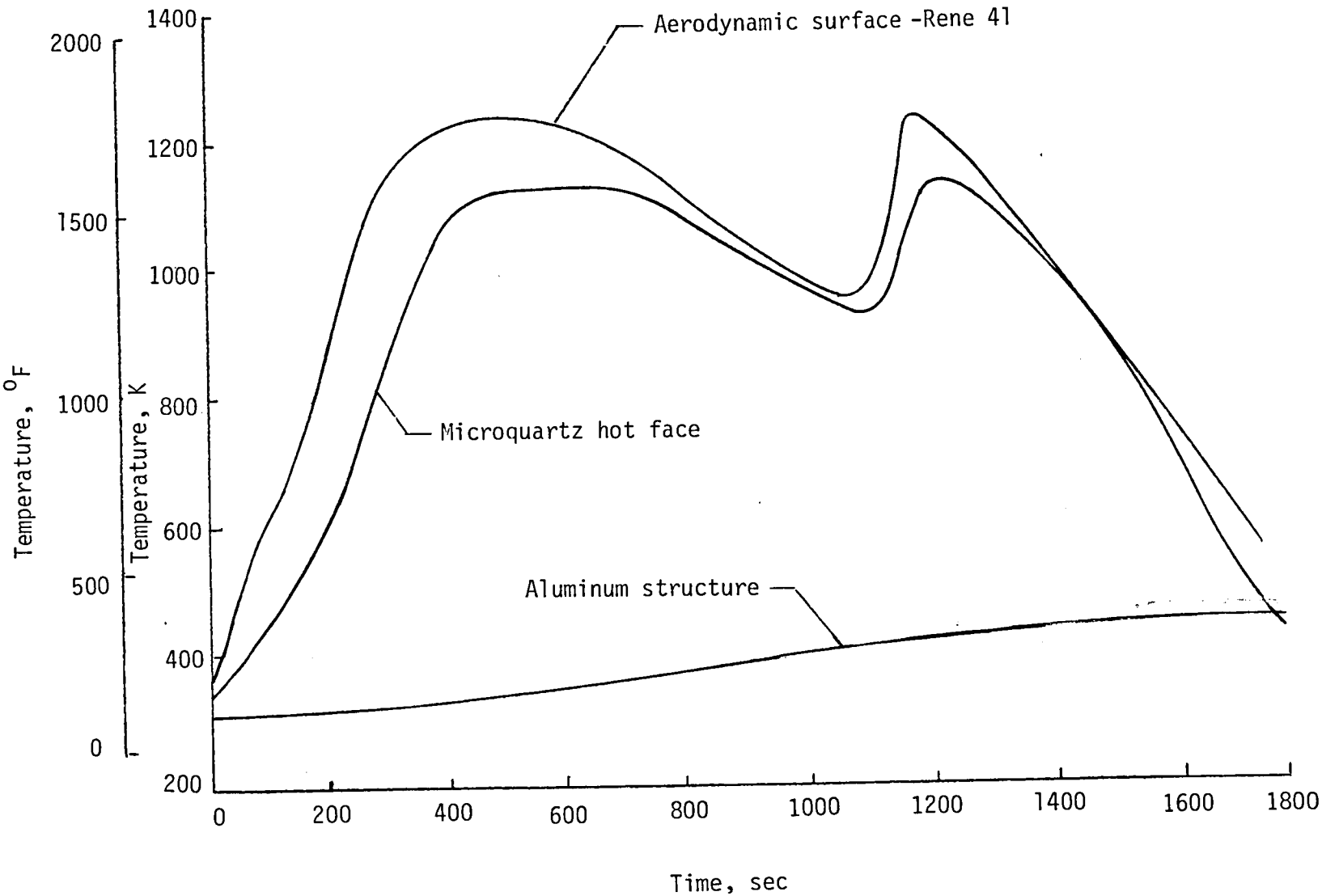

Figure 16.- Temperature history of space shuttle body point 1700.

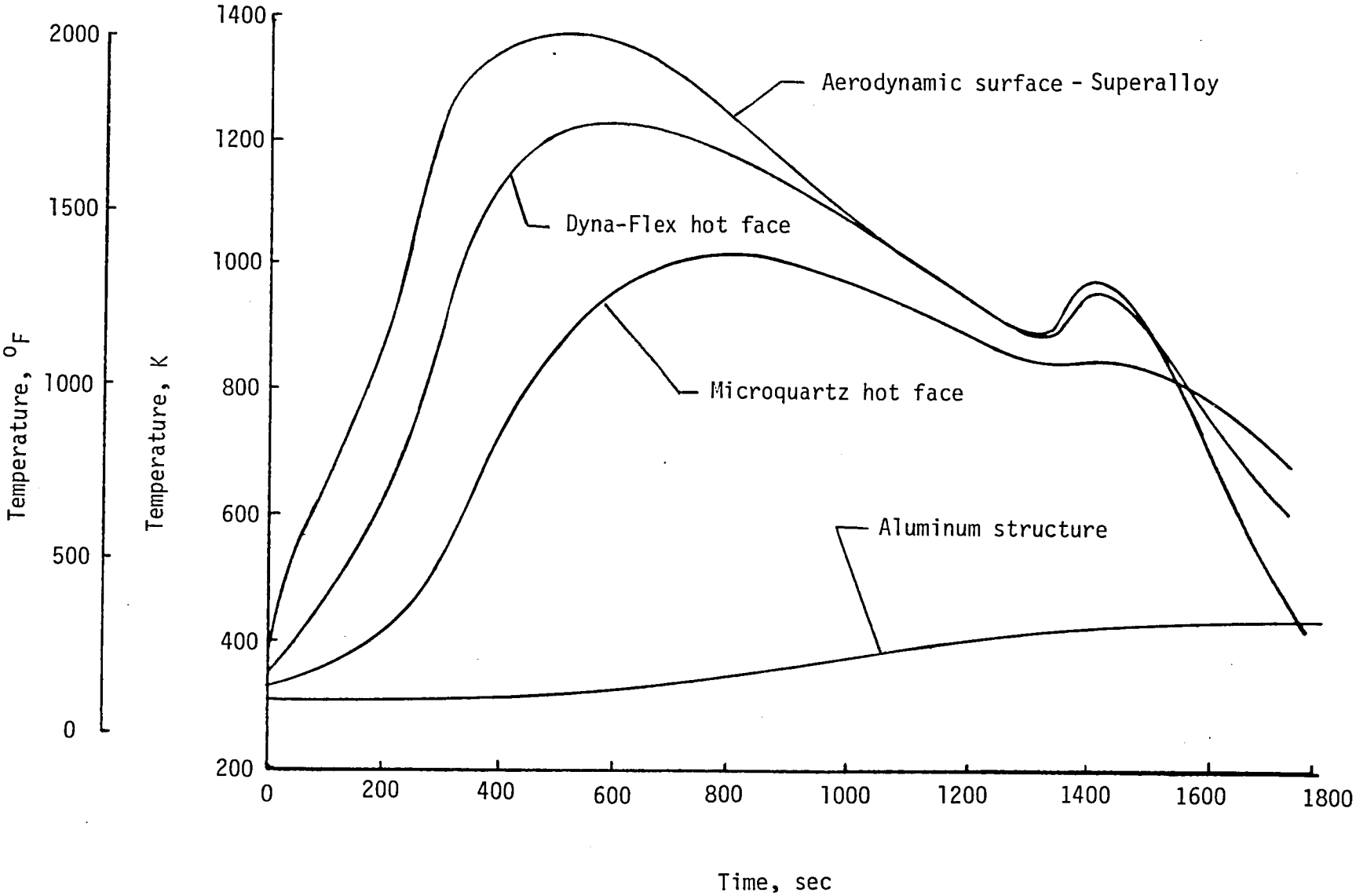

Figure 17.- Temperature history of space shuttle body point 1300.

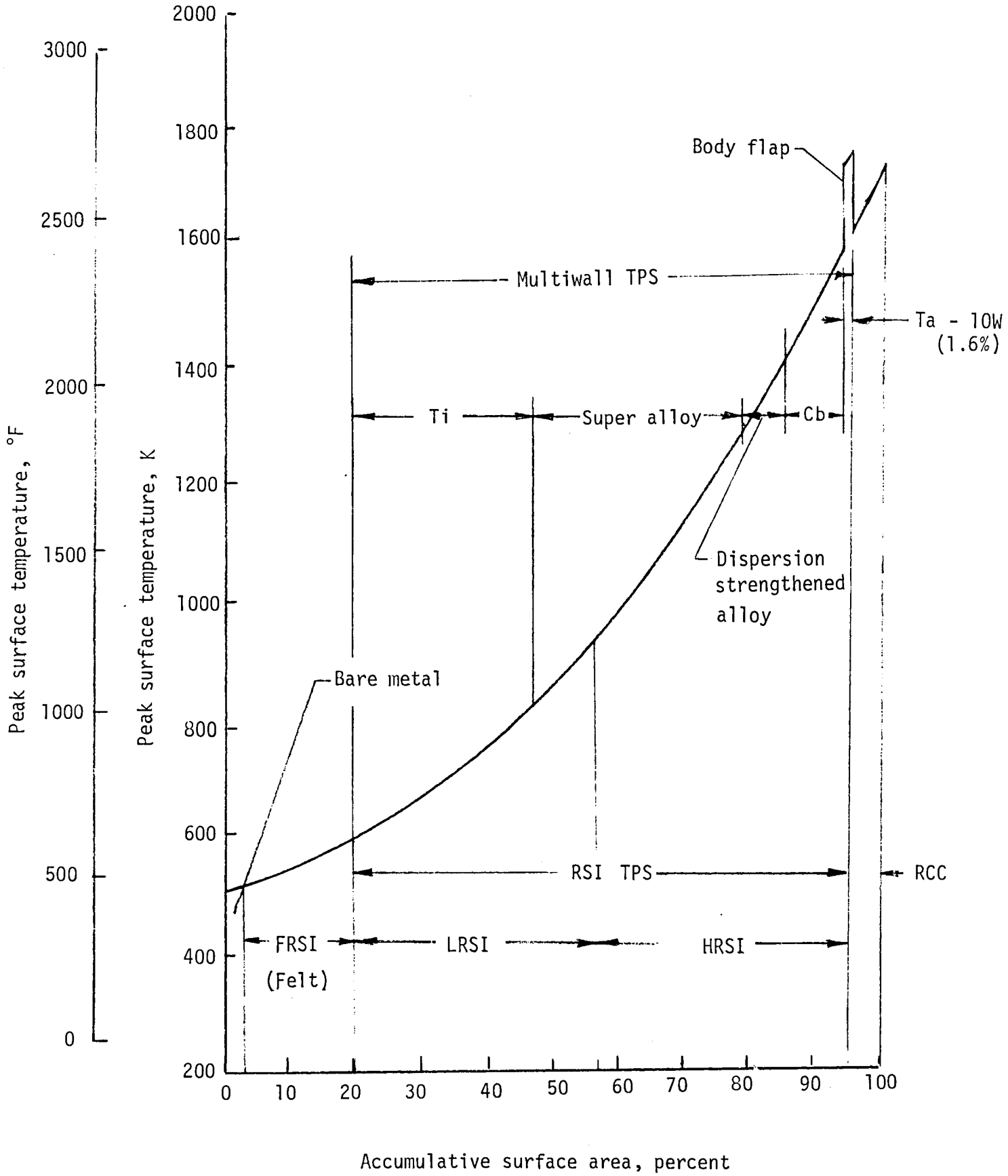

Figure 18.- Percentage surface area as a function of peak surface temperature and various TPS.

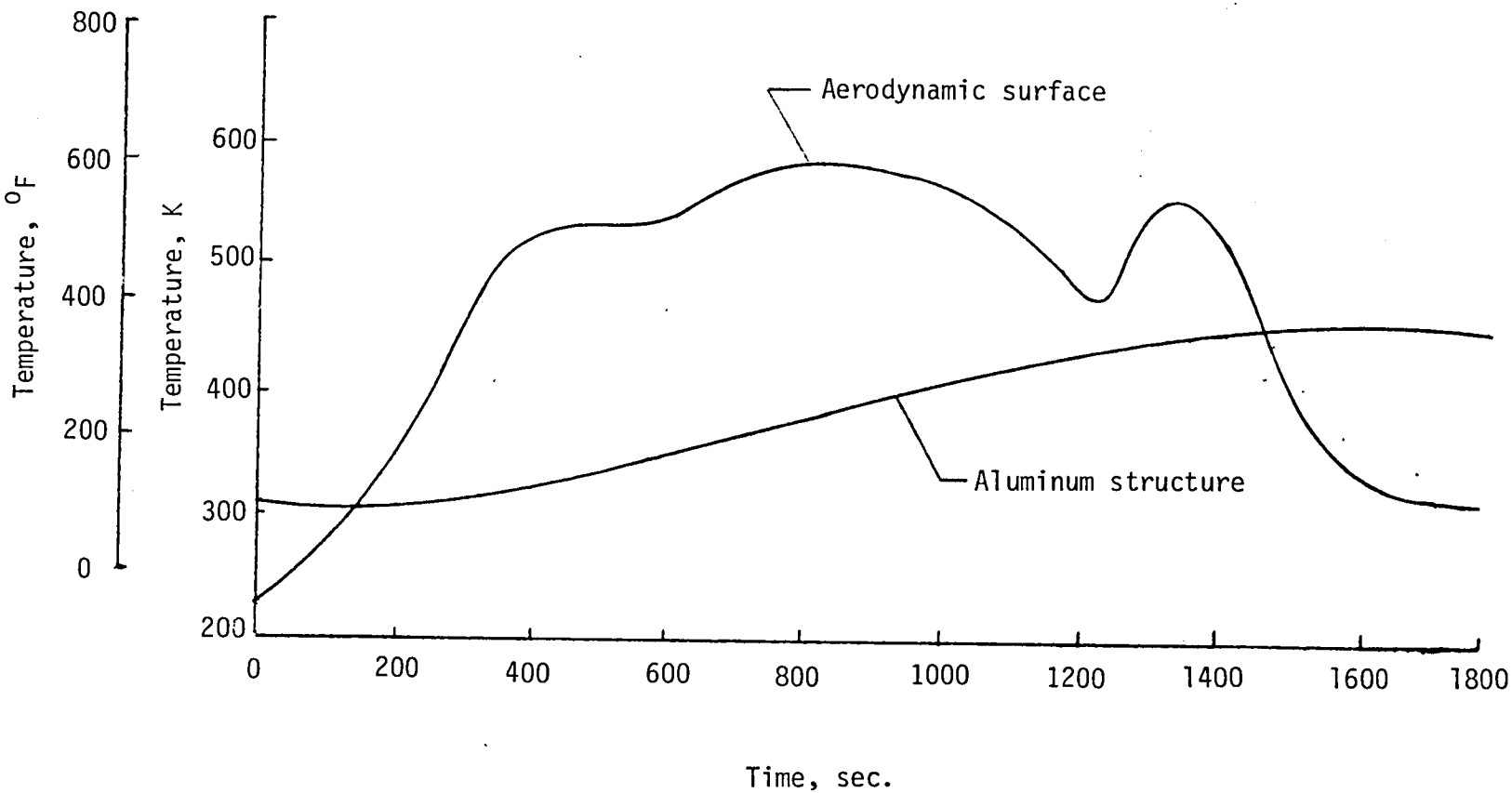

Figure 19.- Temperature history of space shuttle body point 3554 with titanium multiwall TPS.

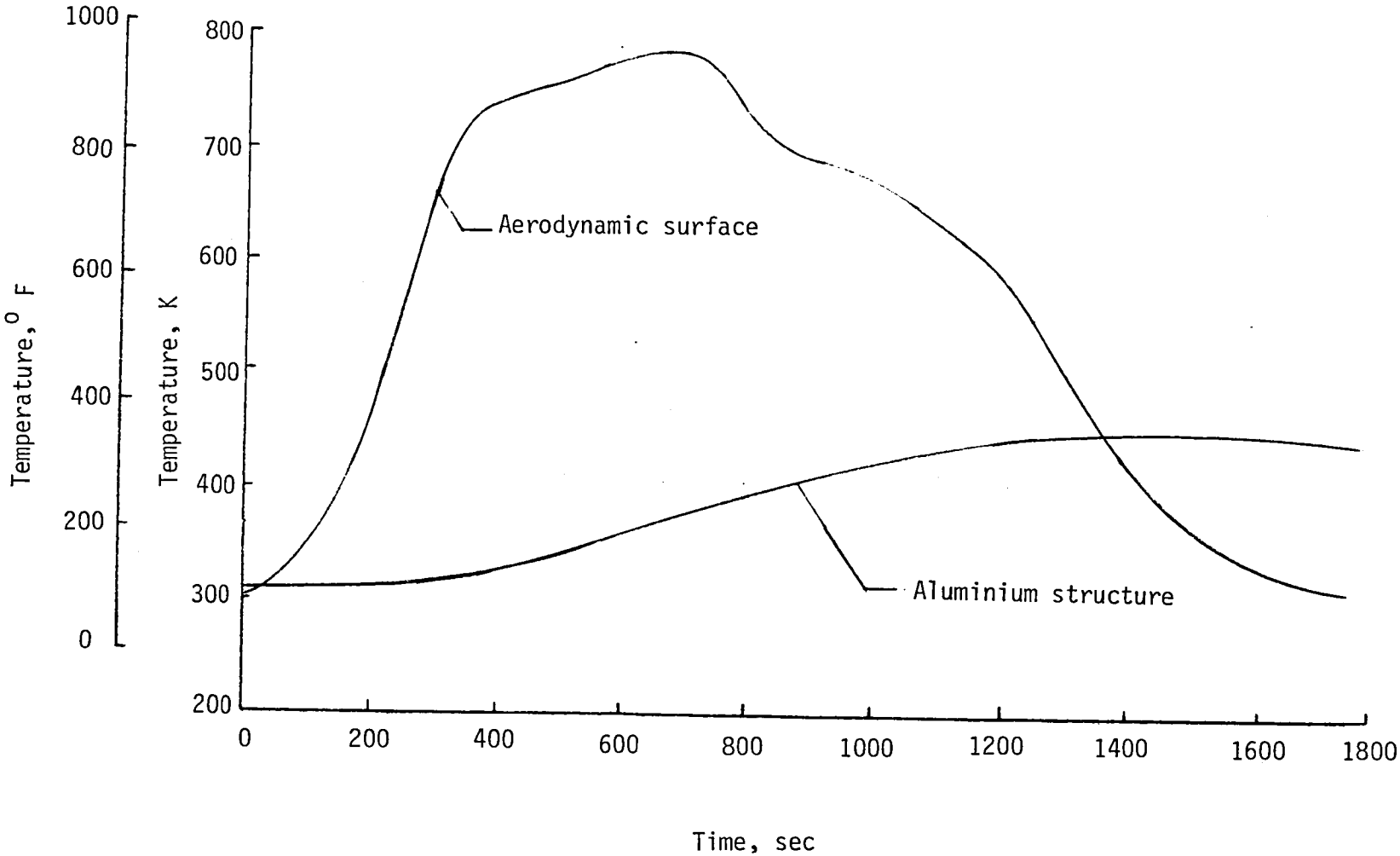

Figure 20.- Temperature history of space shuttle body point 3140 with titanium multiwall TPS.

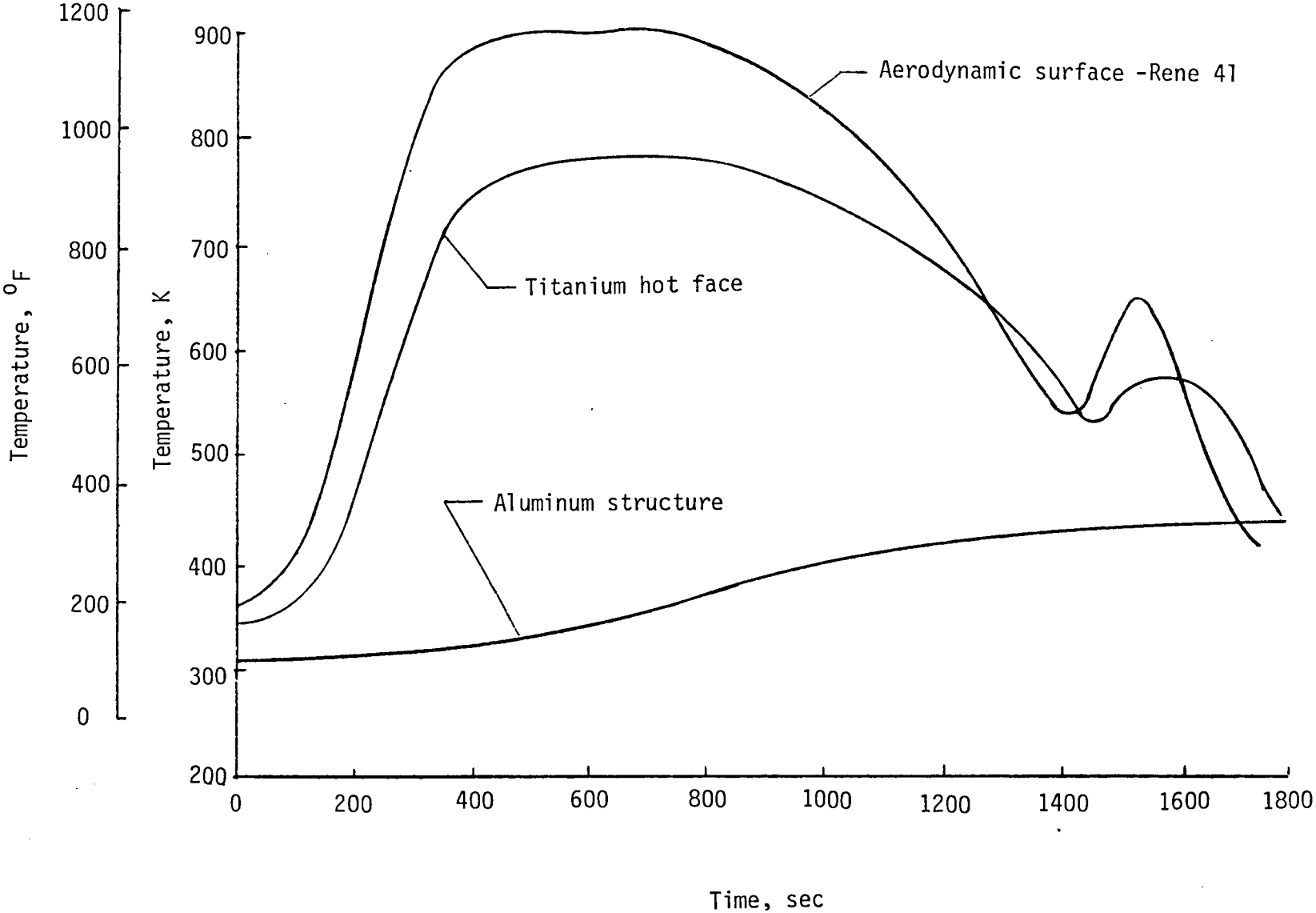

Figure 21.- Temperature history of space shuttle body point 3154 with bimetal multiwall TPS.

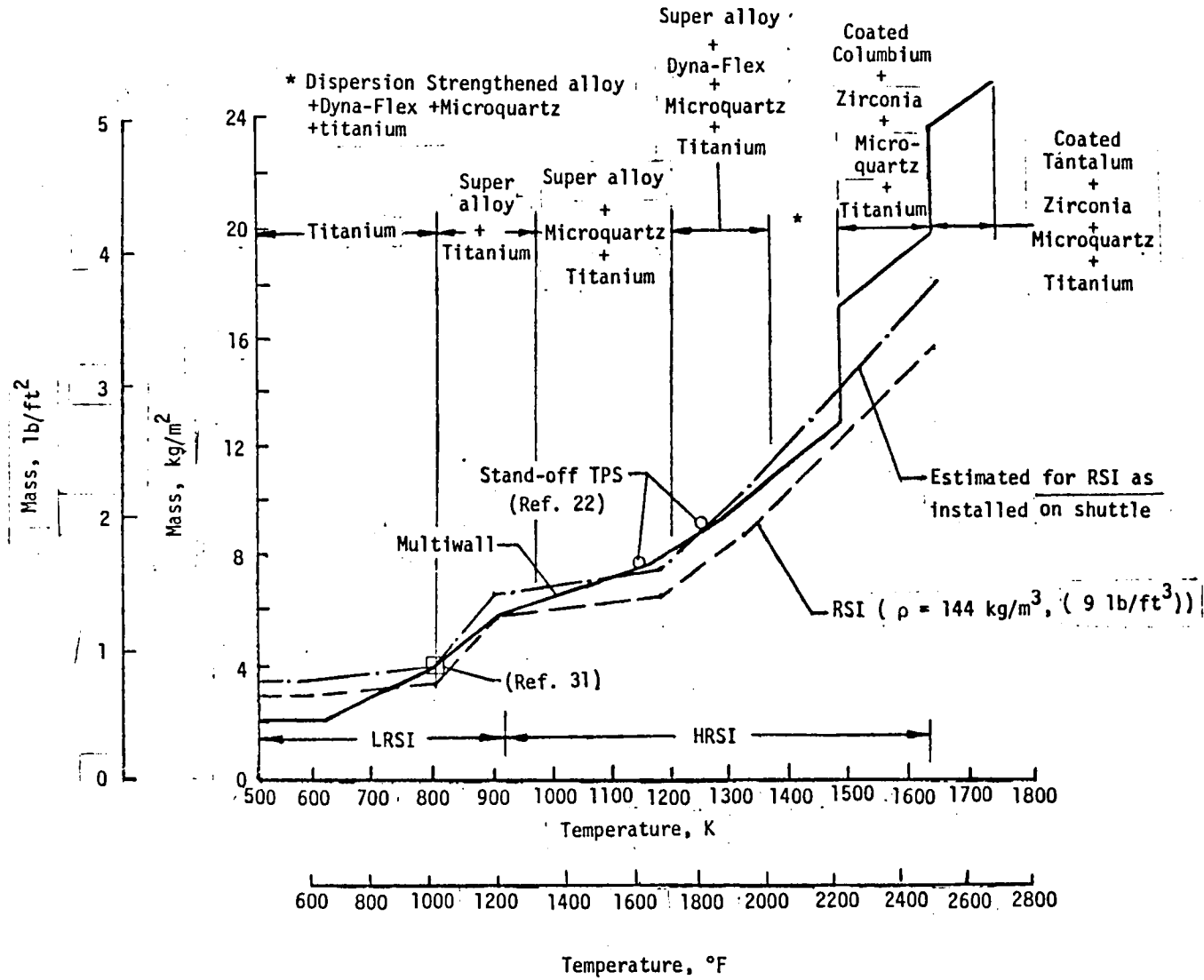

Figure 22.- Unit area masses vs. peak surface temperature for various TPS.

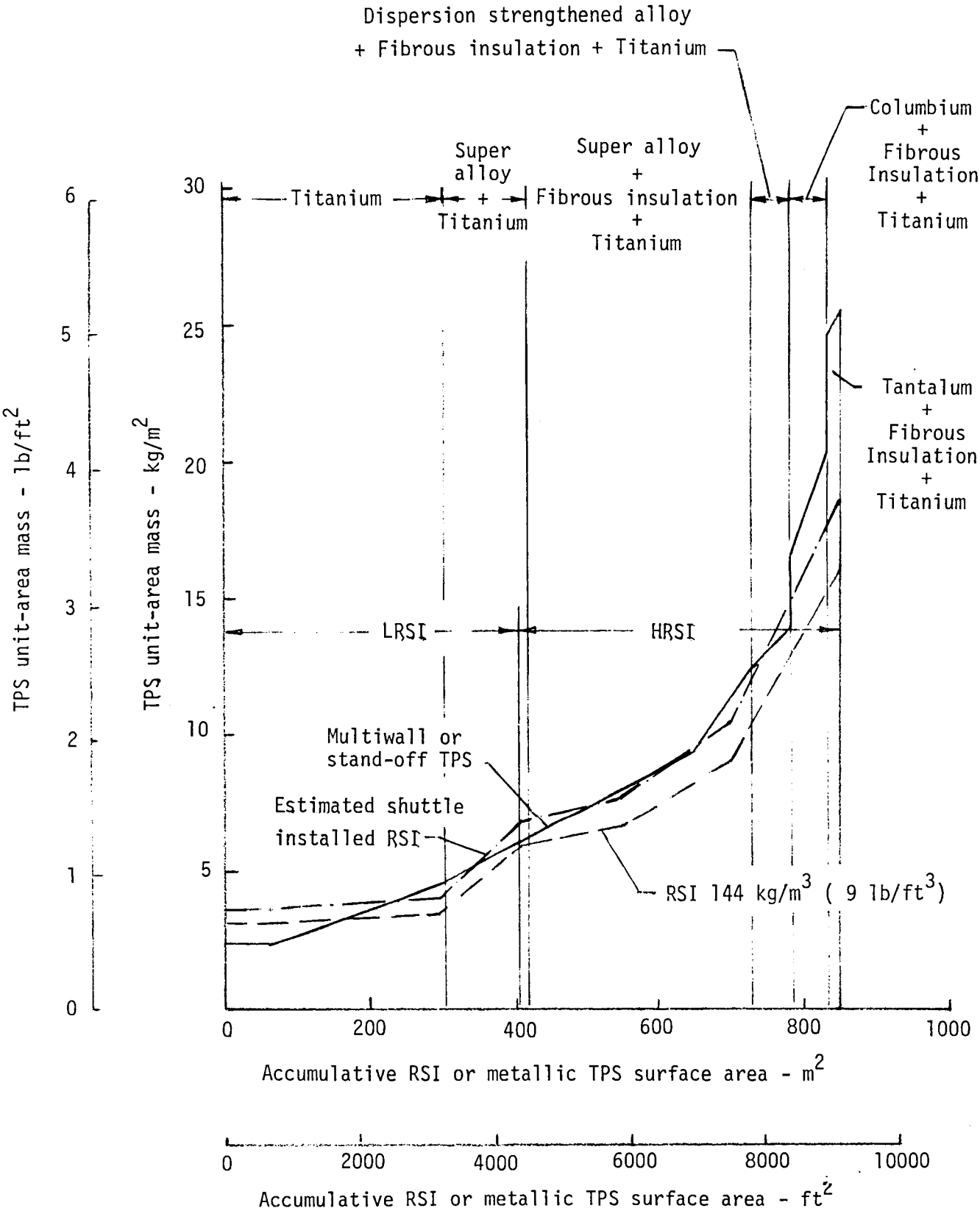

Figure 23.- Unit-area mass of various TPS as a function of shuttle surface area covered with RSI or metallic TPS which is 75 percent of the total wetted area.

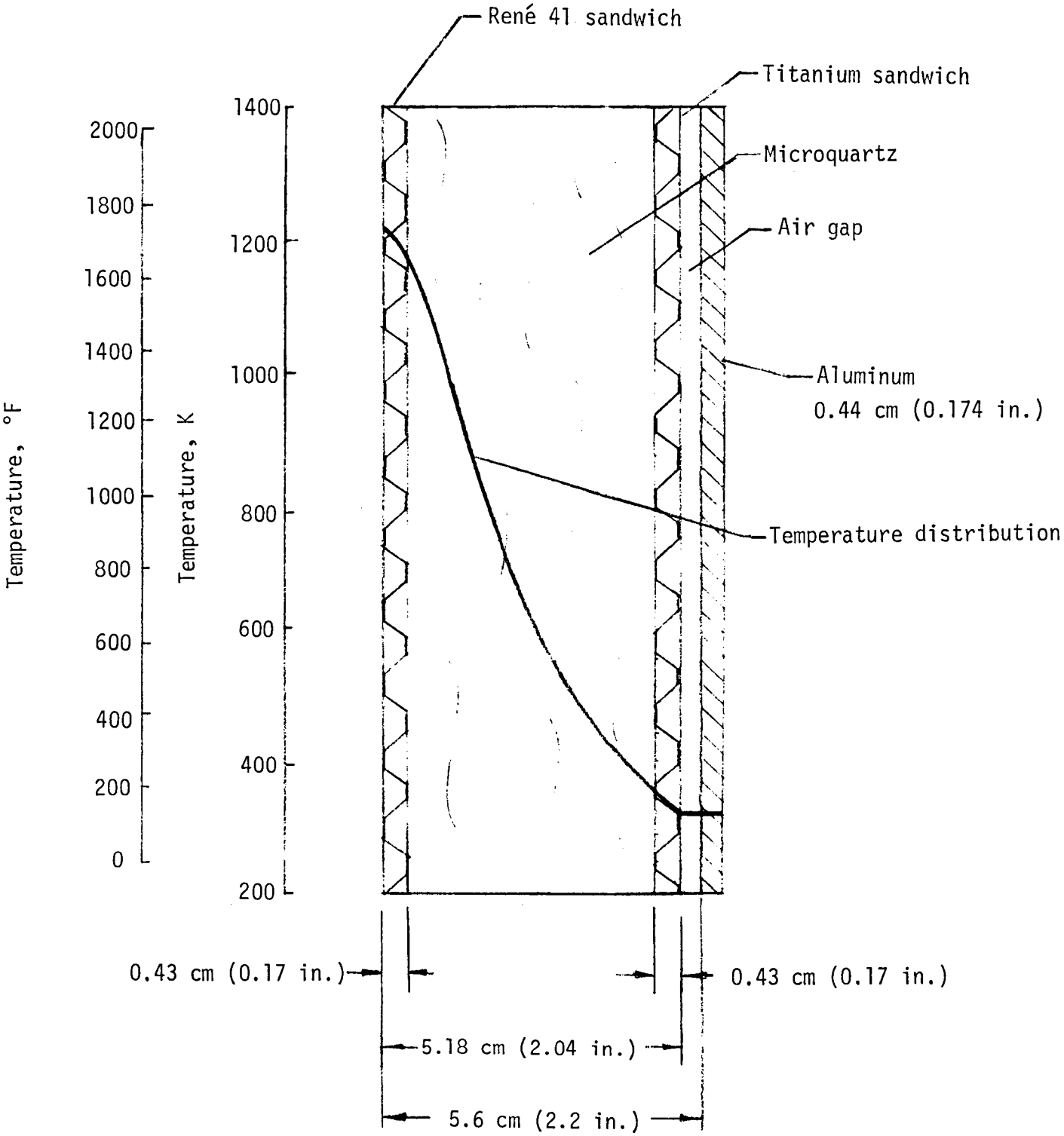

Figure 24.- Temperature distribution through multiwall tile for peak heating at body point 1700.

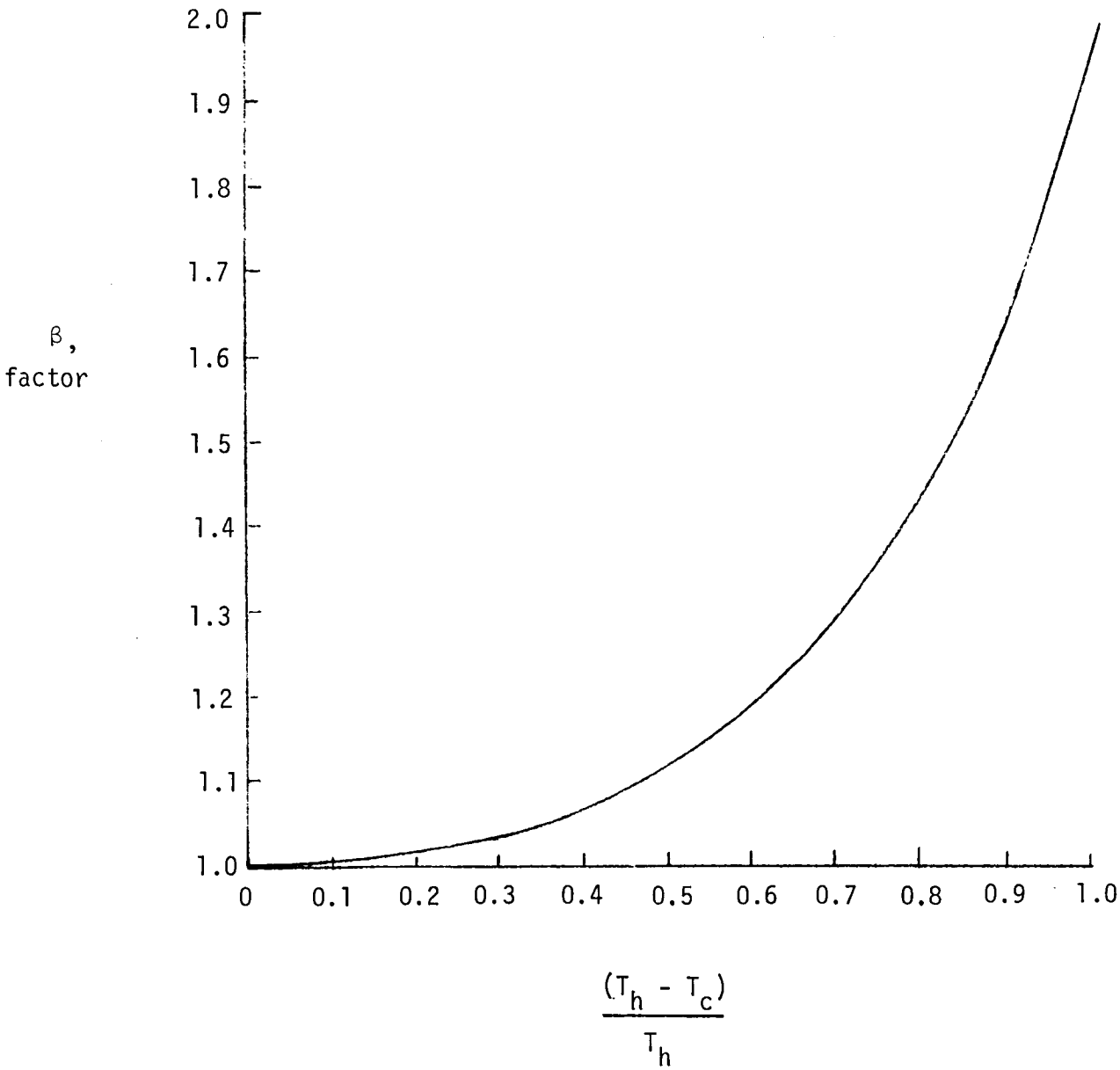

Figure 25.- Plot of factor, β, equation (A5), as a function of $(T_h - T_c)/T_h$.

1. Report No.	2. Government Accession No.	3. Recipient's Catalog No.
NASA TM-81780		

4. Title and Subtitle	5. Report Date
A Design Assessment of Multiwall, Metallic Stand-off, and RSI Reusable Thermal Protection Systems Including Space Shuttle Application	April 1980
	6. Performing Organization Code
7. Author(s)	8. Performing Organization Report No.
L. Robert Jackson and Sidney C. Dixon	
	10. Work Unit No.
9. Performing Organization Name and Address	505-31-73
NASA Langley Research Center Hampton, VA 23665	11. Contract or Grant No.
	13. Type of Report and Period Covered
12. Sponsoring Agency Name and Address	Technical Memorandum
National Aeronautics and Space Administration Washington, DC 20546	14. Sponsoring Agency Code

15. Supplementary Notes

16. Abstract Three reusable thermal protection systems of current interest are Reusable Surface Insulation (RSI), metallic stand-off TPS, and multiwall TPS. TPS design goals, a description of each system, and an assessment of how well each system satisfies the design goals is given. Multiwall TPS is described in some detail, and analyses useful for design of multiwall are included in the Appendix.

Results indicate that multiwall has the potential to satisfy the TPS design goals better than the other systems. The total mass of the stand-off TPS and of multiwall TPS are each comparable to that of RSI for shuttle application. Moreover, the metallic systems require less primary structure mass than the RSI system; since the nonbuckling skin criteria, required for RSI, may be removed. Continued development of multiwall TPS is required to verify its potential and to provide the necessary data base for design.

17. Key Words (Suggested by Author(s))	18. Distribution Statement
Insulation Thermal Protection Systems Space Shuttle	Unclassified - Unlimited Subject Category 16

19. Security Classif. (of this report)	20. Security Classif. (of this page)	21. No. of Pages	22. Price*
Unclassified	Unclassified	94	$6.00

* For sale by the National Technical Information Service, Springfield, Virginia 22161